

UNCLASSIFIED

AD NUMBER	
AD500268	
CLASSIFICATION CHANGES	
TO:	UNCLASSIFIED
FROM:	CONFIDENTIAL
LIMITATION CHANGES	
TO: Approved for public release; distribution is unlimited.	
FROM: Distribution authorized to U.S. Gov't. agencies and their contractors; Administrative/Operational Use; DEC 1968. Other requests shall be referred to Rocket Propulsion Lab., Edwards AFB, CA.	
AUTHORITY	
AFRPL ltr 16 Mar 1978; AFRPL ltr 16 Mar 1978	

THIS PAGE IS UNCLASSIFIED

THIS REPORT HAS BEEN DELIMITED
AND CLEARED FOR PUBLIC RELEASE
UNDER DOD DIRECTIVE 5200.20 AND
NO RESTRICTIONS ARE IMPOSED UPON
ITS USE AND DISCLOSURE.

DISTRIBUTION STATEMENT A

APPROVED FOR PUBLIC RELEASE;
DISTRIBUTION UNLIMITED.

SECURITY

MARKING

The classified or limited status of this report applies to each page, unless otherwise marked.

Separate page printouts MUST be marked accordingly.

THIS DOCUMENT CONTAINS INFORMATION AFFECTING THE NATIONAL DEFENSE OF THE UNITED STATES WITHIN THE MEANING OF THE ESPIONAGE LAWS, TITLE 18, U.S.C., SECTIONS 793 AND 794. THE TRANSMISSION OR THE REVELATION OF ITS CONTENTS IN ANY MANNER TO AN UNAUTHORIZED PERSON IS PROHIBITED BY LAW.

NOTICE: When government or other drawings, specifications or other data are used for any purpose other than in connection with a definitely related government procurement operation, the U.S. Government thereby incurs no responsibility, nor any obligation whatsoever; and the fact that the Government may have formulated, furnished, or in any way supplied the said drawings, specifications, or other data is not to be regarded by implication or otherwise as in any manner licensing the holder or any other person or corporation, or conveying any rights or permission to manufacture, use or sell any patented invention that may in any way be related thereto.

**Best
Available
Copy**

CONFIDENTIAL

AFRPL-TR-68-159-Vol II ✓

TCO-57-9-8

Copy No.

AD 500268

FINAL REPORT
DEMONSTRATION OF 156 INCH MOTOR WITH
SEGMENTED FIBERGLASS CASE AND ABLATIVE NOZZLE

VOLUME II--STATIC TEST AND HYDROBURST (U)

CONTRACT AF 04(611)-11603 ✓

December 1968

Prepared for

AIR FORCE
ROCKET PROPULSION LABORATORY
DIRECTORATE OF LABORATORIES
AIR FORCE SYSTEMS COMMAND
UNITED STATES AIR FORCE
Edwards AFB, California

THIOKOL CHEMICAL CORPORATION
WASATCH DIVISION
Brigham City, Utah

DDC
MAR 24 1969

IN ADDITION TO SECURITY REQUIREMENTS WHICH MUST BE MET, THIS
DOCUMENT IS SUBJECT TO SPECIAL EXPORT CONTROLS AND EACH
TRANSMITTAL TO FOREIGN NATIONALS MAY BE MADE ONLY WITH
PRIOR APPROVAL OF AFRPL (RPPR/STINFO) EDWARDS AFB,
CALIFORNIA, 93523.

CONFIDENTIAL

SPECIAL NOTICES

Qualified users may obtain copies of this report from the Defense Documentation Center.

Do not return this copy. When not needed, destroy in accordance with pertinent security regulations.

When U. S. Government drawings, specifications, or other data are used for any purpose other than a definitely related Government procurement operation, the Government thereby incurs no responsibility nor any obligations whatsoever, and the fact that the Government may have formulated, furnished, or in any way supplied the said drawings, specifications, or other data, is not to be regarded by implication or otherwise, or in any manner licensing the holder or any other person or corporation, or conveying any rights or permission to manufacture, use, or sell any patented invention that may in any way be related thereto.

RECEIVED IN	
OFFICE	ACTIVE SECTION <input checked="" type="checkbox"/>
DATE	DEF. SECTION <input checked="" type="checkbox"/>
TO: [illegible]	
FROM: [illegible]	
SUBJECT: [illegible]	
DISTRIBUTION AVAILABILITY CODE	
DATE	STATUS OF SPECIAL
2	

1973

CONFIDENTIAL

AFRPL-TR-68-159-Vol 2

TCO-57-9-8

FINAL REPORT. 1: 1/2 11/7
DEMONSTRATION OF 156 INCH MOTOR WITH
SEGMENTED FIBERGLASS CASE AND ABLATIVE NOZZLE.

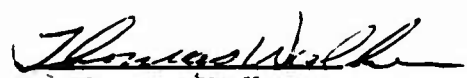
VOLUME II--STATIC TEST AND HYDROBURST (U).


CONTRACT AF 04(611)-11603/

(11) D...
(12) 1: 1/2

Prepared by

THIOKOL CHEMICAL CORPORATION
WASATCH DIVISION
Brigham City, Utah


Thomas Walker
Program Manager


Robert Zeigler
Project Engineer

IN ADDITION TO SECURITY REQUIREMENTS WHICH MUST BE MET, THIS DOCUMENT
IS SUBJECT TO SPECIAL EXPORT CONTROLS AND EACH TRANSMITTAL TO FOREIGN
NATIONALS MAY BE MADE ONLY WITH PRIOR APPROVAL OF AFRPL (RPPRUSTINE),
EDWARDS, CALIFORNIA 93523.

DOWNGRADED AT 3 YEAR INTERVALS
DECLASSIFIED AFTER 12 YEARS
DOD DIR 5200.10

THIS MATERIAL CONTAINS INFORMATION AFFECTING THE NATIONAL DEFENSE OF THE
UNITED STATES WITHIN THE MEANING OF THE ESPIONAGE LAWS, TITLE 18, U.S.C.,
SECTIONS 793 AND 794, THE TRANSMISSION OR REVELATION OF WHICH IN ANY MANNER
TO AN UNAUTHORIZED PERSON IS PROHIBITED BY LAW.

Publications No. 0968-20171 ✓

CONFIDENTIAL

m/2 1: 2 2 6 1

FOREWORD

This final technical engineering report documents all efforts and results relative to Contract AF 04(611)-11603, "Demonstration of 156 Inch Motor with Segmented Fiberglass Case and Ablative Nozzle." The program motor, designated by the Air Force as the 156-8 rocket motor, was identified as the TU-312L.02 motor for internal processing at Thiokol.

The contract with Thiokol Chemical Corporation, Wasatch Division, was performed under the overall direction of SAMSO with technical direction by Captain Richard Neely (RPMMS), Solid Rocket Division of the Air Force Rocket Propulsion Laboratory, Directorate of Laboratories (DOL), Air Force Systems Command, Edwards, California.

The report is organized into two volumes. Volume I describes the motor design and fabrication, and Volume II covers the motor static test and hydroburst. The report contains no classified information extracted from other documents.

This document has been reviewed and approved.

Charles R. Cooke
Chief, Solid Rocket Division
AFRPL, Edwards, California

TABLE OF CONTENTS

		<u>Page</u>
I	INTRODUCTION AND SUMMARY	1
II	TEST OBJECTIVES	2
III	MOTOR ASSEMBLY AND INSTRUMENTATION	3
	A. Motor Assembly.	3
	B. Instrumentation	5
IV	STATIC TEST	11
	A. Test Objective Fulfillment.	11
	B. Test Results	11
	1. Ballistic Performance.	11
	2. Case Performance	18
	3. Seal and Insulation Performance.	33
	4. Ignition System Performance	47
	5. Nozzle Performance.	54
	6. Accelerometer Data	71
V	HYDROBURST TEST.	83
	A. Introduction.	83
	B. Bladder Repair and Case Installation.	83
	1. Bladder Repair	83
	2. Case Installation	84
	C. Instrumentation	85
	D. Test Results and Analysis	85
VI	CONCLUSIONS AND RECOMMENDATIONS.	97

LIST OF ILLUSTRATIONS

<u>Figure</u>		<u>Page</u>
1	Quench System	6
2	156-8 Motor Prepared for Static Test	7
3	Instrumentation List and Drawing Notes	8
4	Instrumentation Layout Drawing	9
5	Camera Location	10
6	Predicted and Actual Chamber Pressure, 70° F	14
7	Predicted and Actual Thrust, 70° F	15
8	Predicted and Actual Pressure Decay Rates	20
9	Predicted and Actual Thrust Decay Rates	21
10	Measured Strain (S044) of Skirt Overwrap	22
11	Aft Skirt and Cylinder Strain Data	24
12	Center Segment Hoop Strain	31
13	Insulation Performance Summary	36
14	Insulation Performance, Aft Joint - Center Segment	38
15	Insulation Performance, Forward Joint - Aft Segment	39
16	Measured Erosion Rate vs Mach No., V-44 Insulation, Aft Dome	40
17	Predicted V-44 Erosion Rate Based on Predicted Gas Flow Rate	41

LIST OF ILLUSTRATIONS (Cont)

<u>Figure</u>		<u>Page</u>
18	V-44 Insulation Erosion Rate and Convective Heat Transfer Coefficient	43
19	Erosion Analysis of Silica Cloth Phenolic Ring	44
20	Aft Dome Erosion Data	45
21	Asbestos Filled NBR and Silica Cloth Phenolic Erosion Rate vs Mach No.	46
22	Damaged Center Segment Bladder	48
23	Damaged Bladder and Case, Forward Segment	49
24	Damaged Bladder in Forward and Center Segments	50
25	Predicted and Actual Igniter Performance	52
26	Post-Test View of 156-8 Nozzle	55
27	Closeup of Nozzle, Internal View	56
28	Erosion Pockets in Throat Section, 100 Deg Location	57
29	Erosion Pockets in Throat Section, 280 Deg Location	58
30	Inlet Section	59
31	Throat Section Showing Gas Penetration	60
32	Hot Spot on Steel Inlet Structure	62
33	Throat Backup Ring	63
34	Melted Throat Ring Material	64
35	Nozzle Erosion and Char Profile.	67
36	Temperature Plots (T201 thru T205)	68

LIST OF ILLUSTRATIONS (Cont)

<u>Figure</u>		<u>Page</u>
37	Temperature Plots (T206 thru T210)	69
38	156-8 Nozzle Instrumentation	70
39	Strain Plots (S201 thru S206)	72
40	Strain Plots (S207 thru S212)	73
41	Strain Plots (S213 thru S217)	74
42	Strain Plots (S218 thru S222)	75
43	Strain Plots (S223 thru S227)	76
44	Strain Plots (S228 thru S232)	77
45	Strain Plots (S233 thru S236)	78
46	Aft Nozzle PSD vs Frequency in Vertical Direction	79
47	Aft Nozzle PSD vs Frequency in Horizontal Direction	80
48	Aft Harness PSD vs Frequency in Longitudinal Direction. . .	81
49	Forward Harness PSD vs Frequency in Vertical Direction. .	82
50	Hydroburst Instrumentation Layout	86
51	Hydroburst Pressure Chart	87
52	Case Crack Propagation at Burst	88
53	Photographic Sequence of Hydroburst.	90
54	Hoop Displacement, Forward Segment	91
55	Circumferential Strain Data	93

LIST OF TABLES

<u>Table</u>		<u>Page</u>
I	Ballistic Performance.	12
II	Motor Specifications	19
III	Skirt Maximum Strains, Displacements, and Temperatures	25
IV	Maximum Strains, Displacements, and Temperatures for the Case	28
V	Maximum Strains, Displacements, and Temperatures for Clevis Joints	34
VI	Igniter Performance	51
VII	Predicted Versus Actual Nozzle Erosion Rates and Char Depths	66
VIII	Extensometer Readings at Burst Pressure	95
IX	Strain Readings at Burst Pressure	96

SECTION I

(U) INTRODUCTION AND SUMMARY

- (U) The 156-8 rocket motor was static tested successfully on 25 Jun 1968 at the Wasatch Division of Thiokol Chemical Corporation under contract AF 04(611)-11603. The motor static test and subsequent hydroburst test culminated effort which started in early 1963 with the inception of the 623A program. The primary test objectives were to successfully static test fire the segmented, fiberglass, 156 in. diameter motor followed by the hydroburst test of the case. The motor was static test fired in accordance with the requirements of Thiokol Document TWR-2048, Amendment II, dated 26 Jan 1968, titled "Static Firing Test Requirements for 156-8 (TU-312L.02) Rocket Motor." The hydroburst test was performed in accordance with the requirements of Thiokol Document TWR-2454, dated 12 Jan 1968, titled "Hydroburst Test Requirements for TU-312L.02 Rocket Motor Case."
- (U) All systems performed satisfactorily during the static test. The case was subsequently hydroburst tested, successfully completing the program objectives. This volume contains the detailed results of the static firing and hydroburst tests, as well as conclusions and recommendations resulting from the overall program.

SECTION II

(U)

TEST OBJECTIVES

1. Demonstration of a large segmented fiberglass rocket motor.
2. Performance demonstration of a segmented 156 in. diameter fiberglass case.
3. Performance demonstration of joint seal and insulation on a large segmented rocket motor.
4. Performance demonstration of a headend ignition system in a 156 in. diameter rocket motor.
5. Performance demonstration of a large fixed ablative nozzle on a 156 in. diameter motor.

SECTION III

(U) MOTOR ASSEMBLY AND INSTRUMENTATION

(U) A. MOTOR ASSEMBLY

(U) The first step of the motor assembly was to install the igniter booster motor in the forward segment in the horizontal position. This was done at the manufacturing area.

(U) The balance of the assembly was performed in the test bay. Preparation for the assembly was made in the test bay by installing the axial load train and thrust adapter and aligning them. The forward straight-line mover supports were installed. Next, the forward segment was received in the test bay where it was lifted from the transporter and then mated to the thrust adapter and straight-line movers. It was supported with jacks and the joint protector removed. At this point, three outside clevis legs of the forward segment joint were found to have been damaged. The details of the analysis and rework are covered in Section II-C, Vol I.

(U) The center segment was then received at the test area, lifted from the transporter, and its joint protector removed.

(U) Upon attempting to mate the segments it was discovered that they would not engage. The case of the center segment had sagged 1/4 in. away from the Epocast filler in the harness on both ends and was out-of-round. Roundness checks made on the ends of both segments verified that the forward end of the center segment had deflected into an oval shape such that the pitch plane diameter was too small and the yaw plane diameter was too large. The comparative diameters are as follows:

	<u>Pitch Diameter (in.)</u>	<u>Yaw Diameter (in.)</u>
Forward segment	153.686	153.684
Center segment	153.413	154.075

- (U) Rounding brackets were fabricated and assembled to the harness. Each bracket consisted of a shoe to fit the 156-8 case contour, a jack screw, and a bracket which attached to the harness and through which the jack screws were threaded. Thirty-six of these jack screws were fabricated and were installed on the forward segment from 57 to 123 deg and from 227 to 303 degrees.
- (U) The brackets were incrementally and systematically torqued to a 46 ft-lb maximum. At this point the forward end of the center segment appeared to be compatible with the forward segment joint. The segments were then successfully mated. Pins were then installed and the segments supported with jacks.
- (U) The aft segment was then received at the test bay, lifted from the transporter, and the joint protectors removed from the aft end of the center segment and from the forward end of the aft segment. The rounding jacks were installed on the aft end of the center segment. This joint, which was fabricated with less clearance than the forward joint, was then matched with rounding jacks as much as possible. Although both were the same shape, the inside of the tongue on the aft segment interfered with the inside leg of the clevis on the center segment. This can be attributed to an inward deflection due to rounding jack pressure. Since the joint had a high structural factor of safety (see Section II, Vol I) shims were removed on the inside of the tongue until a fit was achieved. One shim was removed from 52 shim stacks and two from two shim stacks.
- (U) Following assembly of the aft segment to the center segment, the aft straight-line mover supports were installed. The jacks supporting the motor at the joint harness rings were then lowered to place the weight on the forward and aft skirts. As the weight came to bear on the skirts and into the forward and aft harness rings, it became evident that the aft skirt was failing and would not carry the weight of the motor. The jacks at the segment joints were then raised to relieve the weight from the aft skirt. A glass fabric overwrap was designed and installed. Details of the analysis and rework are covered in Section II-C-3, Vol I.
- (U) Following completion of the segment assembly, the CO₂ quench system consisting of a CO₂ storage having a capacity of at least 8,000 lb of CO₂, was installed.

Piping having a minimum ID of 0.391 in. led to the six injection ports around the periphery of the igniter. Check valves were fitted in each line. The system was pressure tested to 1,200 psig prior to installation on the motor. Figure 1 shows the installed quench system.

(U) A leak test was then performed by installing a pressure plate over the aft polar opening and a dummy S & A on the igniter. The loaded case assembly was pressurized to 50 psig for 1/2 hour. No pressure drop was evident. The segment joints, igniter joint, and quench system fittings were tested for leaks with Leak-Tec solution.

(U) The nozzle was then dryfitted and the potting gap measured. Fuller vacuum bag compound was then applied to the nozzle joint and the nozzle installed.

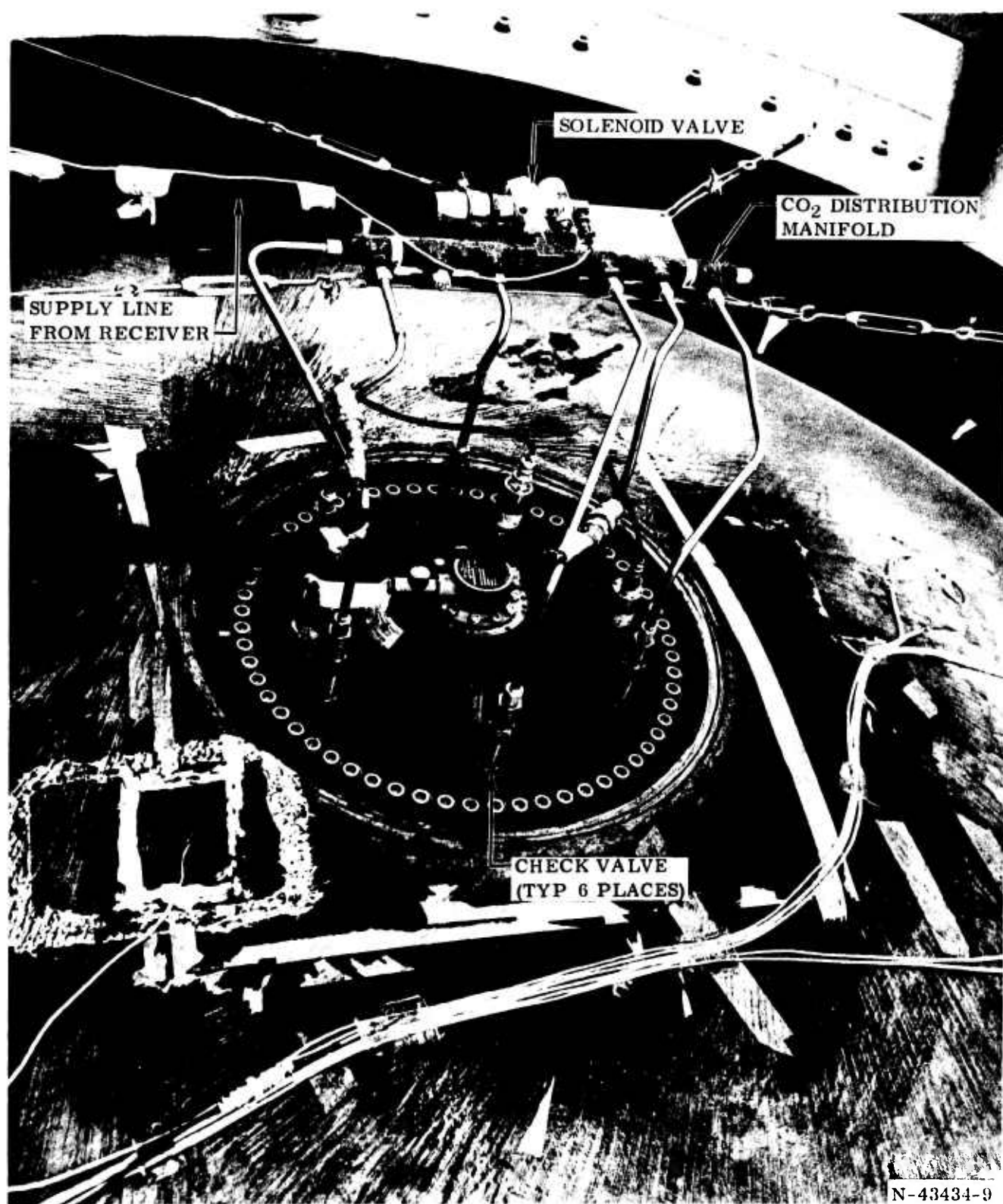
(U) After completion of the motor assembly, the antflight devices were installed.

(U) Figure 2 shows the 156-8 motor assembly prepared for static test.

(U) B. INSTRUMENTATION

(U) The motor was instrumented in accordance with Figures 3 and 4. In addition to the instrumentation shown in Figures 3 and 4, three strain gages were added at the damaged shim stack at zero degrees. All instrumentation was installed, calibrated and checked out prior to static test.

(U) The static test was covered by a minimum of 10 motion picture cameras. Figure 5 gives the location and frame rate of the exposure.



(U) Figure 1. Quench System

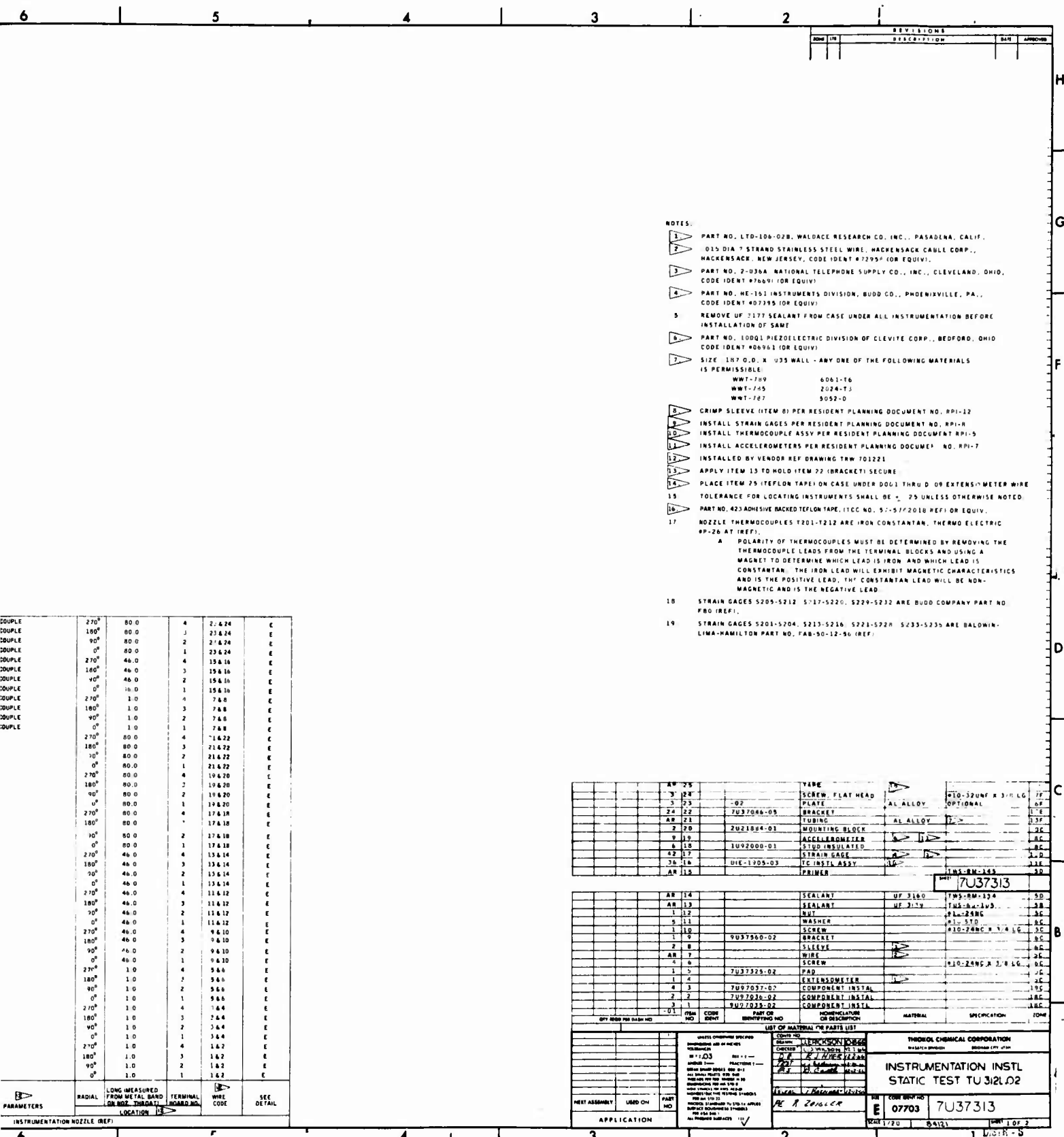


N43434-4

(U) Figure 2. 156-8 Motor Prepared for Static Test

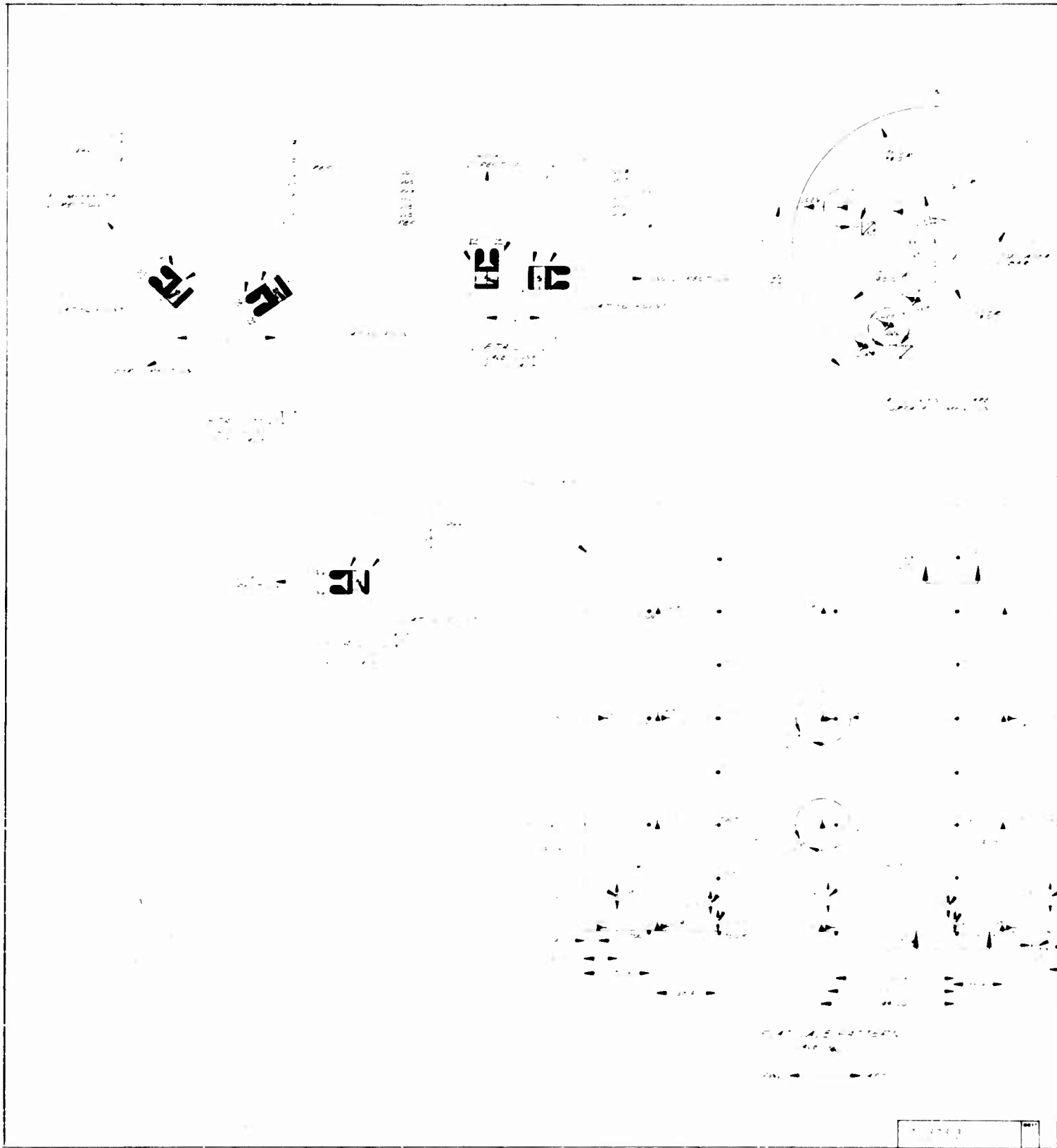
A206	ACCEL. HORIZONTAL	NOZZLE, DETAIL F
A205	ACCEL. VERTICAL	NOZZLE, VIEW T-T
A204	ACCEL. HORIZONTAL	NOZZLE, DETAIL F
A203	ACCEL. VERTICAL	NOZZLE, VIEW T-T
A202	ACCEL. HORIZONTAL	NOZZLE, DETAIL F
A201	ACCEL. VERTICAL	NOZZLE, VIEW T-T
A003	ACCEL. VERTICAL	CASE, DETAIL C
A002	ACCEL. LONGITUDINAL	CASE, DETAIL C
A001	ACCEL. VERTICAL	CASE, DETAIL B
T036	THERMOCOUPLE + 270°	AFT FLANGE, DETAIL D
T034	THERMOCOUPLE + 70°	AFT FLANGE, DETAIL D
T033	THERMOCOUPLE + 0°	AFT FLANGE, DETAIL D
T032	THERMOCOUPLE + 270°	AFT DOME, AFT VIEW
T031	THERMOCOUPLE + 180°	AFT DOME, AFT VIEW
T030	THERMOCOUPLE + 90°	AFT DOME, AFT VIEW
T029	THERMOCOUPLE + 0°	AFT DOME, AFT VIEW
T028	THERMOCOUPLE + 0°	AFT SEGMENT, DETAIL P
T027	THERMOCOUPLE + 0°	AFT SEGMENT, DETAIL P
T026	THERMOCOUPLE + 0°	AFT SEGMENT, DETAIL P
T025	THERMOCOUPLE + 0°	AFT SEGMENT, DETAIL P
T024	THERMOCOUPLE + 315°	AFT MOTOR JOINT, VIEW S-S
T023	THERMOCOUPLE + 270°	AFT MOTOR JOINT, VIEW S-S
T022	THERMOCOUPLE + 225°	AFT MOTOR JOINT, VIEW S-S
T021	THERMOCOUPLE + 180°	AFT MOTOR JOINT, VIEW S-S
T020	THERMOCOUPLE + 135°	AFT MOTOR JOINT, VIEW S-S
T019	THERMOCOUPLE + 90°	AFT MOTOR JOINT, VIEW S-S
T018	THERMOCOUPLE + 45°	AFT MOTOR JOINT, VIEW S-S
T017	THERMOCOUPLE + 0°	AFT MOTOR JOINT, VIEW S-S
T016	THERMOCOUPLE + 270°	CENTER SEGMENT, FLAT PATTERN
T015	THERMOCOUPLE + 180°	CENTER SEGMENT, FLAT PATTERN
T014	THERMOCOUPLE + 90°	CENTER SEGMENT, FLAT PATTERN
T013	THERMOCOUPLE + 0°	CENTER SEGMENT, FLAT PATTERN
T012	THERMOCOUPLE + 315°	FWD MOTOR JOINT, VIEW S-S
T011	THERMOCOUPLE + 270°	FWD MOTOR JOINT, VIEW S-S
T010	THERMOCOUPLE + 225°	FWD MOTOR JOINT, VIEW S-S
T009	THERMOCOUPLE + 180°	FWD MOTOR JOINT, VIEW S-S
T008	THERMOCOUPLE + 135°	FWD MOTOR JOINT, VIEW S-S
T007	THERMOCOUPLE + 90°	FWD MOTOR JOINT, VIEW S-S
T006	THERMOCOUPLE + 45°	FWD MOTOR JOINT, VIEW S-S
T005	THERMOCOUPLE + 0°	FWD MOTOR JOINT, VIEW S-S
T004	THERMOCOUPLE + 270°	FWD SEGMENT, FLAT PATTERN
T003	THERMOCOUPLE + 180°	FWD SEGMENT, FLAT PATTERN
T002	THERMOCOUPLE + 90°	FWD SEGMENT, FLAT PATTERN
T001	THERMOCOUPLE + 0°	FWD SEGMENT, FLAT PATTERN
S041	STRAIN FIBER	AFT DOME DETAIL C
S040	STRAIN FIBER	AFT DOME DETAIL C
S039	STRAIN FIBER	AFT DOME DETAIL H
S038	STRAIN CIRCUMFERENTIAL	AFT DOME DETAIL H
S037	STRAIN FIBER	AFT DOME DETAIL H
S036	STRAIN CIRCUMFERENTIAL	AFT DOME DETAIL H
S035	STRAIN FIBER	AFT DOME DETAIL H
S034	STRAIN CIRCUMFERENTIAL	AFT DOME DETAIL H
S033	STRAIN FIBER	AFT DOME DETAIL H
S032	STRAIN CIRCUMFERENTIAL	AFT DOME DETAIL H
S031	STRAIN FIBER	FWD DOME DETAIL G
S030	STRAIN FIBER	FWD DOME DETAIL G
S029	STRAIN FIBER	FWD DOME DETAIL G
S028	STRAIN FIBER	FWD DOME DETAIL H
S027	STRAIN CIRCUMFERENTIAL	FWD DOME DETAIL H
S026	STRAIN FIBER	FWD DOME DETAIL H
S025	STRAIN CIRCUMFERENTIAL	FWD DOME DETAIL H
S024	STRAIN FIBER	FWD DOME DETAIL H
S023	STRAIN CIRCUMFERENTIAL	FWD DOME DETAIL H
S022	STRAIN LONGITUDINAL	AFT SKIRT DETAIL L
S021	STRAIN LONGITUDINAL	AFT SKIRT DETAIL L
S020	STRAIN HOOP	CASE DETAIL K
S019	STRAIN LONGITUDINAL	CASE DETAIL J
S018	STRAIN HOOP	CASE DETAIL J
S017	STRAIN HOOP	CASE DETAIL J
S016	STRAIN LONGITUDINAL	CASE DETAIL J
S015	STRAIN HOOP	CASE DETAIL J
S014	STRAIN HOOP	CASE DETAIL K
S013	STRAIN LONGITUDINAL	CASE DETAIL J
S012	STRAIN HOOP	CASE DETAIL J
S011	STRAIN HOOP	CASE DETAIL K
S010	STRAIN LONGITUDINAL	CASE DETAIL J
S009	STRAIN HOOP	CASE DETAIL J
S008	STRAIN HOOP	CASE DETAIL K
S007	STRAIN LONGITUDINAL	CASE DETAIL J
S006	STRAIN HOOP	CASE DETAIL J
S005	STRAIN HOOP	CASE DETAIL K
S004	STRAIN LONGITUDINAL	CASE DETAIL J
S003	STRAIN HOOP	CASE DETAIL J
S002	STRAIN LONGITUDINAL	FWD SKIRT DETAIL L
S001	STRAIN LONGITUDINAL	FWD SKIRT DETAIL L
D010	DISP CASE SEGMENT	CASE DETAIL R
D009	DISP LONGITUDINAL	CASE SEE FLAT PATTERN
D008	DISP LONGITUDINAL	CASE SEE FLAT PATTERN
D007	DISP HOOP	CASE SEE FLAT PATTERN
D006	DISP HOOP	CASE SEE FLAT PATTERN
D005	DISP HOOP	CASE SEE FLAT PATTERN
D004	DISP HOOP	CASE SEE FLAT PATTERN
D003	DISP HOOP	CASE SEE FLAT PATTERN
D002	DISP HOOP	CASE SEE FLAT PATTERN
D001	DISP HOOP	CASE SEE FLAT PATTERN
D000	DISP HOOP	CASE SEE FLAT PATTERN

INSTRUMENT CODE	PARAMETER	LOCATION	INSTRUMENT CODE	PARAMETER	LOCATION	INSTRUMENT CODE	PARAMETER	LOCATION	INSTRUMENT CODE	PARAMETER	LOCATION		
7212	THERMOCOUPLE	270°	80.0	4	2.424	E	7211	THERMOCOUPLE	180°	80.0	2	23.424	E
7210	THERMOCOUPLE	90°	80.0	1	23.424	E	7209	THERMOCOUPLE	0°	80.0	1	23.424	E
7208	THERMOCOUPLE	270°	46.0	4	15.416	E	7207	THERMOCOUPLE	180°	46.0	3	15.416	E
7206	THERMOCOUPLE	90°	46.0	2	15.416	E	7205	THERMOCOUPLE	0°	46.0	1	15.416	E
7204	THERMOCOUPLE	270°	1.0	4	7.68	E	7203	THERMOCOUPLE	180°	1.0	3	7.68	E
7202	THERMOCOUPLE	90°	1.0	2	7.68	E	7201	THERMOCOUPLE	0°	1.0	1	7.68	E
5236	STRAIN	270°	80.0	4	11.422	E	5235	STRAIN	180°	80.0	3	21.422	E
5234	STRAIN	90°	80.0	2	21.422	E	5213	STRAIN	0°	80.0	1	21.422	E
5232	STRAIN	270°	80.0	4	19.420	E	5231	STRAIN	180°	80.0	2	19.420	E
5230	STRAIN	90°	80.0	2	19.420	E	5229	STRAIN	0°	80.0	1	19.420	E
5228	STRAIN	270°	80.0	4	17.418	E	5227	STRAIN	180°	80.0	3	17.418	E
5226	STRAIN	90°	80.0	2	17.418	E	5225	STRAIN	0°	80.0	1	17.418	E
5224	STRAIN	270°	46.0	4	15.414	E	5223	STRAIN	180°	46.0	3	15.414	E
5222	STRAIN	90°	46.0	2	15.414	E	5221	STRAIN	0°	46.0	1	15.414	E
5220	STRAIN	270°	46.0	4	11.412	E	5219	STRAIN	180°	46.0	3	11.412	E
5218	STRAIN	90°	46.0	2	11.412	E	5217	STRAIN	0°	46.0	1	11.412	E
5216	STRAIN	270°	46.0	4	9.410	E	5215	STRAIN	180°	46.0	3	9.410	E
5214	STRAIN	90°	46.0	2	9.410	E	5213	STRAIN	0°	46.0	1	9.410	E
5212	STRAIN	270°	1.0	4	5.66	E	5211	STRAIN	180°	1.0	3	5.66	E
5210	STRAIN	90°	1.0	2	5.66	E	5209	STRAIN	0°	1.0	1	5.66	E
5208	STRAIN	270°	1.0	4	1.42	E	5207	STRAIN	180°	1.0	3	1.42	E
5206	STRAIN	90°	1.0	2	1.42	E	5205	STRAIN	0°	1.0	1	1.42	E
5204	STRAIN	270°	1.0	4	1.42	E	5203	STRAIN	180°	1.0	3	1.42	E
5202	STRAIN	90°	1.0	2	1.42	E	5201	STRAIN	0°	1.0	1	1.42	E

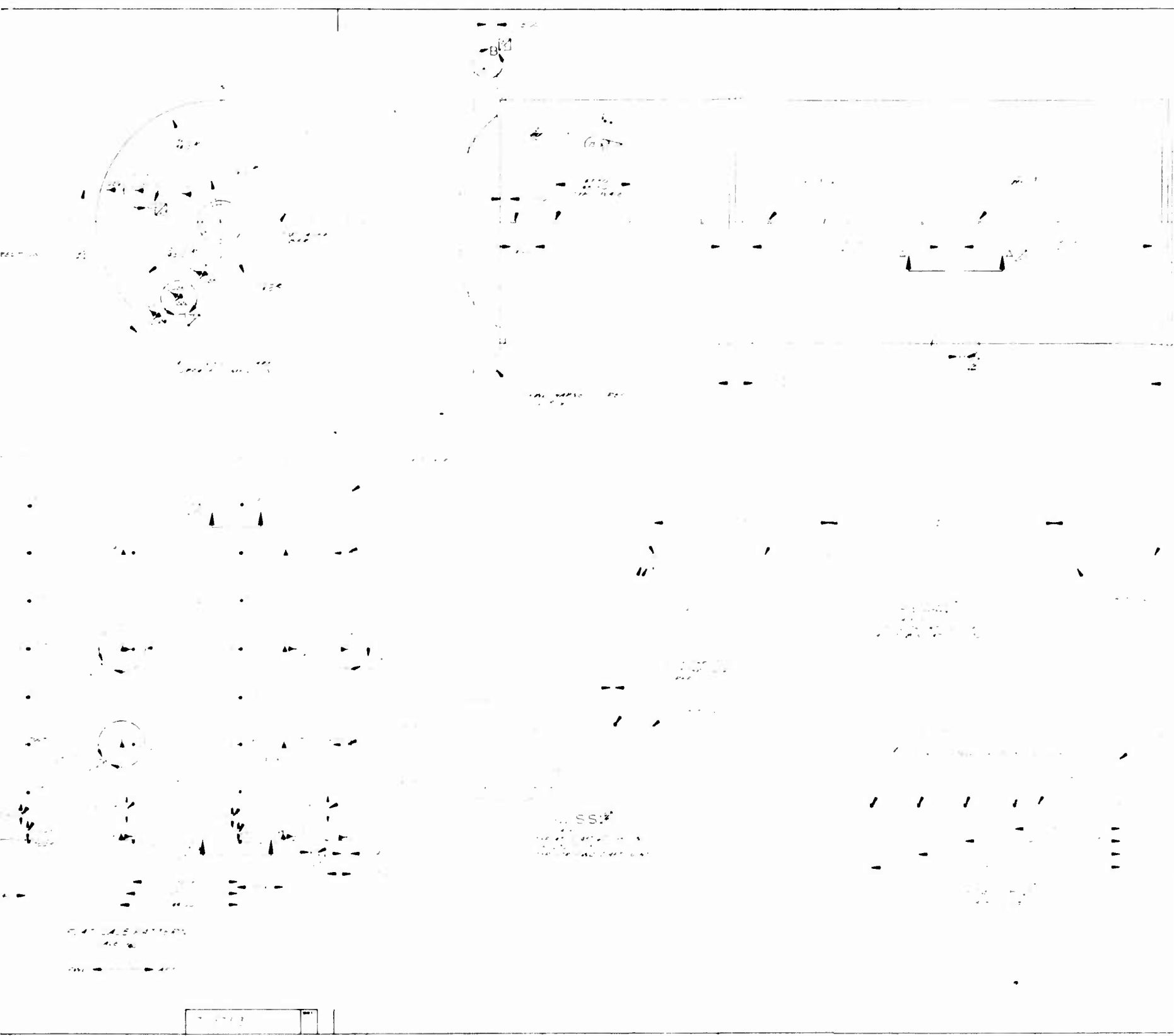


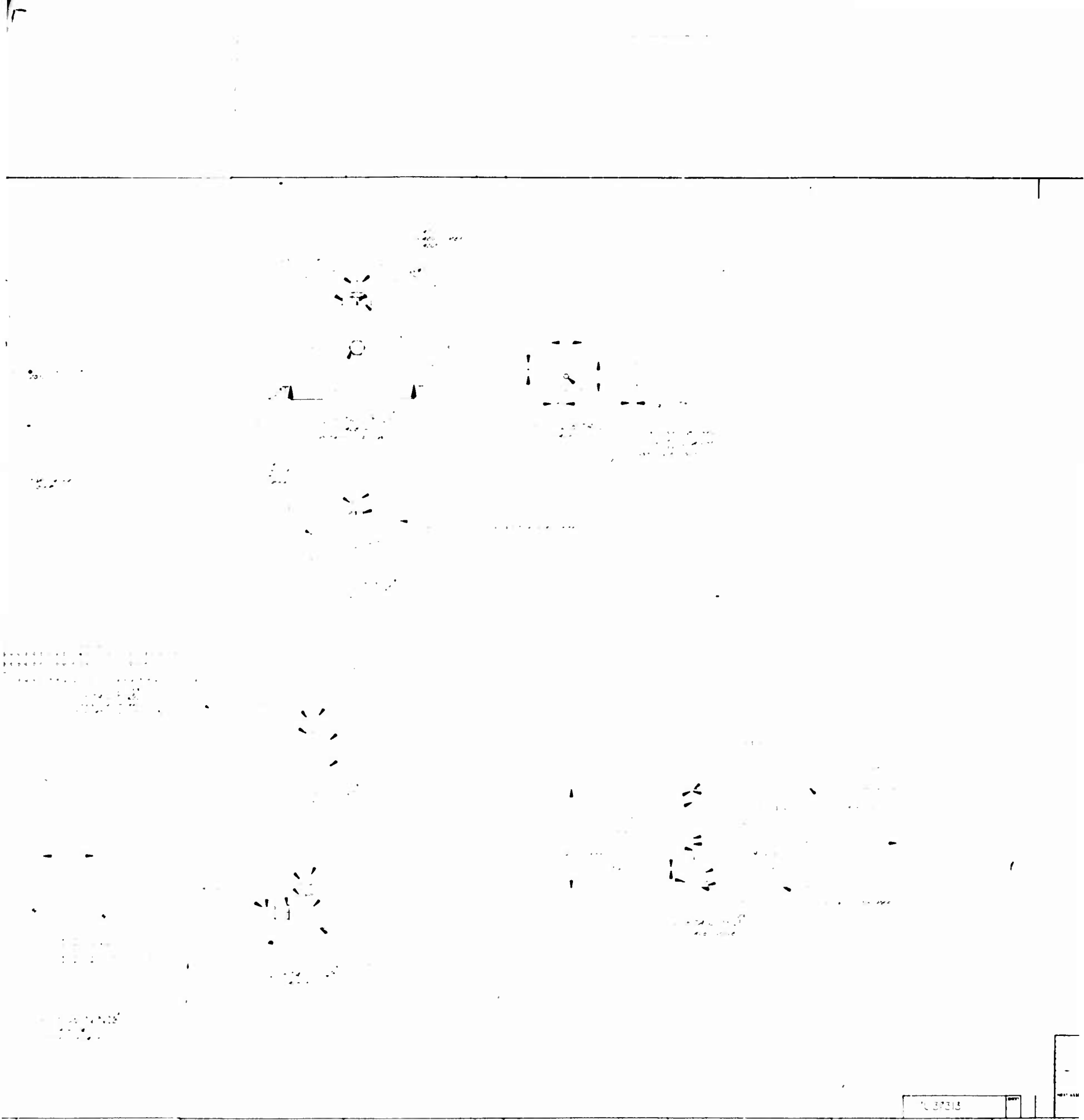
(U) Figure 3. Instrumentation List and Drawing Notes

2



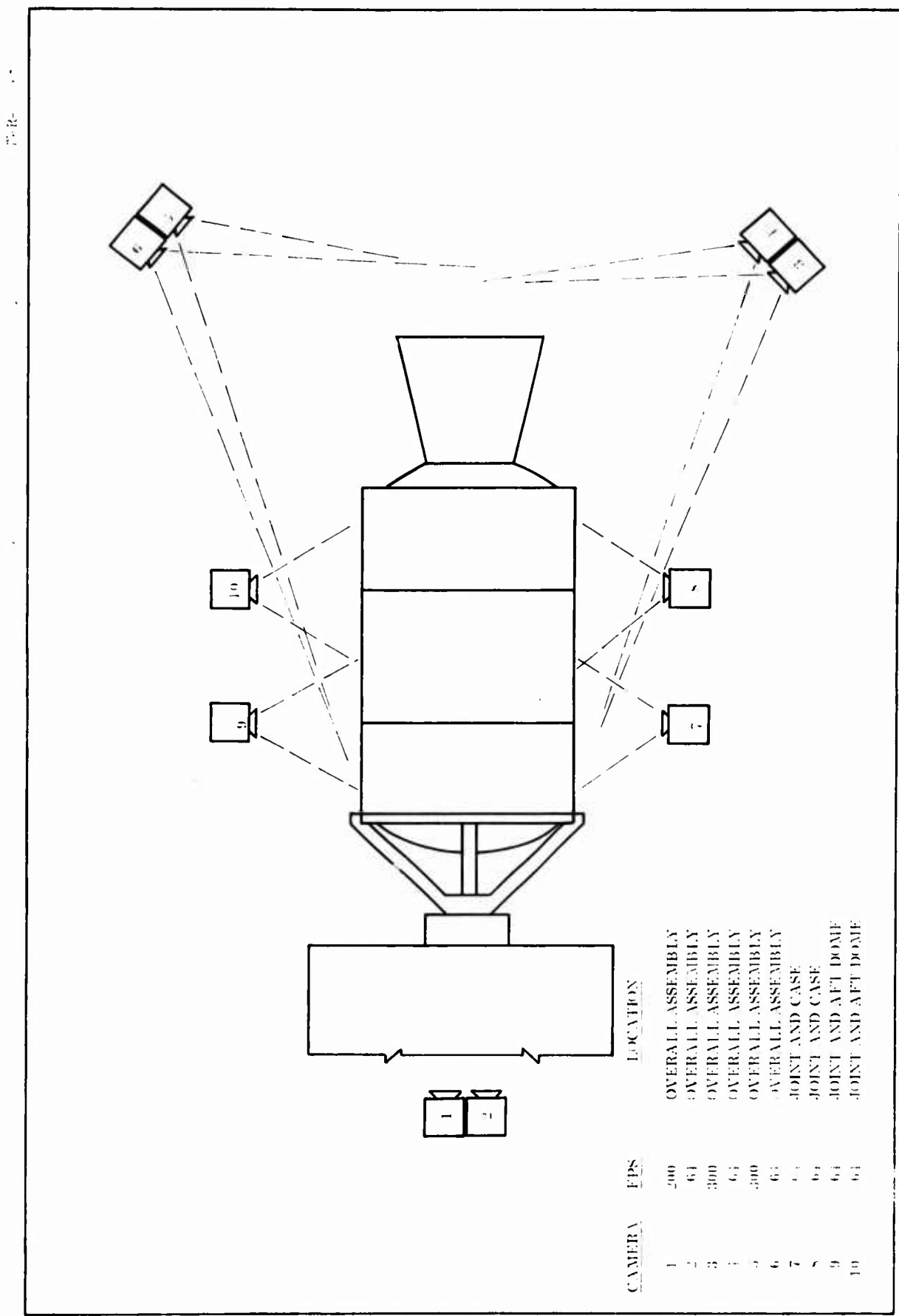
1





7

		REV. 1.0 DATE: 11/1/77 BY: [Signature] CHECKED: [Signature]	



(U) Figure 5. Camera Location

CONFIDENTIAL

SECTION IV

(U) STATIC TEST

(U) A. TEST OBJECTIVE FULFILLMENT

(C) All static test objectives were fulfilled. The 156-8 motor fired for an action time of 123.8 sec meeting all parameters very closely to predicted. The large segmented fiberglass case withstood the internal pressure and loads except the aft skirt overwrap reinforcement which was not under evaluation.

(C) The joint seal and insulation performed satisfactorily with no hot spots due to marginal insulation. The head end ignition system satisfactorily ignited the grain in 0.453 second. The large fixed ablative nozzle effectively withstood the environment of the firing.

(U) B. TEST RESULTS

(U) 1. BALLISTIC PERFORMANCE

(U) Performance of the 156-8 motor was satisfactory and close to predicted for the full duration of operation. Comparisons of measured and predicted ballistic performance data, plus propellant configuration data, are presented in Table I. Predicted and measured pressure and thrust versus time characteristics for the 156-8 motor are presented in Figures 6 and 7, respectively.

(U) Measured pressure and thrust values showed minor deviation from the predicted values in three areas: (1) the motor operated at a slightly lower average action time pressure and for a longer action time than was predicted; (2) a sudden, unpredicted rise in pressure and thrust occurred at 109 sec; and (3) the motor operating pressure and thrust for the first 20 sec were below the predicted levels.

CONFIDENTIAL

TABLE I
(C) BALLISTIC PERFORMANCE

Test Conditions

Motor Conditioning Temperature (°F)	70
Ambient Temperature (°F)	85
Ambient Pressure (psia)	12.4

Web Time Performance	<u>Predicted</u>	<u>Measured</u>
Web Time* (sec)	117.8	117.8
Average Pressure (psia)	744	734
Maximum Pressure (psia)	806	806
Average Thrust (lbf)	1,006,500	993,492
Maximum Thrust (lbf)	1,077,700	1,088,754
Impulse (lbf-sec)	118,518,400	117,063,137

Action Time Performance

Action Time** (sec)	121.3	123.8
Average Pressure (psia)	732	712
Average Thrust (lbf)	990,400	960,847
Impulse (lbf-sec)	120,124,600	118,972,800
Specific Impulse (lbf-sec/lbm)	243	242.2
Measured Thrust Coefficient	1.512	1.500

Propellant Data

Burning Rate at 1,000 psia (in./sec)	0.353	0.351
Burning Rate Exponent	0.21	0.21
Characteristic Velocity (ft/sec)	5,180	5,195

Propellant Configuration

Port Diameter, Nominal (in.)	--	76.49
Web Thickness (in.)	--	38.741
Web Fraction	--	0.503
Propellant Weight (lbm)	494,442	492,619
Port Area/Throat Area, Initial	--	5.38
Propellant Mass Fraction	--	0.926

*Web time is defined as the time interval from 75 percent of maximum pressure during rise to the point of pressure-time trace which lies on the line bisecting the angle formed by the tangents to the trace prior to and immediately after the beginning of tailoff.

**Action time is defined as the time interval from 75 percent of maximum pressure during rise to 10 percent maximum pressure during tailoff.

CONFIDENTIAL

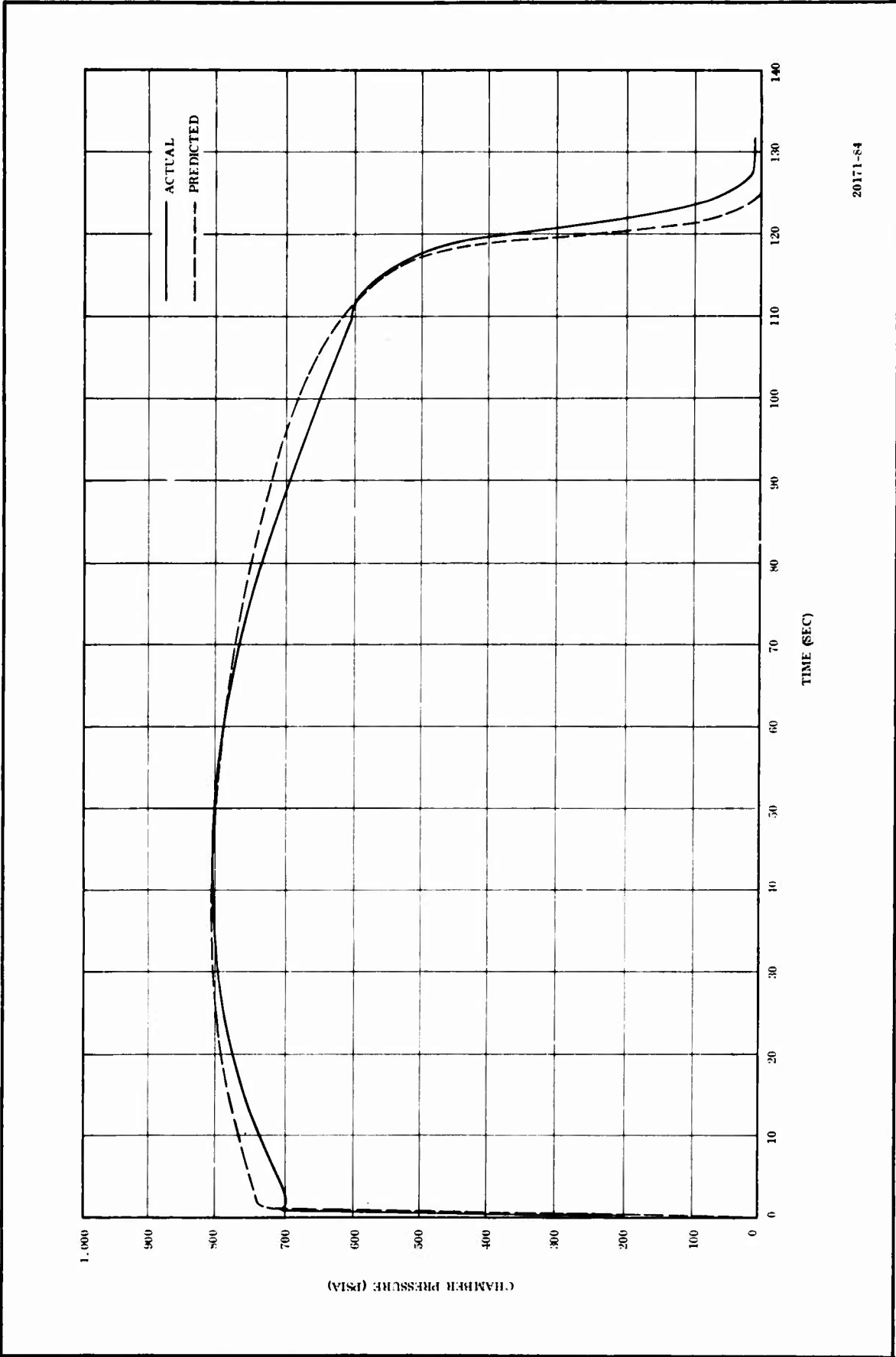
TABLE I (Cont)

(C) BALLISTIC PERFORMANCE

	<u>Predicted</u>	<u>Measured</u>
Corrected Data		
Reference Specific Impulse (lbf-sec/lbm)	248.0	247.89
Average Web Time Sea Level Thrust (lbf)	993,300	979,800
Web Time Sea Level Impulse (lbf-sec)	116,956,500	115,422,000
Maximum Thrust (lbf)	1,064,000	1,075,100
Average Action Time Sea Level Thrust (lbf)	977,900	947,200
Action Time Sea Level Impulse (lbf-sec)	118,609,100	117,259,400
Sea Level Specific Impulse (lbf-sec/lbm)	239.9	238.8

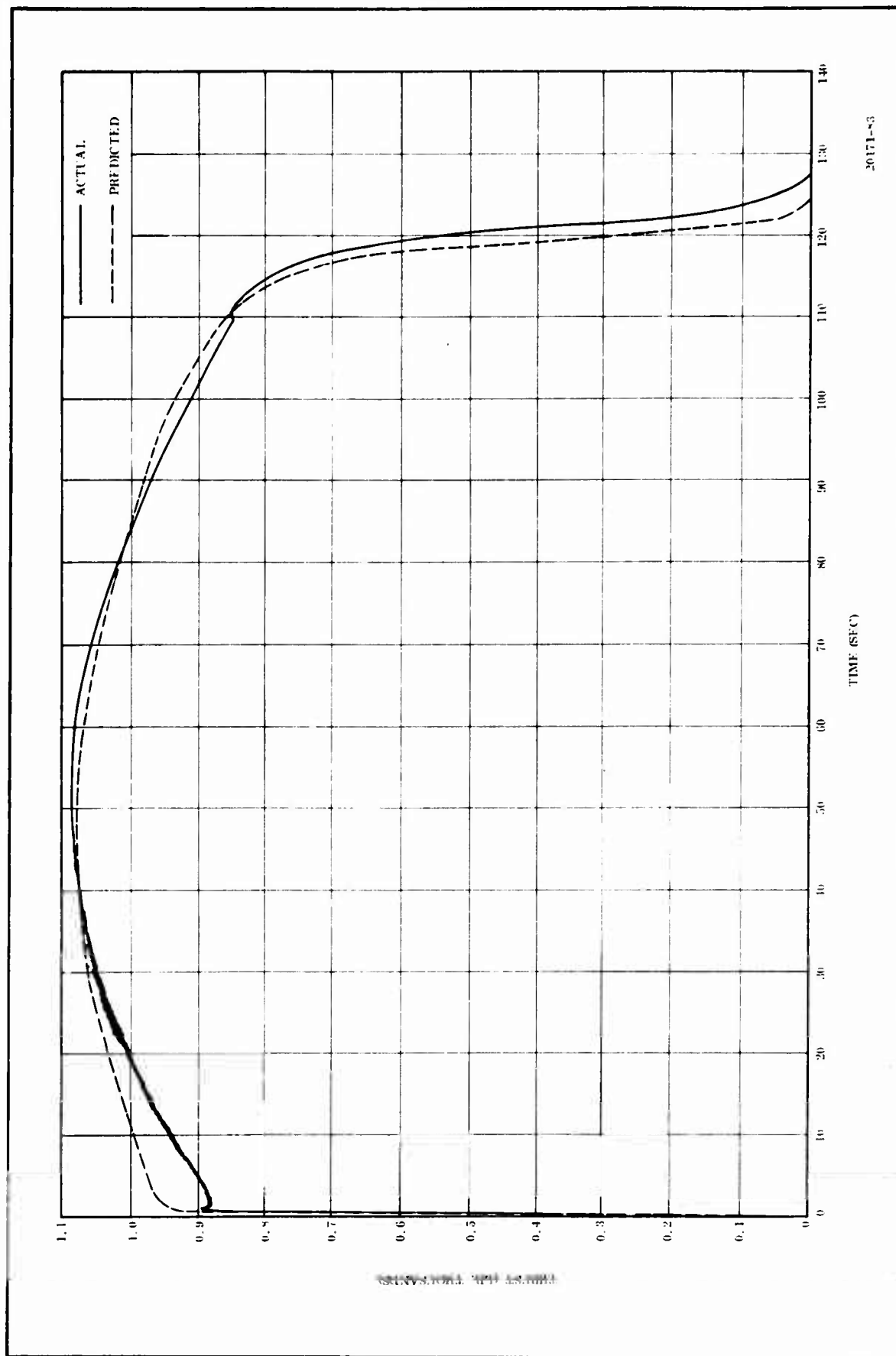
$\Delta A_s = 2,140$ sq in. or 1.45 percent

$\Delta P = 10$ psi



(C) Figure 6. Predicted and Actual Chamber Pressure, 70°F

CONFIDENTIAL



(C) Figure 7. Predicted and Actual Thrust, 70°F

CONFIDENTIAL

- (U) The cylindrical perforate grain configuration used in the 156-8 motor theoretically had no propellant sliver at web burnout. However, many factors, such as batch-to-batch propellant burning rate variations, influence the uniformity of web burnout along the length of the motor and both the size and configuration of the propellant sliver. The size and shape of the propellant sliver remaining at web burnout determines the shape and duration of the tailoff portion of motor operation.
- (U) Due to the difficulty in predicting the sliver configuration, empirical data from motors of similar design, are frequently used to predict motor tailoff characteristics. The 156-8 motor tailoff prediction was based on the results of the previously tested 156-1C motor. The prediction of tailoff duration ($t_a - t_o$) and the pressure integral during tailoff was based on the assumption that the sliver configuration in the 156-1C and 156-8 motors would be similar.
- (U) The longer than predicted tailoff duration and the lower than predicted average pressure during tailoff resulted in an extended motor action time and a reduction in the overall average motor pressure during the action time interval. This performance apparently resulted from a more nonuniform propellant sliver than demonstrated by the 156-1C test. The slight difference in predicted and actual pressure and thrust decay rates can be directly attributed to deviations in the propellant sliver configuration.
- (U) Also contributing to the motor tailoff discrepancy was a marked pressure rise at 109 sec (Figure 6). This pressure buildup had the effect of delaying the beginning of motor pressure decay and essentially prolonging the tailoff time.
- (U) Analysis indicated that the pressure anomaly occurring at 109 sec was probably due to the unrepaired voids and folds in the last 4 in. of the propellant web of the forward segment. Calculations showed that at 109 sec the flame front

CONFIDENTIAL

had burned approximately 36 in. into the propellant web. The region was known to contain propellant voids and folds. As the flame front reached the separated propellant portions, an increased amount of burning surface area was created, thus rapidly increasing motor chamber pressure. A hot spot occurred in the case wall in the cylindrical portion of the forward segment and was probably associated with the pressure rise.

- (U) The low pressure and thrust operation during the first 20 sec of motor firing is not fully explainable but is characteristic of large cylindrical perforate (CP) grain motors. Approximately 75 percent of the initial burning surface of the 156-8 was the CP bore surface, which was subjected to moderate strain during motor pressurization. Test data have shown that propellant in a strained condition has a reduced burning rate.* It is possible that the strained condition of the propellant was a factor causing the initial low pressure and thrust levels.
- (U) The total measured propellant weight in the motor was 492,619 lbm, which is 1,823 lbm lower than the predicted weight listed in Table I. The measured useful propellant weight was 491,139 lbm and was used in determining the measured delivered specific impulse.
- (C) The delivered specific impulse of 242.2 sec was only 0.8 sec lower than predicted. This difference was partially due to the lower operating pressure. When corrected to reference conditions (1,000 psia, sea level, $\alpha = 15$ deg, and optimum expansion), the 156-8 reference specific impulse of 247.89 sec was only 0.11 sec less than the predicted value of 248.0.
- (C) The reference specific impulse of 247.89 reflects a combustion efficiency of 94.4 percent [reference specific impulse (1,000 psia, sea level, optimum expansion, $\alpha = 15$ deg) divided by theoretical reference specific impulse (1,000 psia, sea level,

*Macbeth, A. W.: Effects of Propellant Strain on Motor Burning Rate (U). Contract AF 33(600)-36514, Thiokol Chemical Corporation, Wasatch Division, 15 Jul 1964.

CONFIDENTIAL

optimum expansion, $\alpha = 0$ deg)]. The demonstrated efficiency of 94.4 percent compares favorably with the predicted efficiency of 94.5 percent based on historical efficiency data.

(C) The propellant used in the 156-8 motor had a burning rate of 0.306 in./sec at 700 psia when tested in a 5 in. CP (TU-131) motor. At a pressure of 744 psia, this burning rate increases to 0.310 in./sec. A scaleup factor of 1.07 is then used to predict the full size motor burning rate of 0.332 in./sec at 744 psia. The close correlation of predicted and measured action time substantiates the 7 percent burning rate scaleup from the batch check motor burning rate to the predicted burning rate in the full size motor.

(U) Motor performance specified in Exhibit A to the Work Statement is compared with measured data in Table II. Predicted and actual values of pressure and thrust decay rates are presented in Figures 8 and 9.

(U) 2. CASE PERFORMANCE

(U) a. Skirt Performance--The skirts were designed to support the case during static test. Thrust was taken through the forward skirt so that the stresses in the skirts were induced by discontinuities plus axial compression.

(U) The aft skirt failed during motor assembly in the test stand. The failure occurred in the skirt laminate and not between the laminate and rubber shear ply. The damaged skirt was repaired by applying a 0.030 in. layer of rubber and 44 layers (15 in. wide) of 181 style E glass wrapped around the motor in the damaged area. The details of this repair are covered in Section II-C-3 of Volume I.

(U) During static test the repaired skirt supported the motor as intended but after firing it was noted that the 181E glass overwrap had failed. It developed five longitudinal cracks which were induced by hoop strain. The strain time trace indicated that the failure started at $T + 1.13$ sec (Figure 10). Movies also showed the failure developing during that period. The case pressure at 1.13 sec was 700 psig.

CONFIDENTIAL

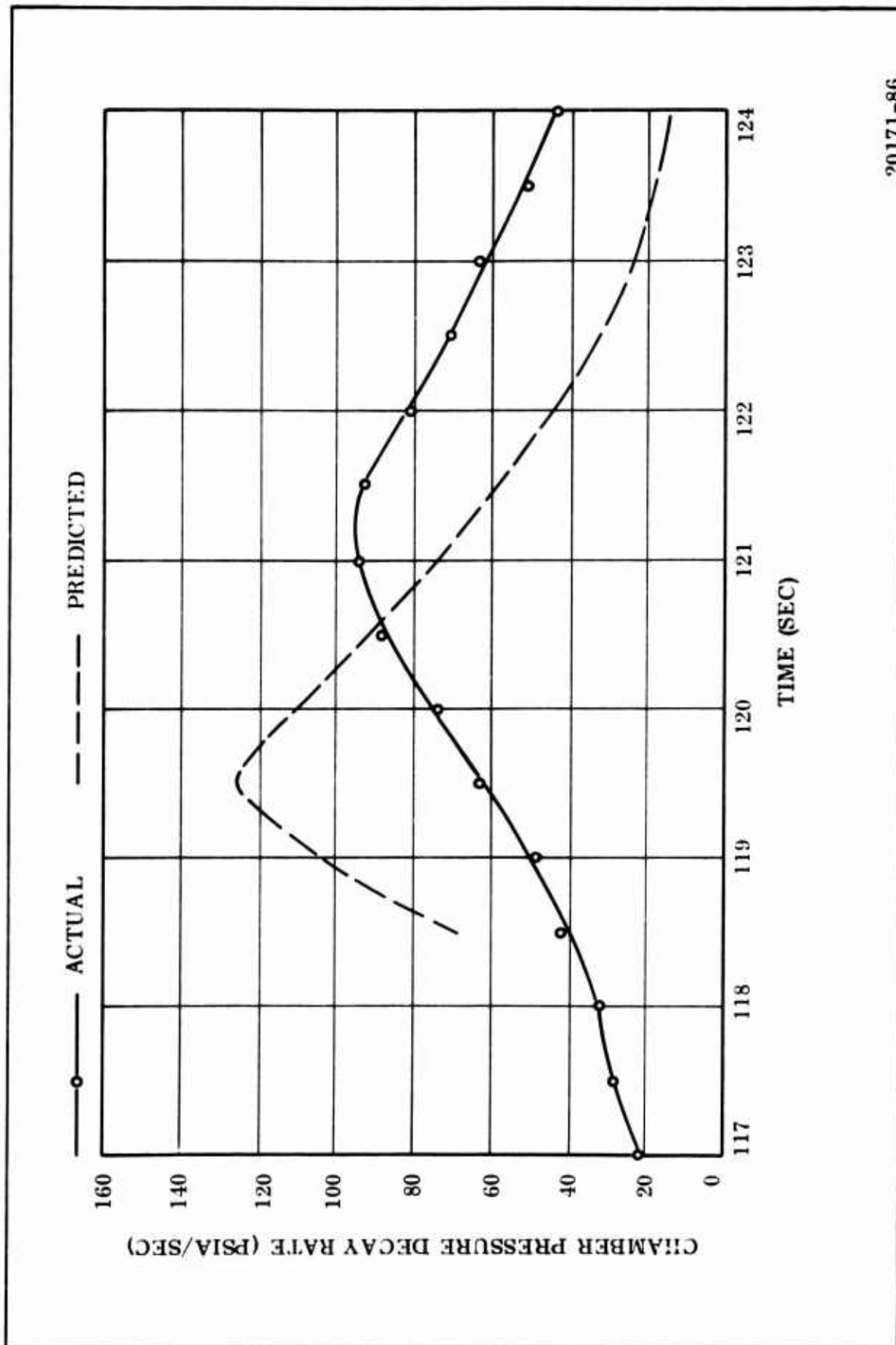
TABLE II
(C) MOTOR SPECIFICATIONS

	<u>Required</u>	<u>Measured</u>
Mass Fraction	0.91*	0.926
Burning Time Average Thrust, Sea Level (lbf)	900,000	979,800
Burning Time (sec)	115-120	117.8
Total Impulse, Sea Level (lbf-sec)	120,000,000**	117,259,400
Tailoff Impulse, Sea Level (lbf-sec)	5,400,000**	2,421,300
Nozzle Throat Diameter, Initial (in.)	32.96	32.954

*Minimum specified value.

**Maximum specified value.

CONFIDENTIAL

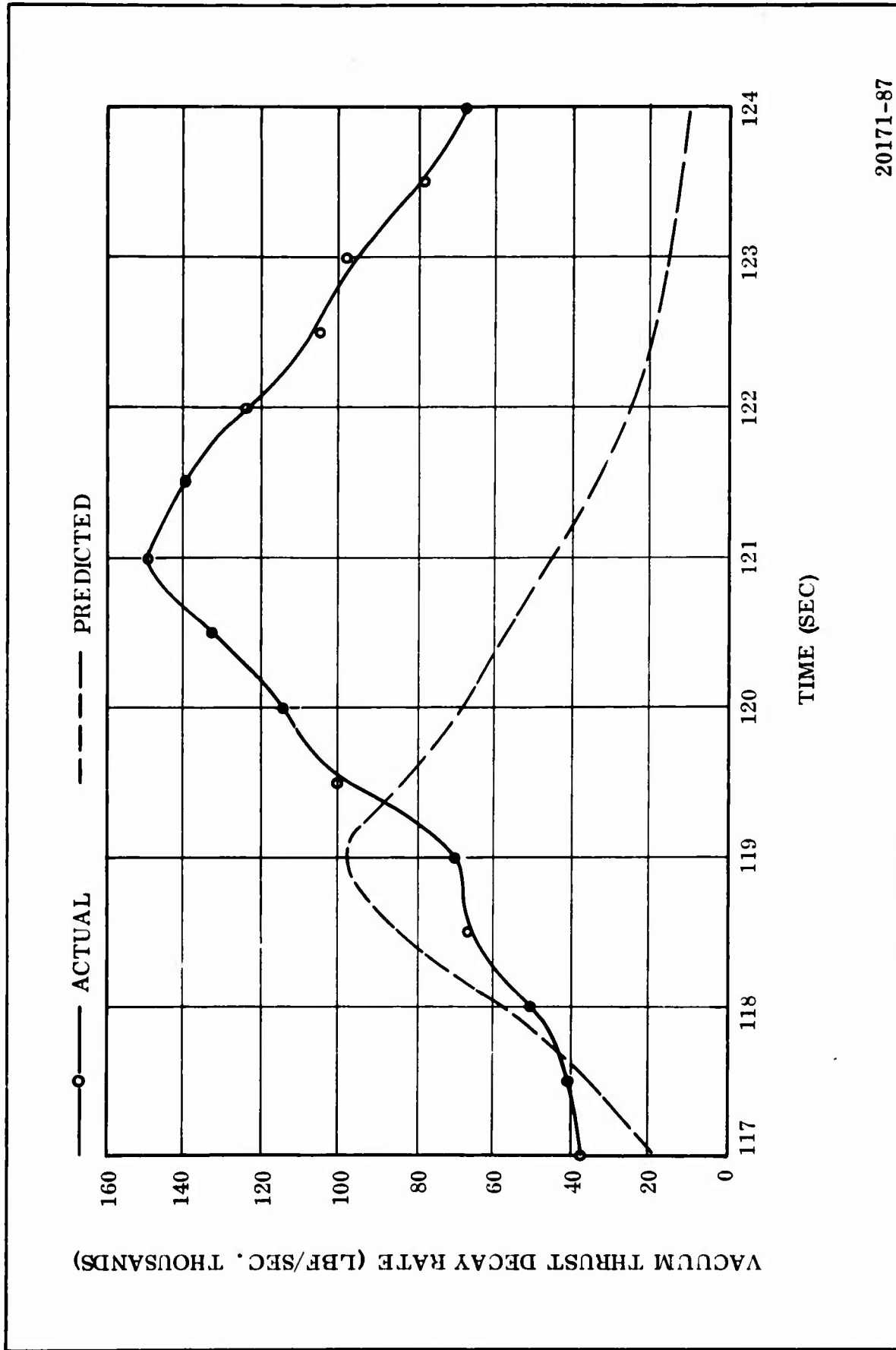


20171-86

(C) Figure 8. Predicted and Actual Pressure Decay Rates

CONFIDENTIAL

CONFIDENTIAL

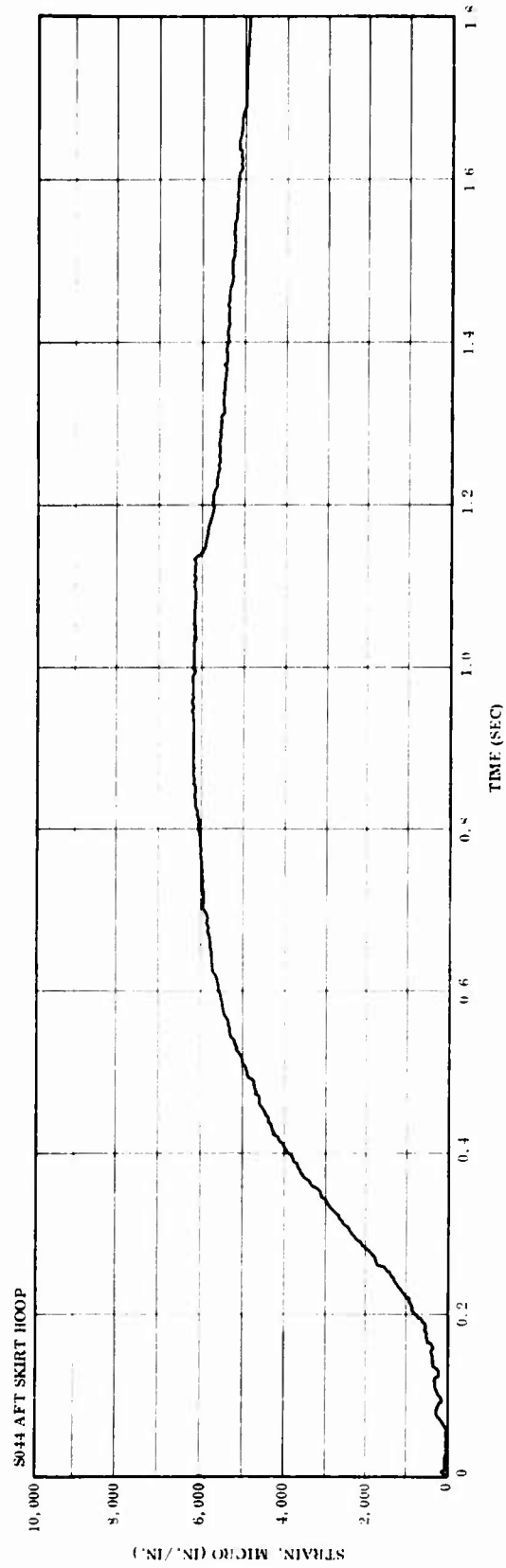


20171-87

(C) Figure 9. Predicted and Actual Thrust Decay Rates

CONFIDENTIAL

CONFIDENTIAL



20171-96

(C) Figure 10. Measured Strain (S044) of Skirt Overwrap

CONFIDENTIAL

CONFIDENTIAL

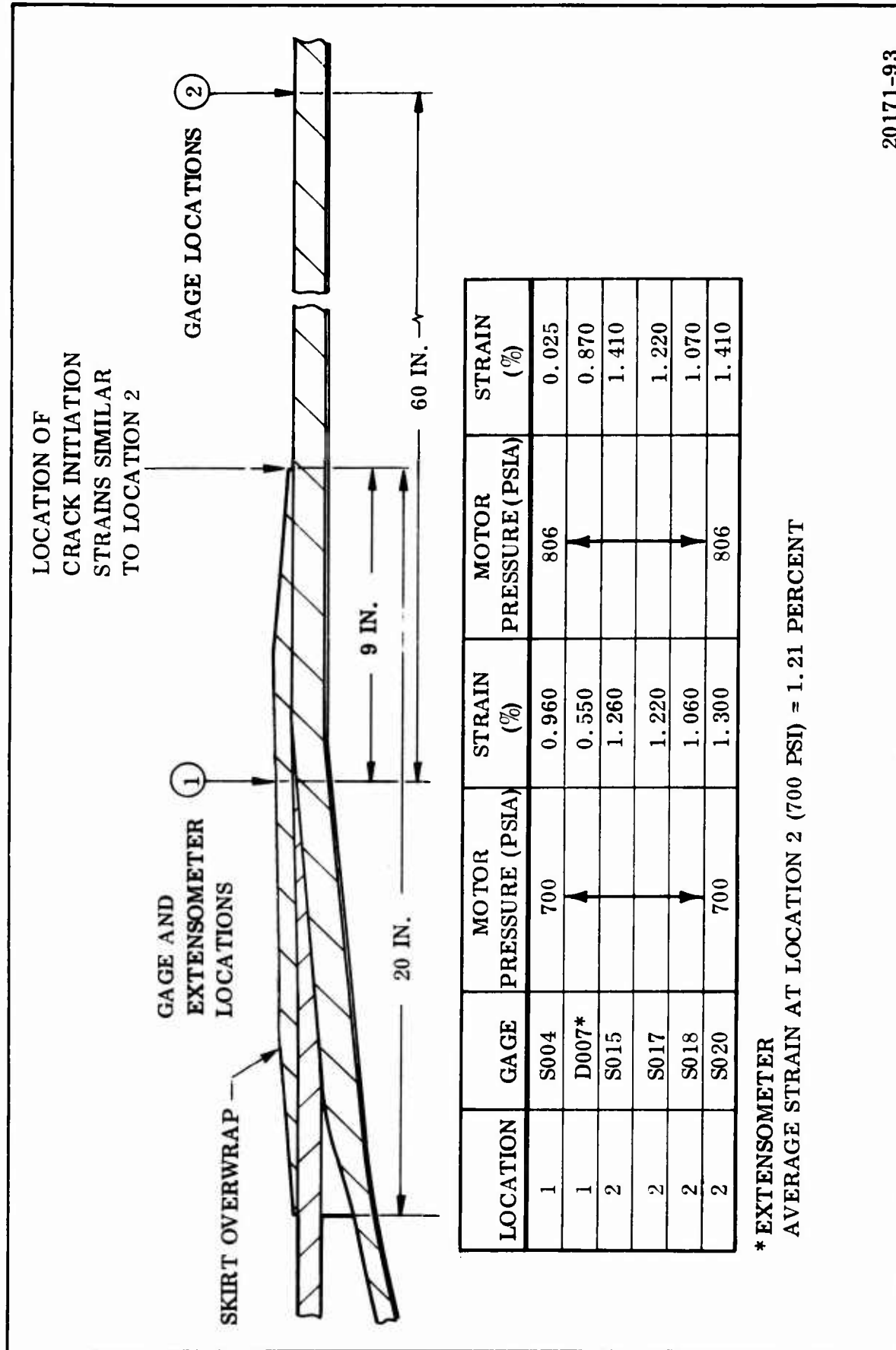
(C) The skirt overwrap extended 8 in. forward on the case, from the forward edge of the skirt (Figure 11). The hoop restraints of the dome and skirt decreased to zero in approximately 7 in. , and the strains at that point were similar to midcylinder strains (Location 2). The average strain at Location 2 (700 psi) was 1.21 percent. The minimum elongation capability of the glass composite overwrap was 1.05 percent. The induced strain at 700 psi was enough to initiate a crack at forward edge of the overwrap. Even though the induced strain was below 1.05 percent at the center of the overwrap, the crack progressed across the overwrap due to stress concentrations.

(C) The strain gage and extensometer at Location 1 indicated the time of failure. The strain gage dropped from 0.960 percent at 700 psig to 0.025 percent at 806 psig while the extensometer strain increased from 0.550 percent at 700 psig to 0.870 percent at 806 psig. The data show that the cracks reduced the overwrap strain and the loss of overwrap stiffness increased the case strain.

(U) Even though the overwrap failed during static firing it did not significantly reduce its shear resistance. The skirt held the motor in position with no indication of sagging or misalignment. Small areas of the overwrap became unbonded during motor tailoff, and the longitudinal cracks prevented the overwrap from returning to its original position during depressurization of the case.

(C) Longitudinal strain gages on the filament wound skirt showed a maximum strain at the top of the motor of -0.2581 percent or -13,834 psi compression due to case expansion which induced bending in the skirts. The safety factor based on compressive buckling stress was 1.29. Temperatures on the skirt were approximately 80°F (Table III).

(C) The forward skirt also had two longitudinal strain gages and a hoop extensometer. The maximum strain, which was at the top of the case, was -0.2617 percent or -14,027 psi compression. Of this stress, 3,700 psi was due to axial compression from motor thrust and the remainder due to bending. The safety factor based on allowable compressive buckling stress was 1.19. The temperatures were from 102 to 121°F (Table III). Instrumentation location is shown in Figure 4.



(C) Figure 11. Aft Skirt and Cylinder Strain Data

CONFIDENTIAL

TABLE III
(C) SKIRT MAXIMUM STRAINS,
DISPLACEMENTS, AND TEMPERATURES

FORWARD SKIRT

Strain Data

<u>Location (deg)</u> <u>0 Deg</u> <u>at Bottom</u>	<u>Strain Gage</u>	<u>Direction</u>	<u>Strain</u> <u>(percent)</u>	<u>Time</u> <u>(sec)</u>
0	S001	Longitudinal	0.262	47.926
180	S002	Longitudinal	-0.183	0.934

Displacement Data

<u>Extensometer</u>	<u>Direction</u>	<u>Displacement</u> <u>(in.)</u>	<u>Time</u> <u>(sec)</u>
D001	Hoop	3.19	46.928

Temperature Data

<u>Temperature Gage</u>	<u>Location (deg)</u> <u>0 Deg at Bottom</u>	<u>Temperature</u> <u>(° F)</u>	<u>Time</u> <u>(sec)</u>
T037	0	102	0.998
T038	0	121	0.988

AFT SKIRT

Strain Data

<u>Location (deg)</u> <u>0 Deg</u> <u>at Bottom</u>	<u>Strain Gage</u>	<u>Direction</u>	<u>Strain</u> <u>(percent)</u>	<u>Time</u> <u>(sec)</u>
0	S021	Longitudinal	-0.258	26.461
180	S022	Longitudinal	-0.229	21.469

Aft Skirt Repair

180	S043	Longitudinal	0.050	0.886
180	S044	Hoop	0.633	0.960

CONFIDENTIAL

TABLE III (Cont)

(C) SKIRT MAXIMUM STRAINS, DISPLACEMENTS, AND TEMPERATURES

AFT SKIRT

Displacement Data

<u>Extensometer</u>	<u>Direction</u>	<u>Displacement (in.)</u>	<u>Time (sec)</u>
D007	Hoop	4.27	54.915

Temperature Data

<u>Temperature Gage</u>	<u>Location (deg) 0 Deg at Bottom</u>	<u>Temperature (° F)</u>	<u>Time (sec)</u>
T025	0	78	132.288
T026	0	78	127.795
T027	0	81	132.288
T028	0	83	130.790

CONFIDENTIAL

- (C) b. Basic Pressure Vessel--The basic pressure vessel performed as intended during the static firing test. The case had a minimum burst pressure of 1,075 psig and the pressure reached a maximum of 806 psig during the static test.
- (C) During static firing, strain gages around the cylinder of the forward segment indicated a maximum hoop strain of 1.31 percent at the top of the cylinder compared to a calculated hoop strain of 1.545 percent at the same pressure (Table IV). See Figure 12 for comparison to hydrotest strain. The safety factor from the strain gage data was 2.08. Temperatures ranged from 97 to 295°F with the maximum at the bottom. The safety factor on strain relates to the glass ultimate design strength of 335 ksi or strain of 2.68 percent. Hoop loading carried by longitudinal windings was considered.
- (C) Strain gages on the forward dome show a maximum strain in the direction of the filament of 1.05 percent and a safety factor of 2.32 (Table IV).
- (C) Center segment strain gage data from the static test indicated a maximum hoop strain at the top of the cylinder of 1.38 percent compared to a calculated value of 1.54 percent at the same pressures (Table IV). See Figure 12 for comparison to hydrotest strain. A hoop extensometer at the center of the segment indicated about 1 in. of radial growth or a strain of 1.29 percent compared to a calculated radial growth of 1.2 in. at the same pressures. The safety factor from strain gage data was 1.98. Temperatures ranged from 123 to 180°F with the maximum at the bottom.
- (C) Aft segment strain gages at the center of the aft cylinder indicated a maximum hoop strain of 1.52 percent at the bottom of the cylinder compared to a calculated value of 1.53 percent at the same pressure (Table IV). See Figure 12 for comparison to hydrotest strain. The safety factor from strain data was 1.92.
- (C) Strain gages on the aft dome showed a maximum in the direction of the filament of 1.07 percent (Table IV). The safety factor was 2.3. The temperatures ranged from 170 to 434°F on the bottom side of the dome. The higher temperatures were caused by radiation from the nozzle exhaust and caused discoloration of the dome. All thermocouple data indicated surface temperatures. The temperature at the center of the glass composite was near ambient.

CONFIDENTIAL

TABLE IV

(C) MAXIMUM STRAINS, DISPLACEMENTS,
AND TEMPERATURES FOR THE CASE

Forward Segment Cylinder

<u>Location (deg)</u> <u>0 Deg</u> <u>at Bottom</u>	<u>Strain Gage</u>	<u>Direction</u>	<u>Strain</u> <u>(percent)</u>	<u>Time</u> <u>(sec)</u>
0	S003	Hoop	1.31	36.445
0	S004	Longitudinal	0.93	27.459
90	S005	Hoop	1.12	38.941
180	S006	Hoop	*	0.787
180	S007	Longitudinal	0.43	0.790
270	S008	Hoop	1.15	0.781

Forward Dome

<u>Distance on</u> <u>Surface to ϕ</u> <u>(in.)</u>	<u>Strain Gage</u>	<u>Direction</u>	<u>Strain</u> <u>(percent)</u>	<u>Time</u> <u>(sec)</u>
85	S023	Hoop	0.91	1.021
85	S024	Along Filament	0.78	0.899
49	S025	Hoop	0.67	0.954
49	S026	Along Filament	0.81	0.934
35	S027	Hoop	0.83	0.899
35	S028	Along Filament	1.05	0.893
85	S029	Along Filament	0.86	36.445
49	S030	Along Filament	0.78	0.947
20	S031	Along Filament	0.91	35.446

Center Segment

<u>Location (deg)</u> <u>0 Deg</u> <u>at Bottom</u>	<u>Strain Gage</u>	<u>Direction</u>	<u>Strain</u> <u>(percent)</u>	<u>Time</u> <u>(sec)</u>
0	S009	Hoop	1.01	0.560
0	S010	Longitudinal	1.06	36.445
90	S011	Hoop	1.38	35.946
180	S012	Hoop	1.38	46.429
180	S013	Longitudinal	1.02	40.438
270	S014	Hoop	*	1.248

*Data not valid.

CONFIDENTIAL

TABLE IV (Cont)

(C) MAXIMUM STRAINS, DISPLACEMENTS, AND TEMPERATURES FOR THE CASE

Aft Segment Cylinder

<u>Location (deg)</u> <u>0 Deg</u> <u>at Bottom</u>	<u>Strain Gage</u>	<u>Direction</u>	<u>Strain</u> <u>(percent)</u>	<u>Time</u> <u>(sec)</u>
0	S015	Hoop	1.42	36.944
0	S016	Longitudinal	0.89	24.464
90	S017	Hoop	1.22	0.938
180	S018	Hoop	1.07	0.896
180	S019	Longitudinal	0.66	35.946
270	S020	Hoop	1.41	26.461

Aft Dome

<u>Distance on</u> <u>Surface to \bar{C}_L</u> <u>(in.)</u>	<u>Strain Gage</u>	<u>Direction</u>	<u>Strain</u> <u>(percent)</u>	<u>Time</u> <u>(sec)</u>
95	S032	Hoop	0.53	43.933
95	S033	Along Filament	0.91	37.942
88	S034	Hoop	0.42	62.403
88	S035	Along Filament	0.75	73.885
69	S036	Hoop	0.42	128.298
69	S037	Along Filament	0.88	129.296
48	S038	Hoop	1.08	127.798
48	S039	Along Filament	1.07	127.798
88	S040	Along Filament	0.76	0.925
69	S041	Along Filament	1.03	46.429
48	S042	Along Filament	1.03	0.922

Displacements

<u>Location</u>	<u>Extensometer</u>	<u>Direction</u>	<u>Displacement</u> <u>(in.)</u>	<u>Time</u> <u>(sec)</u>
Center Segment	D004	Hoop	6.27	56.413
Length of Case	D008	Longitudinal	4.06	42.435
Length of Case	D009	Longitudinal	4.16	42.934
Bottom of Case	D010	Radial	1.01	23.466

CONFIDENTIAL

TABLE IV (Cont)

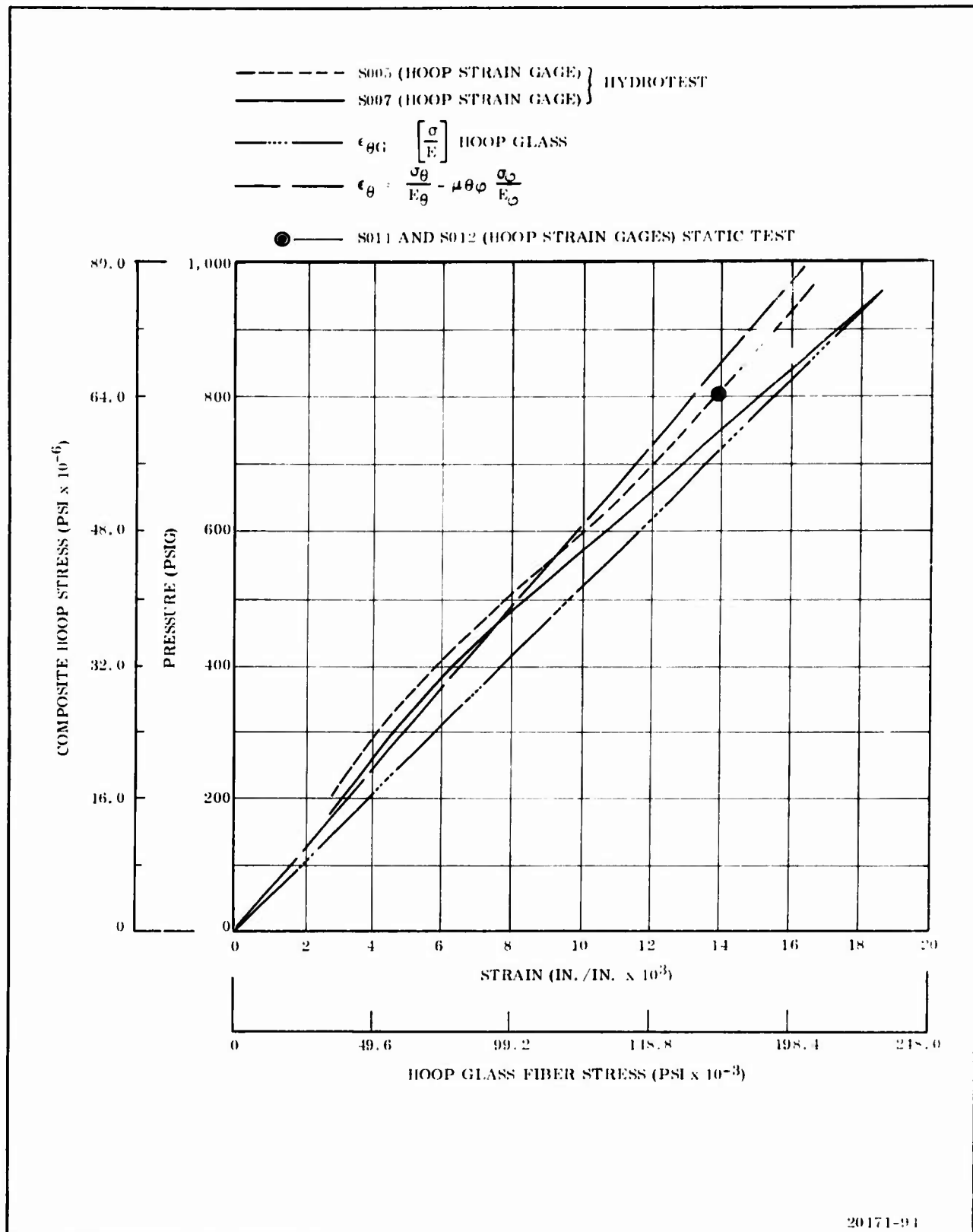
(C) MAXIMUM STRAINS, DISPLACEMENTS,
AND TEMPERATURES FOR THE CASE

Temperatures			
Forward Segment			
<u>Temperature Gage</u>	<u>Location (deg) 0 Deg at Bottom</u>	<u>Temperature (° F)</u>	<u>Time (sec)</u>
T001	0	295	0.998
T002	90	100	0.499
T003	180	126	0.000
T004	270	97	0.499
Center Segment			
T013	0	180	11.981
T014	90	129	0.499
T015	180	123	0.998
T016	270	142	39.437
Aft Dome			
T029	0*	434	129.293
T030	90*	170	127.296
T031	180*	229	132.288
T032	270*	292	132.288
T033	0**	156	127.296
T034	90**	116	127.296
T035	180**	103	103.334
T035	270**	126	131.290

*69 in. to centerline.

**Nozzle flange.

CONFIDENTIAL



(C) Figure 12. Center Segment Hoop Strain

CONFIDENTIAL

CONFIDENTIAL

- (C) Longitudinal extensometers along each side of the motor indicated a strain of 0.82 percent compared to a calculated value of 1.23 percent or a growth of 4.176 in. from tangent-to-tangent compared to a calculated 6.41 in. at the same pressures. Strain gages showed a maximum longitudinal strain of 1.06 percent in the center segment (Table IV). See Figure 4 for instrumentation location.
- (U) The reason for the difference in calculated and measured values of hoop strain is that the calculated value was based on the glass filament strain only while the measured value included the influence of the composite section of polar glass and resin. Strain gage data from the hydrotest of the case are compared with calculated data for filament and composite strains in Figure 12. The graph indicates that the measured values are between the two calculated values, but as the pressure increases the glass crazes and the behavior moves more toward the glass filament and away from the composite calculated value. The static firing results correlate closely with the hydrotest results as shown by the point plotted on the graph. Hydrotest data indicate the longitudinal strain behaves in a similar manner.
- (U) Inspection of the case interior after static test revealed that the insulative bladder was burned through and several layers of glass were burned. The loose glass was removed and the bladder repaired before hydroburst test (see Section V). Inspection of the polar bosses revealed no cracks and it appeared that the bosses did not yield during static firing.
- (U) c. Joints--During handling of the forward segment before the static test three of the outside clevis legs were damaged. An analysis (see Section II-C Vol I) was made which indicated that the case could be static fired without joint failure. Undersized pins were put in the holes of these shim stacks and adjacent clevis legs to distribute the load away from the damaged area.
- (C) Longitudinal strain gages were placed on and around the most severely damaged shim stack during the static test. Strain gage S045 was located in the damaged area at the end of the longitudinal slot and S045 and S047 were placed at succeeding slots. The maximum strain on the damaged shim was 0.515 percent

CONFIDENTIAL

compared to a calculated value of 0.601 percent. The strains on the next two shims were 0.857 and 0.716 percent compared to calculated values of 0.833 and 1.026 percent, respectively (Table V). The comparison of strain gage data with analytical data indicates the shims behaved similarly to the manner assumed in that some of the load from the damaged shims was distributed to adjacent shims.

(U) The clevis joint was designed without hoop restraint so that it would expand with the case cylinder, and extensometer data indicated that the hoop displacement in both forward and aft joint was about the same as the cylinder of the case as shown in Table V.

(C) Temperature data on the forward joint indicated a maximum temperature of 689° F at the top of the case which would have charred the fiberglass; however, a visual inspection of the area revealed no damage and therefore it was concluded the temperature gage was in error. Maximum temperature on the forward joint was 154° F. The maximum temperature on the aft joint was 286° F on the side of the motor (Table V).

(U) 3. SEAL AND INSULATION PERFORMANCE

(U) The general performance of the insulation was excellent. The case and insulation were visually examined following static test and left undisturbed except that a new NBR bladder was bonded over the forward and center segment bladders where thermal damage had occurred. Following hydroburst of the case, sectioning of the components and detailed examination were performed. Longitudinal strips of insulation (approximately 4 in. wide) were removed from the forward dome, segment joints, and aft dome for determining the performance of the insulation materials. A summary of the insulation performance is given in Figure 13.

(U) a. Joint Seal and Insulation--The performance of the joint seal and insulation material around the joint seal proved to be very satisfactory. The seal showed no evidence of leakage during the pretest pressure test or during the static test. The loss of insulation material in the joint area was only minor. No gouging of the

CONFIDENTIAL

TABLE V

(C) MAXIMUM STRAINS, DISPLACEMENTS, AND
TEMPERATURES FOR CLEVIS JOINTS

DAMAGED AREA, FORWARD JOINT

<u>Strain Gage</u>	<u>Direction</u>	<u>Strain (percent)</u>	<u>Time (sec)</u>
S045	Longitudinal	0.515	20.970
S046	Longitudinal	0.857	37.942
S047	Longitudinal	0.716	28.957

Displacement

<u>Extensometer</u>	<u>Direction</u>	<u>Displacement (in.)</u>	<u>Time (sec)</u>
D002	Hoop	12.899*	0.205
D003	Hoop	6.36	45.930

Temperature

<u>Location (deg) 0 Deg at Bottom</u>	<u>Temperature Gage</u>	<u>Temperature (° F)</u>	<u>Time (sec)</u>
0	T005	80	0.499
45	T006	85	129.792
90	T007	154	57.906
135	T008	117	0.998
180	T009	689.3*	103.334
225	T010	103	1.498
270	T011	110	0.998
315	T012	88	0.998

*Data not valid.

CONFIDENTIAL

TABLE V (Cont)

(C) MAXIMUM STRAINS, DISPLACEMENTS, AND
TEMPERATURES FOR CLEVIS JOINTS

AFT CLEVIS JOINT

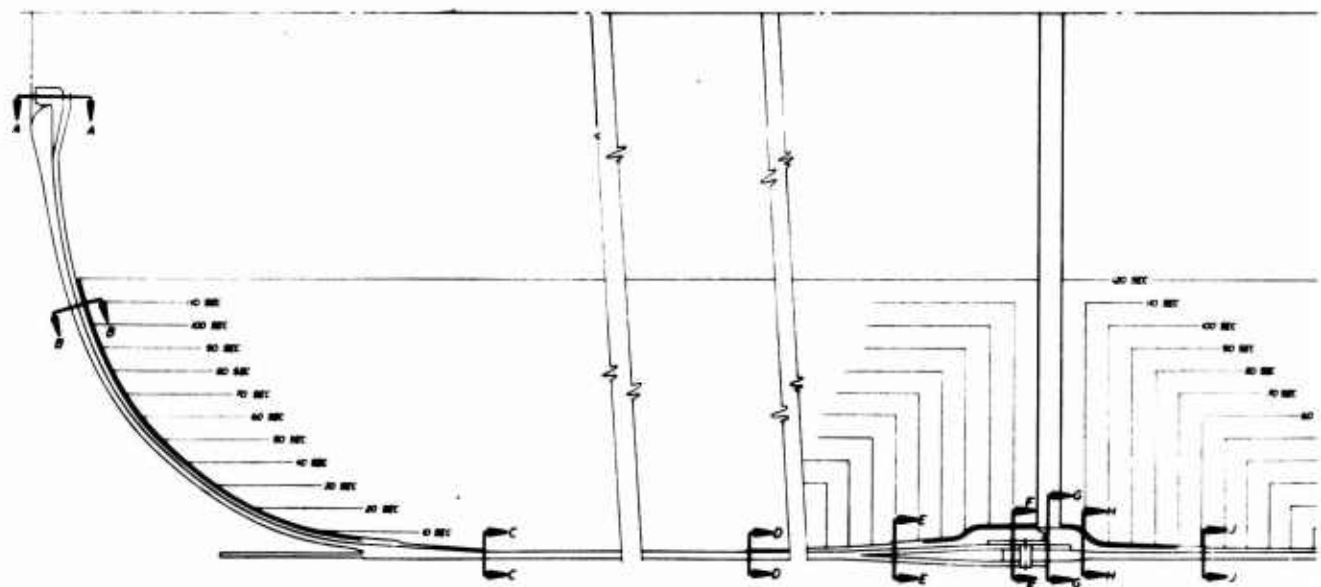
Displacement

<u>Extensometer</u>	<u>Direction</u>	<u>Displacement (in.)</u>	<u>Time (sec)</u>
D005	Hoop	6.54	60.906
D006	Hoop	6.73	51.920

Temperature

<u>Location (deg) 0 Deg at Bottom</u>	<u>Temperature Gage</u>	<u>Temperature (° F)</u>	<u>Time (sec)</u>
0	T017	80	0.998
45	T018	96	0.998
90	T019	110	0.499
135	T020	171	0.998
180	T021	131	0.499
225	T022	286	10.483
270	T023	195	5.491
315	T024	90	0.998

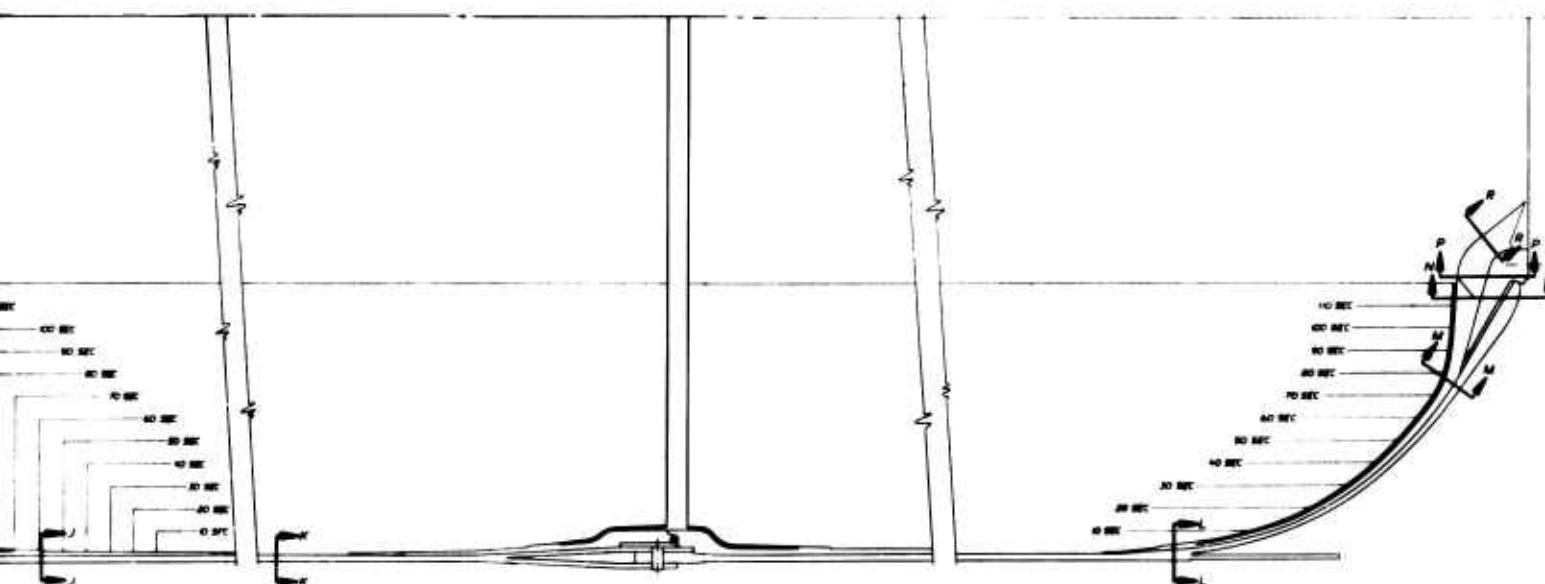
Section	Insulation Material	Location (in.)	Exposure Time (sec)		Predicted Material Loss	
			Web	Effective	Rate (mil/sec)	Depth (in.)
A-A	V-44	13.0 rad	120	--	3.2	0.384
B-B	V-44	41.48 rad	110	120	3.2	0.384
C-C	V-44	Forward dome line	Tailoff	--	3.2	--
D-D	V-44	39.22 fwd of prop face	Tailoff	--	3.2	--
E-E	V-44	19.61 fwd of prop face	60	--	3.2	0.192
F-F	V-44	3.27 fwd of prop face	110	120	3.2	0.384
G-G	V-44	Center of slot	120	--	3.2	0.384
H-H	V-44	3.27 aft of prop face	110	120	3.2	0.384
J-J	V-44	19.61 aft of prop face	60	--	3.2	0.192
K-K	V-45	Cyl area liner & bladder only	Tailoff	--	3.2	--
L-L	V-44	7.5 aft of aft dome datum	4.0	--	3.2	0.013
M-M	V-44	50.93 rad	80	98.4	9.3	0.915
N-N	V-44	40.00 rad	113	120	17.7	2.124
P-P	Silica Phenolic	37.00 rad	120	120	9.3	1.120
R-R	Silica Phenolic	31.5 rad	120	120	17.4	2.090



NOTES:

- ① Thermal protection was provided by a 0.06 in. thick bladder and a 0.085 in. thick liner.
- ② No data. Flap removed to repair bladder for hydrotest.
- ③ Erosion data indicated no loss.

Material Loss Depth (in.)	Added for 1.5 Safety Factor (in.)	Added for Thermal Protect (in.)	Insulation Design Thickness (in.)	Total Insulation Design Thickness (in.)	Combined Safety Factor	Actual Erosion Rate (mil/sec)
0.384	0.192	0.20	0.776	0.80	2.08	1.9
0.384	0.192	0.20	0.776	0.80	2.08	2.7
--	--	0.10	0.100	0.10	--	--
--	--	0.10	0.100	0.10	--	②
0.192	0.096	0.145	0.433	0.50	2.60	②
0.384	0.192	0.20	0.776	1.50	3.91	③
0.384	0.192	0.20	0.776	2.10	5.47	1.70
0.384	0.192	0.20	0.776	1.30	3.39	1.30④ 3.00⑤
0.192	0.096	0.145	0.433	0.50	2.60	0.80
--	--	0.09	0.090	①	--	--
0.013	0.007	0.10	0.120	0.30	23.44	--
0.915	0.458	0.184	1.557	1.60	3.25	7.8
2.124	1.062	0.20	3.386	3.50	2.47	15.9
1.120	0.560	0.365	2.045	4.00	3.66	14.7
2.090	1.045	0.365	3.500	3.55	2.57	13.3



085 in. thick liner. These items not considered in other areas.

- ④ Excluding flap from material loss.
⑤ Including flap as material loss.

20171-45

(C) Figure 13. Insulation Performance Summary

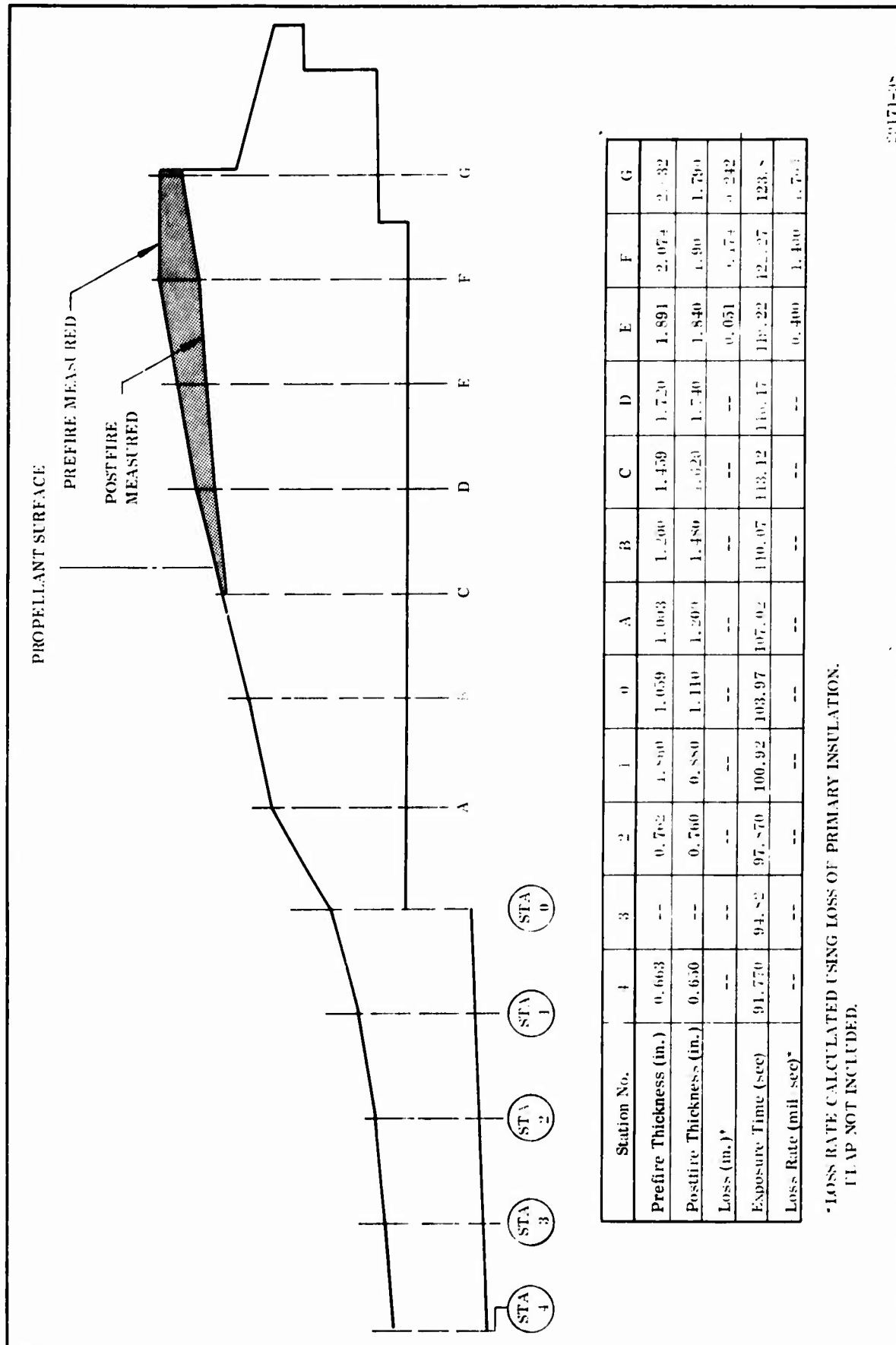
36

CONFIDENTIAL

insulation material occurred at the joint interfaces. There was no evidence of hot gas penetration to the seal areas of either joint, forward to center segment or center to aft segment.

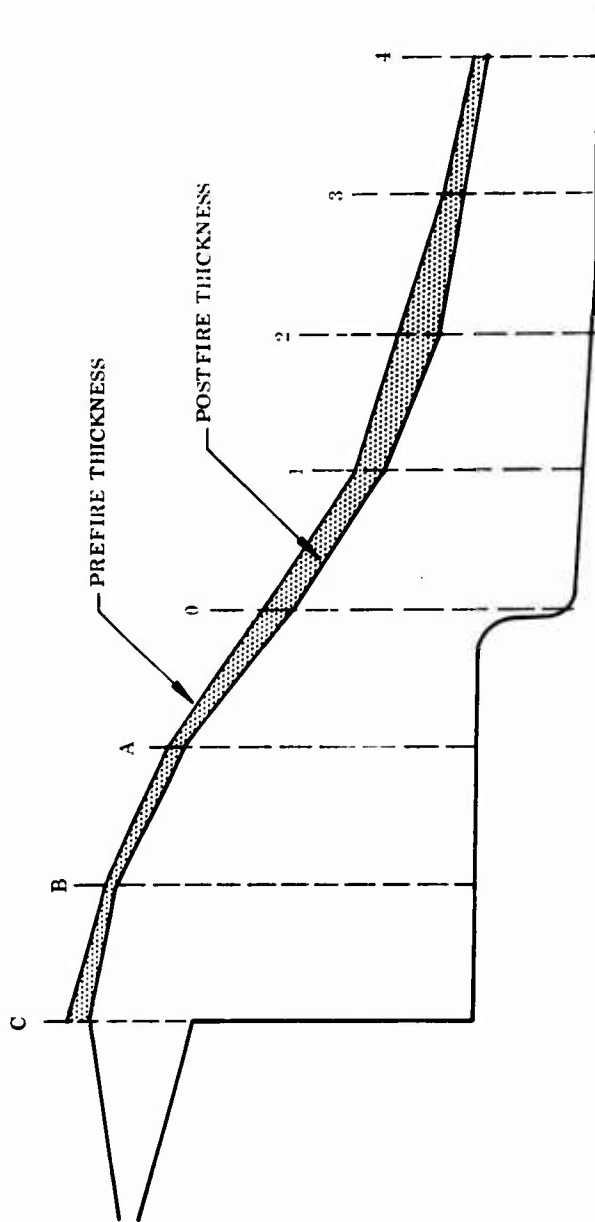
- (C) The joint insulation was measured to determine the insulation loss rate during the test. The maximum loss rate was 4.7 mils/sec in the forward joint. The average material loss rate in both joints was 1.7 mils/sec as compared to a predicted loss rate of 3.2 mils/second. Typical performance data for the joint area is shown in Figures 14 and 15.
- (U) b. Aft Dome Insulation--The aft dome erosion was uniform with no change in the contour at the interface between the asbestos filled NBR (V-44) and the silica cloth phenolic ring as might be expected due to heavy erosion at the point of material change.
- (U) The performance of the insulation materials in the aft dome was evaluated using the design data as a performance base. Insulation design was based upon (1) the empirically established correlation between the material loss rate of silica cloth phenolic (Fiberite MX-2600) and total heat flux (q_T) and (2) the established correlation between the enthalpy heat transfer coefficient (h/cp) and the material loss rate of asbestos filled NBR (V-44). The relation of the aft dome erosion rate of asbestos filled NBR with the velocity of the chamber gases in the aft region was also used in designing the insulation.
- (U) The erosion data from the V-44 and MX-2600 insulation material in the aft dome was obtained by measuring each section of insulation to determine material loss. The exposure time at each station was determined using the propellant burn-back pattern. The material erosion rate was obtained by dividing the material loss by the exposure time.
- (U) The erosion data for the aft dome V-44 insulation were plotted using erosion rate vs Mach number (Figure 16). The good correlation between the erosion data obtained from the V-44 aft dome insulation and the historical data used in the insulation design is shown in Figure 17.

CONFIDENTIAL



(C) Figure 14. Insulation Performance, Aft Joint-Center Segment

CONFIDENTIAL

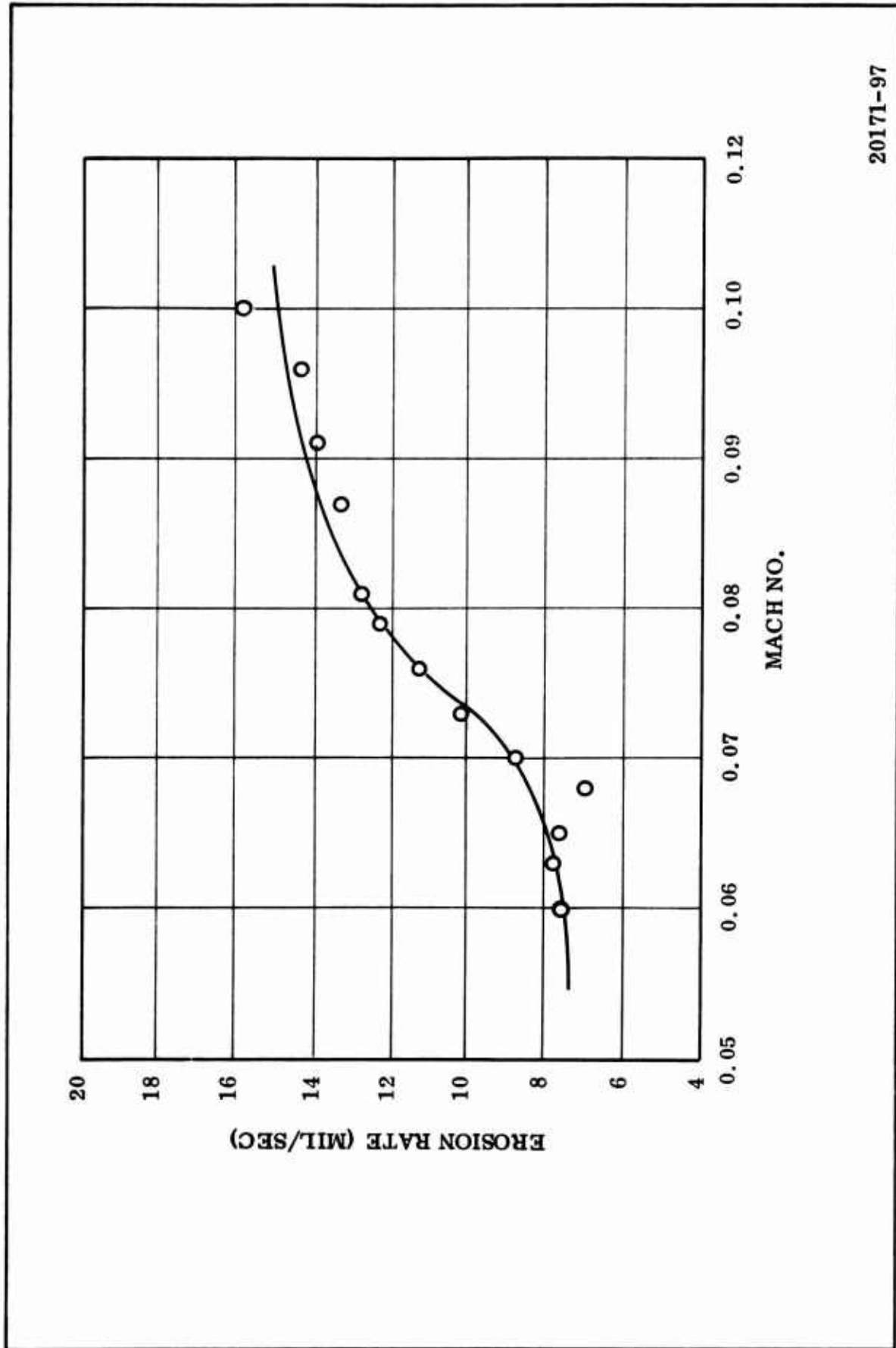


Station No.	C	B	A	0	1	2	3	4
Prefire Thickness (in.)	2.863	2.592	2.178	2.108	1.596	1.336	1.168	0.958
Postfire Thickness (in.)	2.710	2.520	2.060	1.900	1.390	1.080	0.940	0.780
Loss (in.)	0.153	0.072	0.118	0.208	0.206	0.256	0.228	0.178
Exposure Time (sec)	123.8	123.8	123.8	120.75	117.70	114.65	111.60	108.55
Loss Rate (mil/sec)	1.200	0.500	0.900	1.700	1.700	2.200	2.000	1.600

2-171-99

(C) Figure 15. Insulation Performance, Forward Joint-Aft Segment

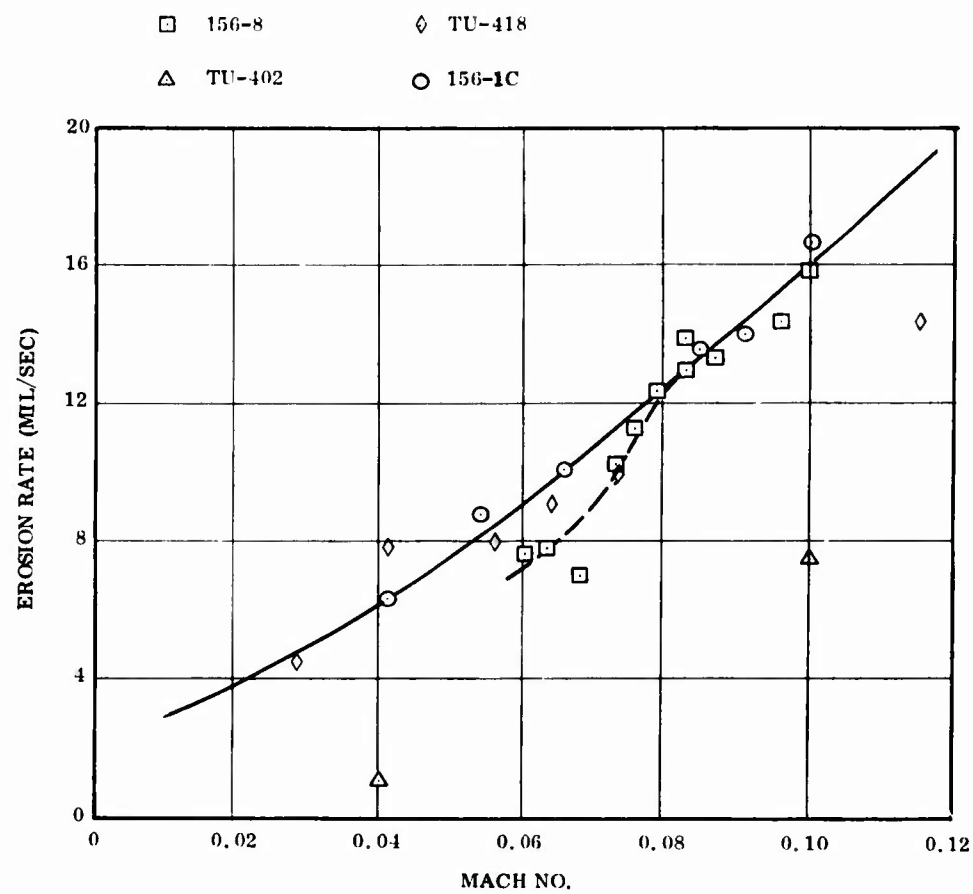
CONFIDENTIAL



(C) Figure 16. Measured Erosion Rate vs Mach No. , V-44 Insulation, Aft Dome

CONFIDENTIAL

CONFIDENTIAL



20171-102

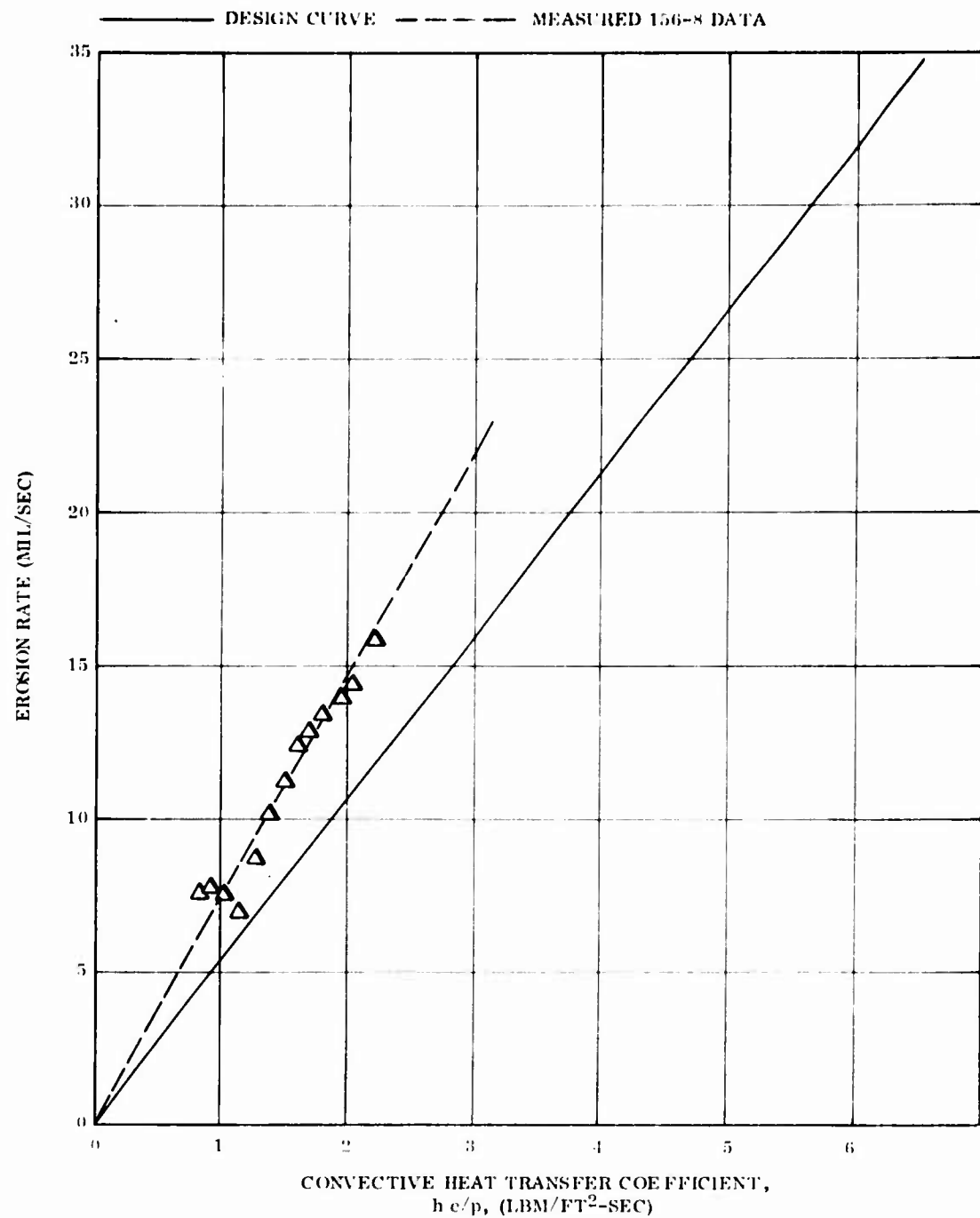
(C) Figure 17. Predicted V-44 Erosion Rate Based on Predicted Gas Flow Rate

CONFIDENTIAL

CONFIDENTIAL

- (U) The erosion data obtained from the V-44 insulation material is correlated with the calculated convective heat transfer coefficient in Figure 18. The data show good correlation between heat transfer coefficient and erosion of asbestos filled NBR obtained from this test. The erosion rate in comparison to the convective heat transfer coefficient was actually higher than the relationship used for the design of the insulation.
- (U) The silica cloth phenolic ring was designed from data obtained from the static test of the TU-465 motor. Using the erosion rate obtained from this test and total heat flux from the design analysis, a new curve was obtained (Figure 19). The new curve shows a higher erosion rate in relation to the total heat flux than used for the design of this motor.
- (U) The gas velocity was also calculated for the area insulated by the silica cloth phenolic ring. The actual erosion vs predicted erosion and the actual erosion rate vs Mach number are shown in Figure 20. Due to the geometry of the part, there was a higher than predicted material loss rate between the 37.0 in. radius and the 32.0 in. radius. The relationship between the erosion of asbestos filled NBR and silica phenolic is shown in Figure 21.
- (U) Examination of the aft dome asbestos filled NBR insulation was made after hydroburst of the case to locate the 1/8 in. dia holes drilled to aid the installation of the insulation. Several holes were located during the examination, but there was no evidence of localized erosion around the holes or excessive erosion of the bonding material used to fill the holes.
- (C) c. Forward Dome Insulation--The forward dome insulation was measured to determine the material loss rate. The maximum rate experienced in this area was 3.5 mils/sec, and the average rate was 2.7 mils/second. The predicted material loss rate for this area was 3.2 mils/second.
- (U) d. Bladder and Bonding Materials--The UF-1149 bonding material between insulation pieces had performed well. No gouging or erosion below the contour of the NBR insulation had occurred in any area.

CONFIDENTIAL

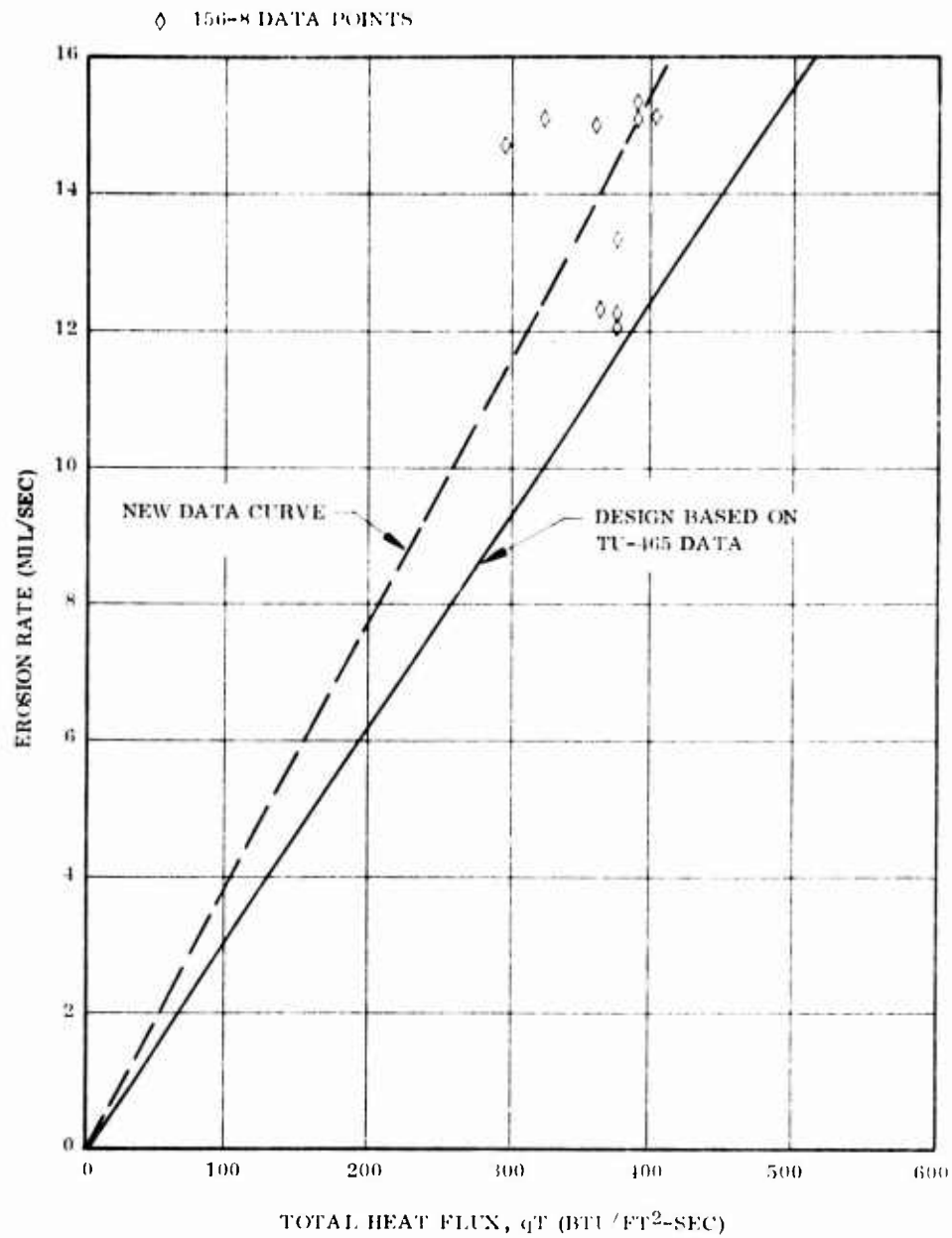


20171-101

(C) Figure 18. V-44 Insulation Erosion Rate and Convective Heat Transfer Coefficient

CONFIDENTIAL

CONFIDENTIAL

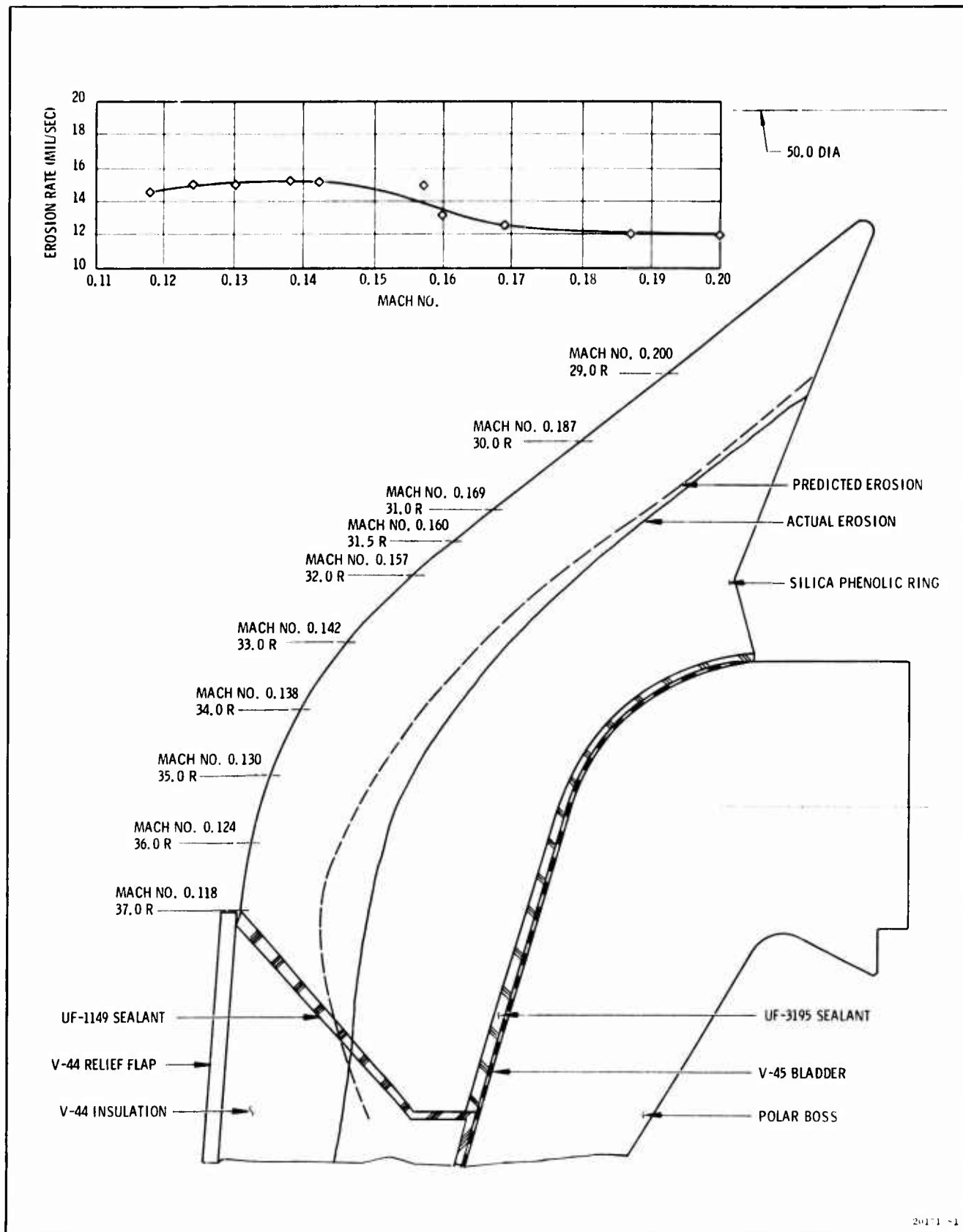


20171-10

(C) Figure 19. Erosion Analysis of Silica Cloth Phenolic Ring

CONFIDENTIAL

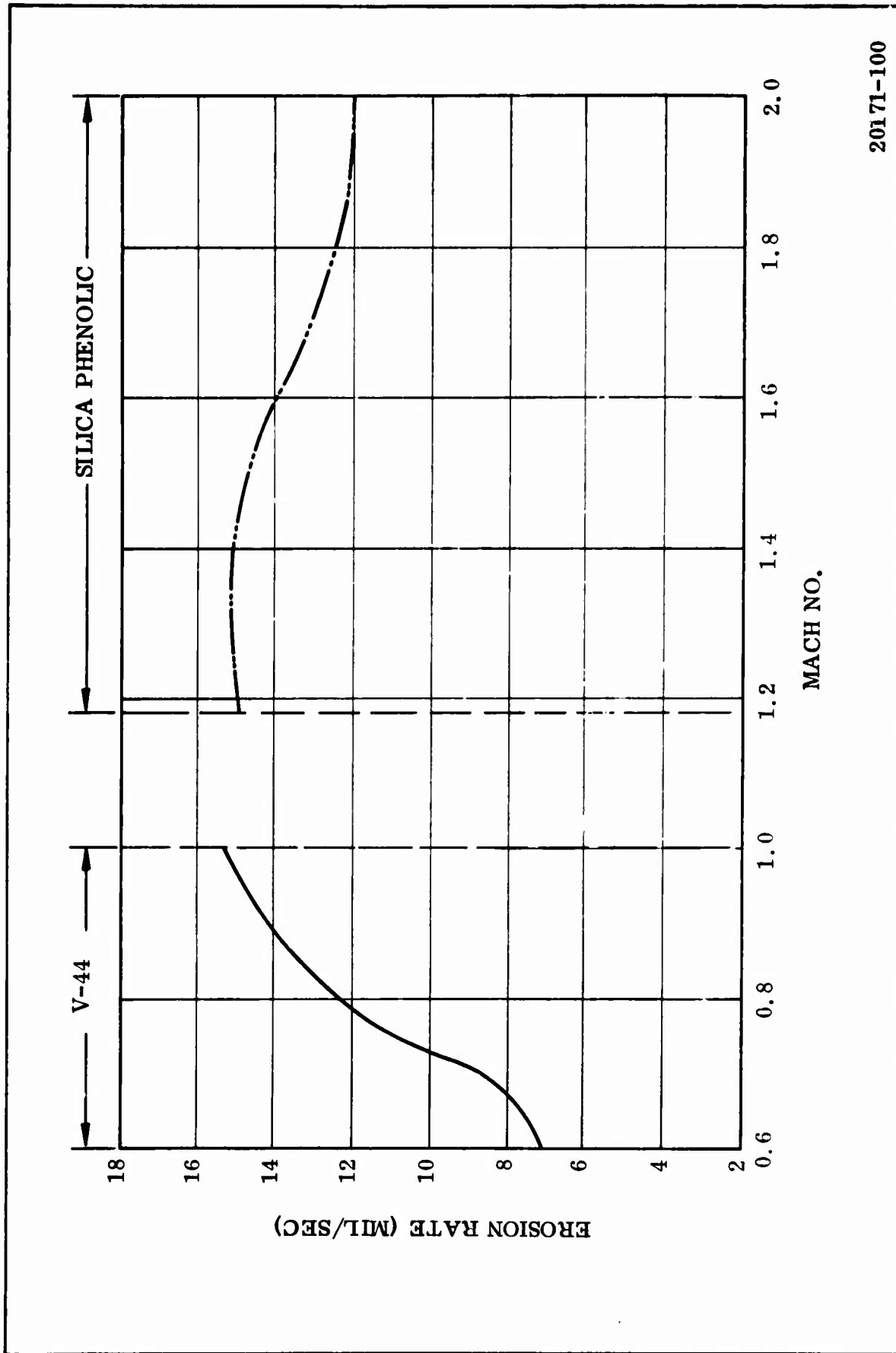
CONFIDENTIAL



(C) Figure 20. Aft Dome Erosion Data

CONFIDENTIAL

CONFIDENTIAL



20171-100

(C) Figure 21. Asbestos Filled NBR and Silica Cloth
Phenolic Erosion Rate vs Mach No.

CONFIDENTIAL

(U) The silica filled NBR bladder had been thermally damaged. The damage in the forward segment was most extensive. In the area from 80 to 120 deg the bladder was burned through as well as two layers of hoop glass and one layer of polar glass (Figure 22). The full extent of the heat effect is covered in Section V, Vol II. The cause of this hot spot was attributed to premature exposure of the case wall due to unrepaired voids in the propellant next to the case wall. Section VIII, Vol I, discusses the events which led to this condition.

(U), The bladder was blistered and unbonded from the case intermittently around the entire circumference of the forward segment (Figure 23). This condition was attributed to post-test heat soak. The CO₂ quench system ports entered the segment around the igniter at a 45 deg angle, which resulted in an impingement point aft of the forward segment bladder. Thus the forward segment bladder was not quenched as effectively as were the center and aft segments.

(U) The center segment bladder was blistered, and holes had burned through mainly in the top (Figure 24). This condition was also attributed to post-test heat soak. The aft segment bladder had only minor holes burned in it.

(U) 4. IGNITION SYSTEM PERFORMANCE

(U) The 156-8 motor was ignited by use of a single nozzle Pyrogen igniter which produced an average mass flow rate of 170 lb/sec for about 0.8 second. Igniter performance and motor ignition data are presented in Table VI and Figure 25.

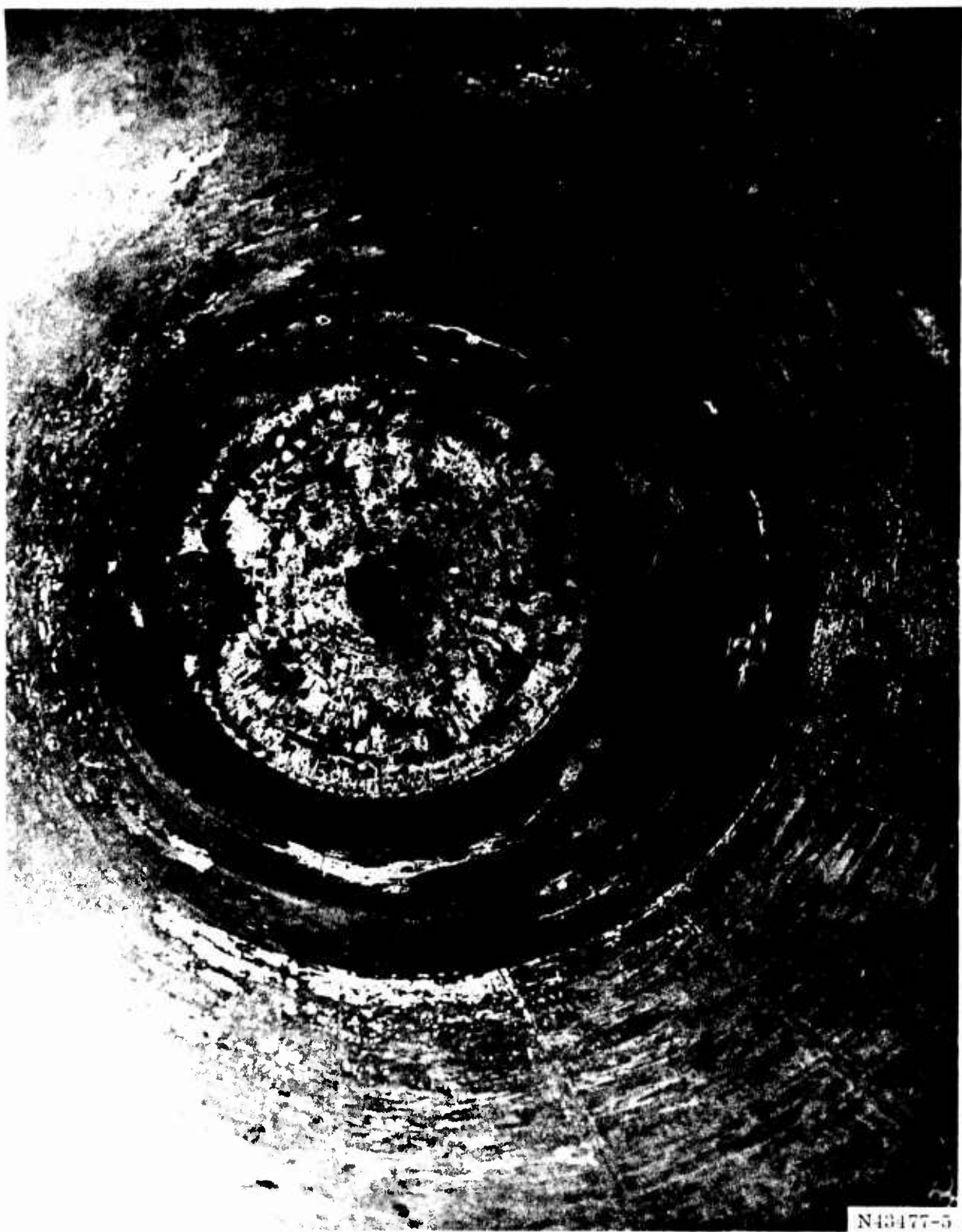
(U) Prior to the motor test, the motor ignition transient had been predicted. In making the prediction, the igniter mass flow was considered entirely adequate for this motor but because the grain port diameter was large and the impingement point of the igniter plume against the grain port was about 19 ft downstream from the igniter nozzle, a long (0.250 sec) lag time or time from beginning of igniter output to the first ignition of motor propellant was predicted. The actual lag time was about 0.125 second. The explanation lies in the fact that this motor had a relatively high L/D ratio making it easier to ignite than a motor with a low L/D. In high L/D



(U) Figure 22. Damaged Center Segment Bladder



(U) Figure 23. Damaged Bladder and Case, Forward Segment



(U) Figure 24. Damaged Bladder in Forward and Center Segments

CONFIDENTIAL

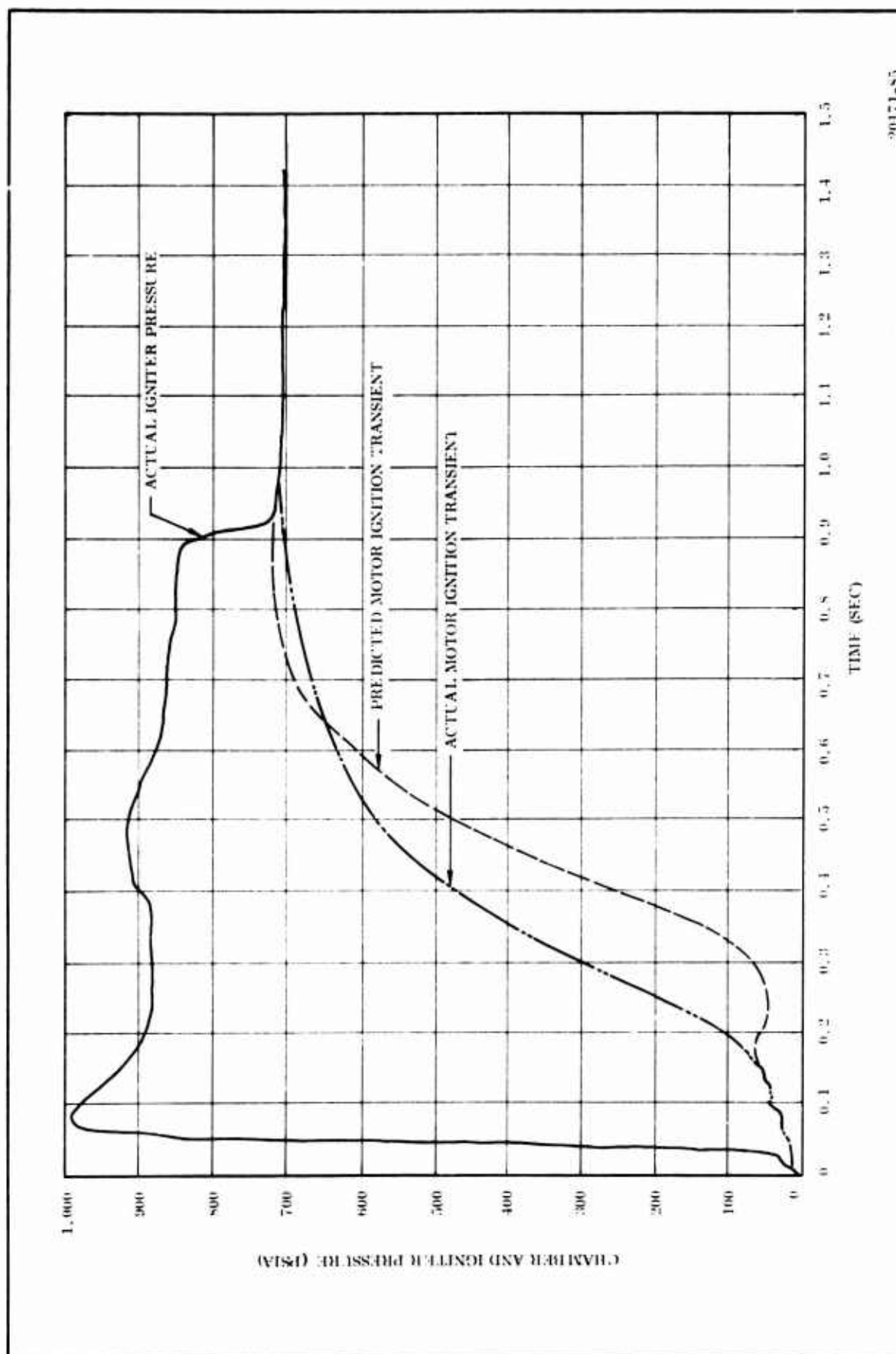
TABLE VI

(C) IGNITER PERFORMANCE

<u>Characteristic</u>	<u>Bench Test</u>	<u>156-8 Prediction</u>	<u>156-8 Motor Test</u>	<u>156-9 Motor Test</u>
First Level Mass Flow Rate (lb/sec)	170	Same As Bench Test	186	190
Burning Time, 10% to 10% of P_{max} (sec)	0.95		0.920	0.875
P_{max} (psia)	1,005		992	985.35
Average Pressure, First Level (psia)	840		920*	940*
Average Pressure, Second Level (psia)	529		860*	725*
Ignition Delay, Igniter Booster, t_0 to 10% P_{max} (sec)	0.040		0.040	0.024
Ignition Interval, Igniter Booster, t_0 to 90% P_{max} (sec)	0.069		0.060	0.040
Motor Ignition Delay, t_0 to 75% P_{max} (sec)	N/A	0.545	0.453	0.240
Motor Maximum Pressure at Ignition (psia)	N/A	725	710	497
Igniter Coefficient (lb/sec/sq in.)	N/A	0.199	0.218	0.196
Total Igniter Impulse (lb/sec)	24,208	N/A	N/A	N/A
Specific Impulse, Delivered (lb-sec/lb)	184.5	N/A	N/A	N/A

*Igniter unchoked before end of first level.
N/A indicates not applicable.

CONFIDENTIAL



(C) Figure 25. Predicted and Actual Igniter Performance

CONFIDENTIAL

motors a greater percentage of the motor grain initial surface area is available for preheating and direct ignition by the igniter exhaust. Less of the surface is hidden in slots and fins. The nozzle is far enough away from the igniter so that little of the igniter heat is lost through the nozzle and a greater percentage is available for ignition and preheat.

- (U) The actual rates of pressure rise in the motor during the flame spreading and chamber filling periods compare very well with the prediction. Flame spreading rates were predicted to be 5,000 in./sec down the grain ports and 250 in./sec down the slots.
- (U) The igniter ballistic performance was normal and agreed with bench test performance during the first 0.390 sec of operation. At that time the motor chamber pressure reached 500 psia and was sufficient to unchoke the igniter throat. The igniter combustion then became affected by motor backpressure, and high pressure burning ensued until all the igniter propellant was consumed. This condition is normal for igniters whose burning time exceeds the motor ignition interval.
- (U) Post-test inspection of the 156-8 ignition system did not reveal any problems. Both internal and external insulation remained. There were no signs of hot spots, leaks, excessive erosion of insulation or melting of case metal parts. The ignition system insulation was of a heavyweight design. No external insulation erosion rate data were obtained inasmuch as no provisions for obtaining these data were included in the test objectives.

CONFIDENTIAL

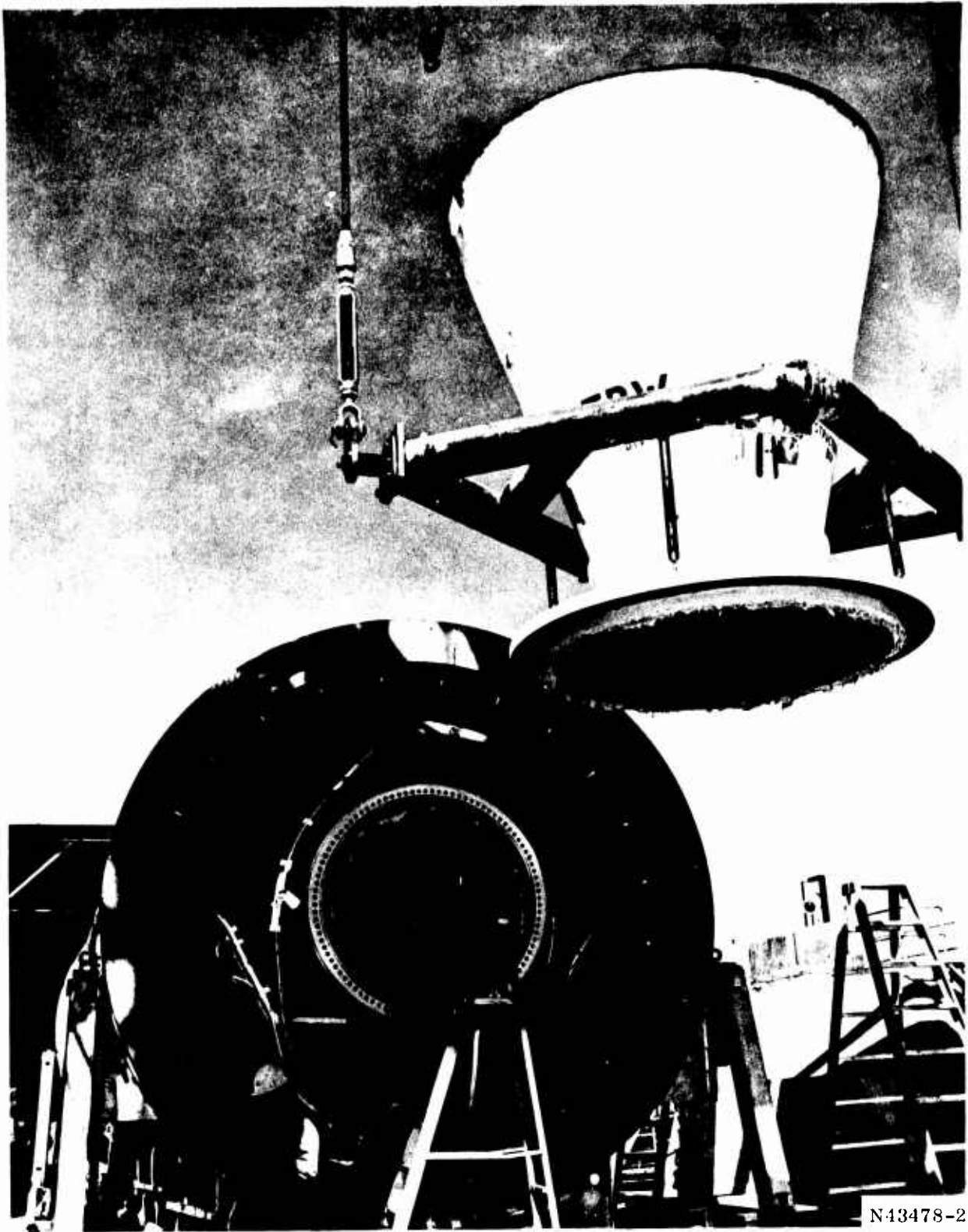
(U) 5. NOZZLE PERFORMANCE

(U) a. General Condition--The nozzle was in excellent post-test condition. Erosion was generally smooth and uniform throughout as can be seen in Figures 26 and 27. Some delamination occurred in the inlet, throat sections and in the tape wrapped carbon cloth cone section downstream of the throat. In the latter section, circumferential delaminations occurred along the tape ply interfaces approximately every 2 to 3 in. axially along the part. The delaminations showed no indications that flow penetration or delamination occurred during the heat soak period after firing.

(U) Two grooves or pocketed areas were eroded in the throat section: one approximately at the 100 deg position (Figure 28) and the other diametrically opposite at 280 deg (Figure 29). At approximately 260 deg, a third erosion pocket occurred in the inlet section just forward of the throat interface and extended a short distance into the throat section (Figure 30).

(C) b. Inlet Section--The inlet section experienced uniform erosion with some very thin delaminations running circumferentially. The delaminations extended in depth through the char layer terminating at the virgin material. An erosion pocket started approximately 3 in. forward of the inlet-throat section interface and extended downstream approximately 5.5 inches. This groove was 2 in. wide at its widest point and 0.4 in. deep at the deepest (Figure 30). A uniform char layer penetrated from 0.65 to 0.75 in. beyond the eroded surface.

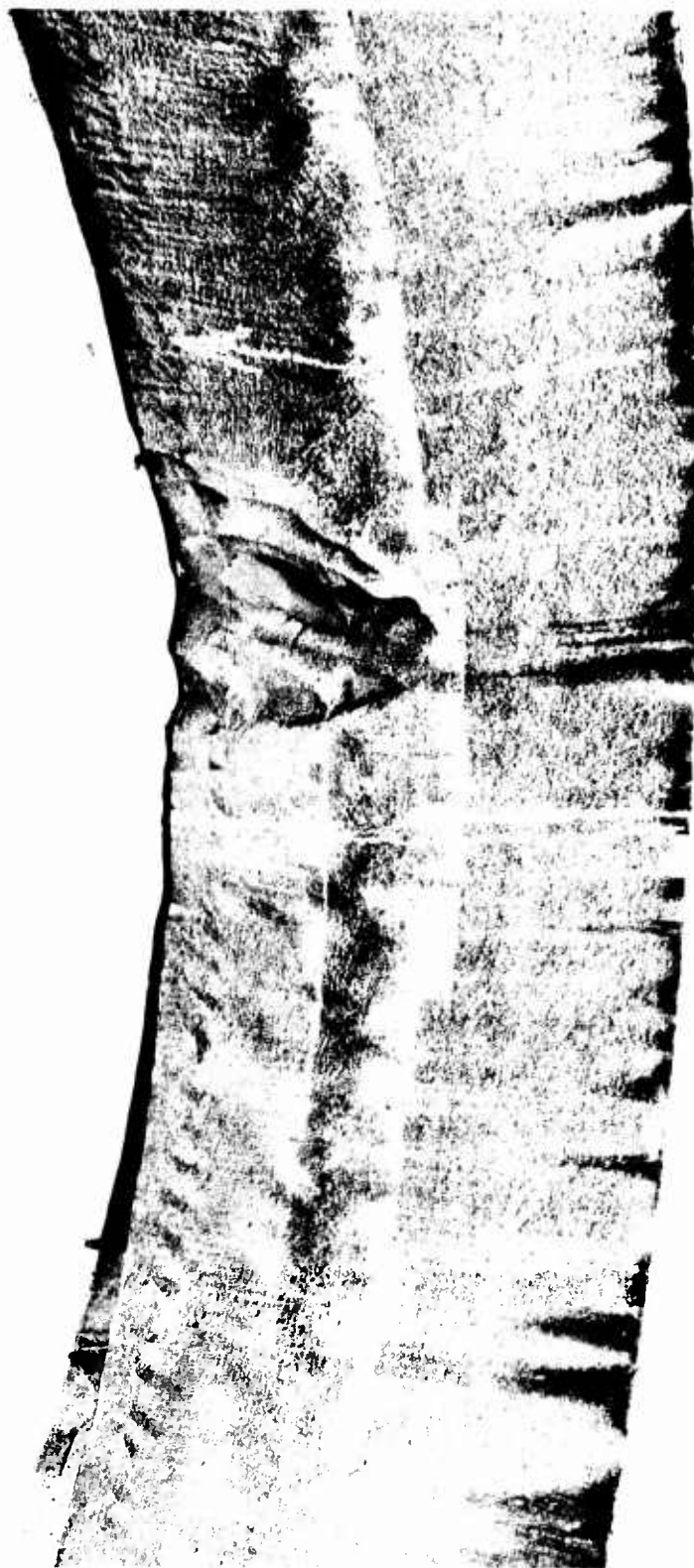
(C) c. Throat Section--In the throat section, the erosion pocket at approximately 100 deg actually consisted of three pockets washed together--starting just forward of the throat section, extending through it, and fading out just aft of the throat-exit cone interface. The center groove was 1.5 in. wide and 3.5 in. long with a maximum depth of 0.8 to 0.9 inch. The two outer grooves were approximately 1 in. wide, 3.5 in. long and 0.4 to 0.5 in. deep (Figure 28). At 280 deg, the pocket was 3 in. wide, 7.5 in. long, and 0.6 to 0.8 in. deep. At this point the inlet-throat interface joint appeared to have opened up, permitting gas to penetrate through the joint (Figure 31)



(U) Figure 26. Post-Test View of 156-8 Nozzle



(U) Figure 27. Closeup of Nozzle, Internal View



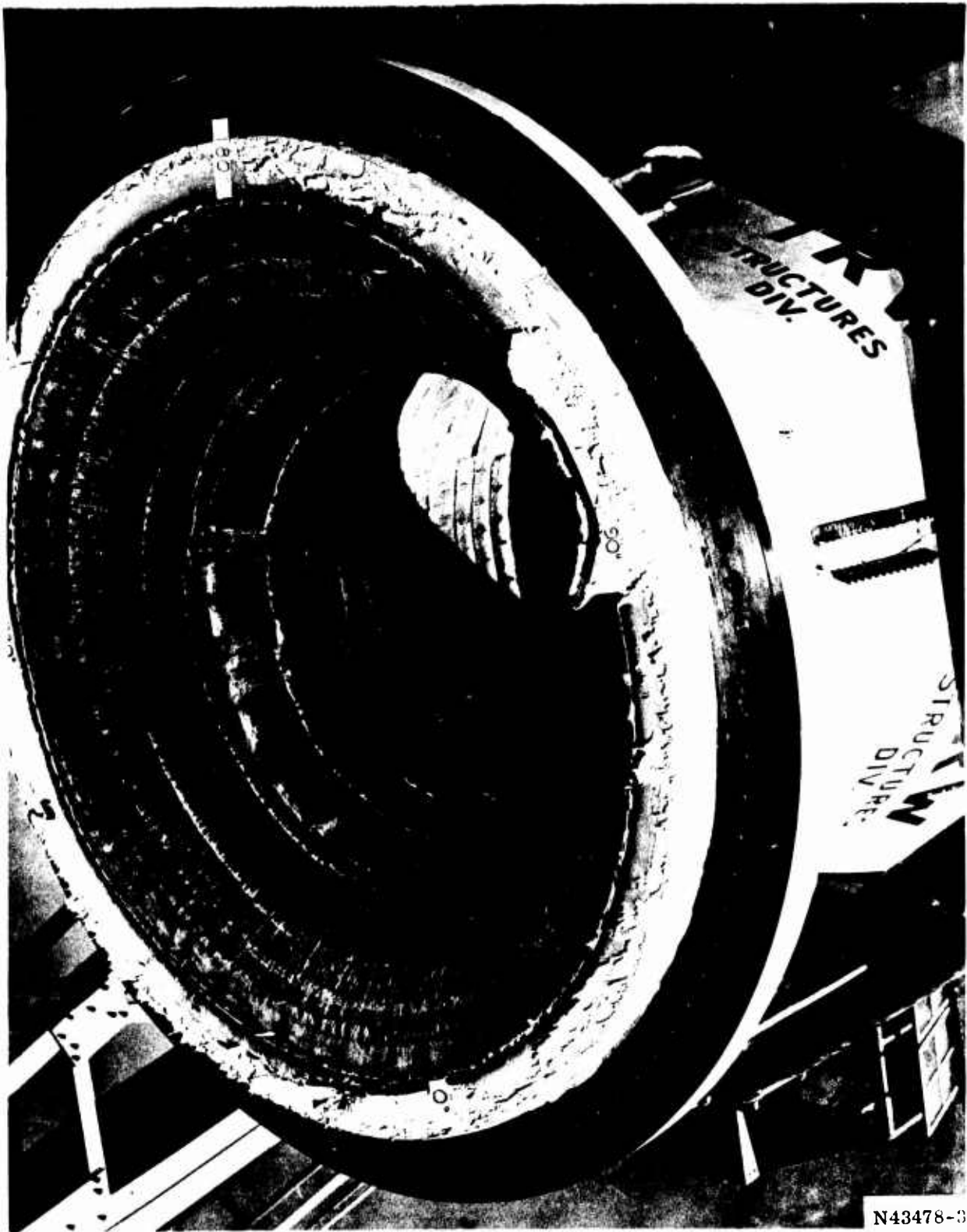
N43478-5

(U) Figure 28. Erosion Pockets in Throat Section, 100 Deg Location



N43478-6

(U) Figure 29. Erosion Pockets in Throat Section, 280 Deg Location



N43478-3

(U) Figure 30. Inlet Section



(U) Figure 31. Throat Section Showing Gas Penetration

CONFIDENTIAL

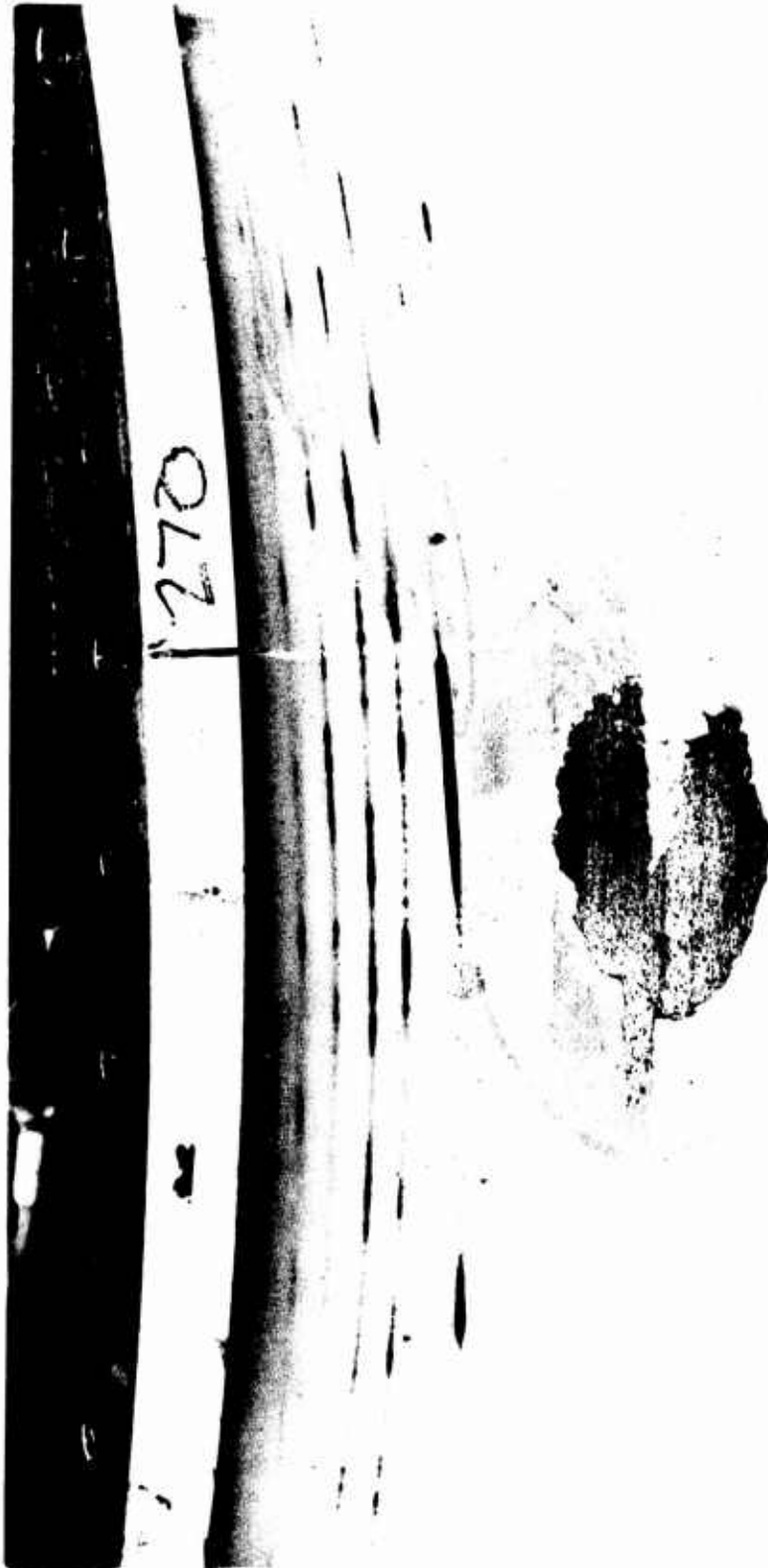
to the steel support structure. Char was uniform except for the immediate area at 280 degrees. Charring extended through the carbon cloth liner and silica backup to approximately 1 in. downstream of the inlet-throat section interface. A section cut through this region revealed a char layer 0.15 to 0.30 in. deep on the OD of the silica running axially along the silica backup-steel interface.

- (U) d. Exit Cone--The carbon cloth exit liner showed numerous circumferential delaminations along the tape ply interfaces axially at 2 to 3 in. intervals (Figure 30). These delaminations extended to the depth of the char layer and were typical for carbon cloth parts. The silica cloth exit cone liner showed the typical dishing erosion just aft of the carbon cloth interface, with normal smooth erosion occurring over the remainder of the cone flow surface.

- (U) There were no abnormal cracks, delaminations, or loss of materials indicative of structural or performance degradation below that of an equivalent hydroclaved part.

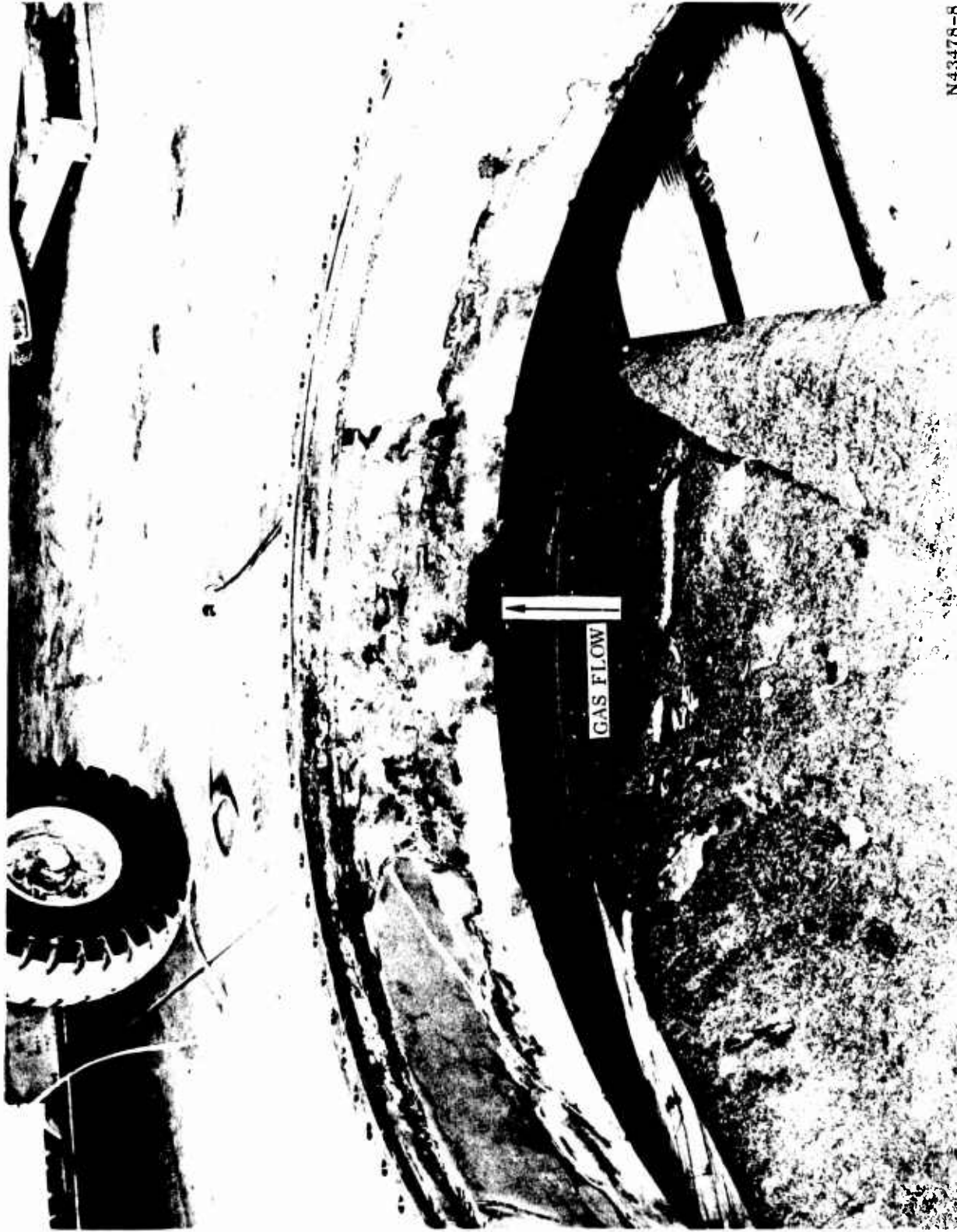
- (C) e. Steel Structure--The inlet and exit cone steel structures performed adequately and showed no adverse effects of the test except for one hot spot located at approximately 280 deg on the inlet structure (Figure 32). After separation of the plastic parts from the steel structure, a melted area was observed on the throat backup ring. Heating effects can be seen to extend from 220 to 330 deg as shown in Figure 33. The forward edge had melted back approximately 0.4 in. for a length of approximately 3 in. at the 250 deg position. At 280 deg a melted spot 0.5 in. wide by 2 in. deep was joined by a spot 1.0 in. deep and circumferentially 4 in. long. These details can be seen in Figure 34. There were small melted spots at approximately 300 and 325 degrees. Gas penetration into the interface and melting of the backup ring resulted in heat reaching the outer steel structure, causing the scorched spot visible in Figure 32. A spot of approximately 2 in. in diameter was scorched and burned at this location.

- (U) The exit cone steel housing was in excellent condition and performed as expected with no evidence of heating or degradation of any form to this component.



N43478-7

(U) Figure 32. Hot Spot on Steel Inlet Structure



(U) Figure 33. Throat Backup Ring



(U) Figure 34. Melted Throat Ring Material

CONFIDENTIAL

(C) f. Erosion and Char Data--Erosion and char values were similar to those experienced previously with the same types of carbon and silica tape wrapped materials fabricated by standard hydroclave methods. Predicted erosion rates and actual values are compared in Table VII. Actual erosion rates were somewhat higher than predicted for the carbon cloth inlet section (actual of 5.52 vs 3.61 mils/sec predicted). Actual throat erosion rate of 6.96 mils/sec is slightly lower than the predicted of 7.57 mils/sec. Erosion rates for the carbon cloth in the forward section of the exit cone were also lower than the predicted (4.75 vs 6.12 mils/sec). The rate in the carbon cloth liner at the carbon-silica interface was higher than predicted due to the influence of the deep silica erosion immediately downstream. Erosion and char profiles are shown in Figure 35. As can be seen, the silica washed out just after leaving the carbon cloth liner which is a typical condition seen in numerous other nozzles. The erosion and char then decreases as the gas approaches the exit plane. Char depths are below predicted values in all materials, as shown in Table VII. For example, in the carbon cloth inlet, predicted char depth is 0.888 in. and actual measured char depth was 0.77 inch. Predicted char depth in the exit cone silica liner was 0.425 in., but the actual was only 0.26 in. at an expansion ratio of 3.0.

(U) g. Instrumentation Data

(C) (1) Thermocouples--Figures 36 and 37 are plots of temperature vs time from the 10 thermocouples during the static test. Instrumentation nomenclature and locations are shown in Figure 38. Thermocouples T201, T202, T203, and T204 are located 1 in. from the metal flange at the nozzle throat. Circumferential locations are noted for each thermocouple on Figure 38 as are the axial distances from the throat flange. All thermocouples were attached to the outside surface of the exit cone.

(C) T201 thru T204 all remained at 75° F, ambient temperature, throughout the test. T205 (Figure 36) rose from ambient shortly after ignition to 215° F at the end of burning time. This rise in temperature was due to radiant reflection of heat from the test bay floor as T205 was located at 0 deg circumferentially. The sudden

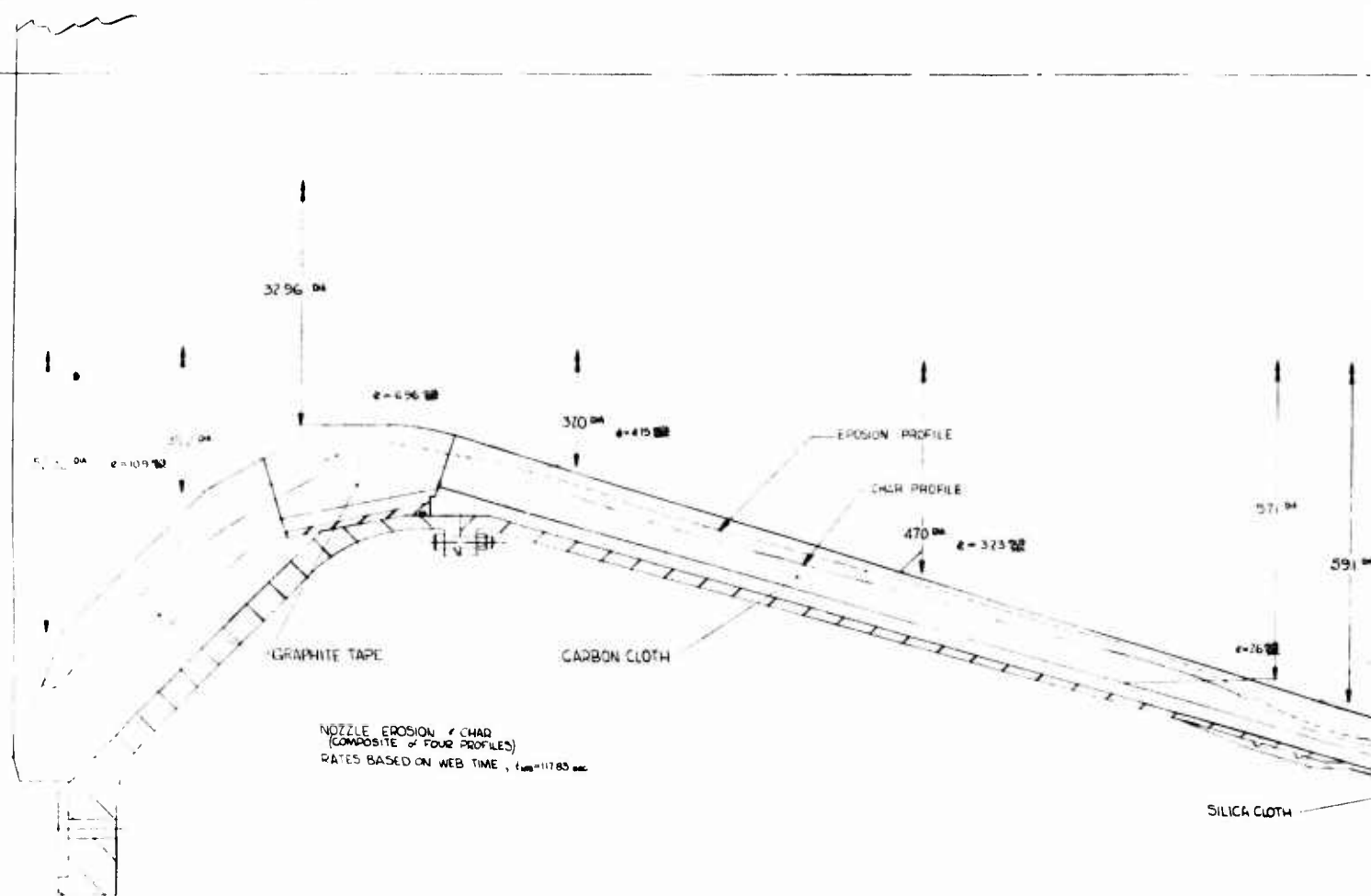
TABLE VII

(C) PREDICTED VERSUS ACTUAL NOZZLE EROSION RATES AND CHAR DEPTHS

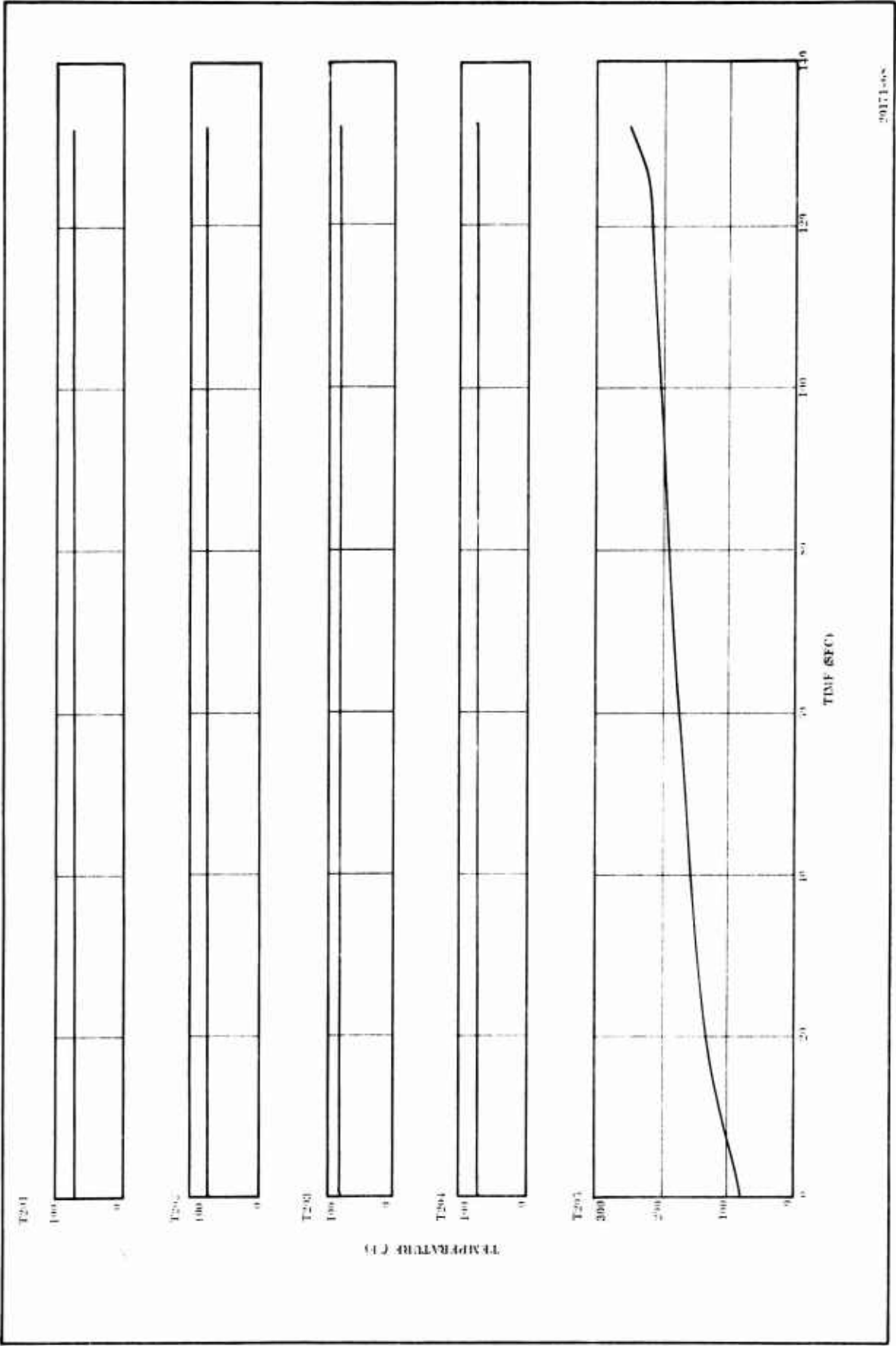
Diameter (in.)	Expansion Ratio	Erosion Rate (mil/sec)		Char Depth (in.)	
		Predicted	Actual	Predicted	Actual
Inlet--Graphite Phenolic Tape					
52.32	2.52	3.61	5.5164	0.888	0.770
39.20	1.414	6.0	10.8631	0.888	0.690
Throat Insert--Graphite Phenolic Tape					
32.96	1.00	7.57	6.9591	0.888	0.660
Exit Cone--Carbon Phenolic Tape					
37.0	1.26	6.12	4.7526	0.8768	0.520
47.0	2.033	3.60	3.2249	0.8424	0.500
57.1	3.00	2.10	2.5460	0.8047	0.340
Exit Cone--Silica Phenolic Tape					
57.1	3.00	8.40	5.4315	0.4248	0.260
59.1	3.215	7.40	9.3354	0.4185	0.280
73.1	4.919	2.80	3.9039	0.3738	0.240
87.2	7.00	0.15	2.2065	0.3431	0.200

CONFIDENTIAL

CONFIDENTIAL



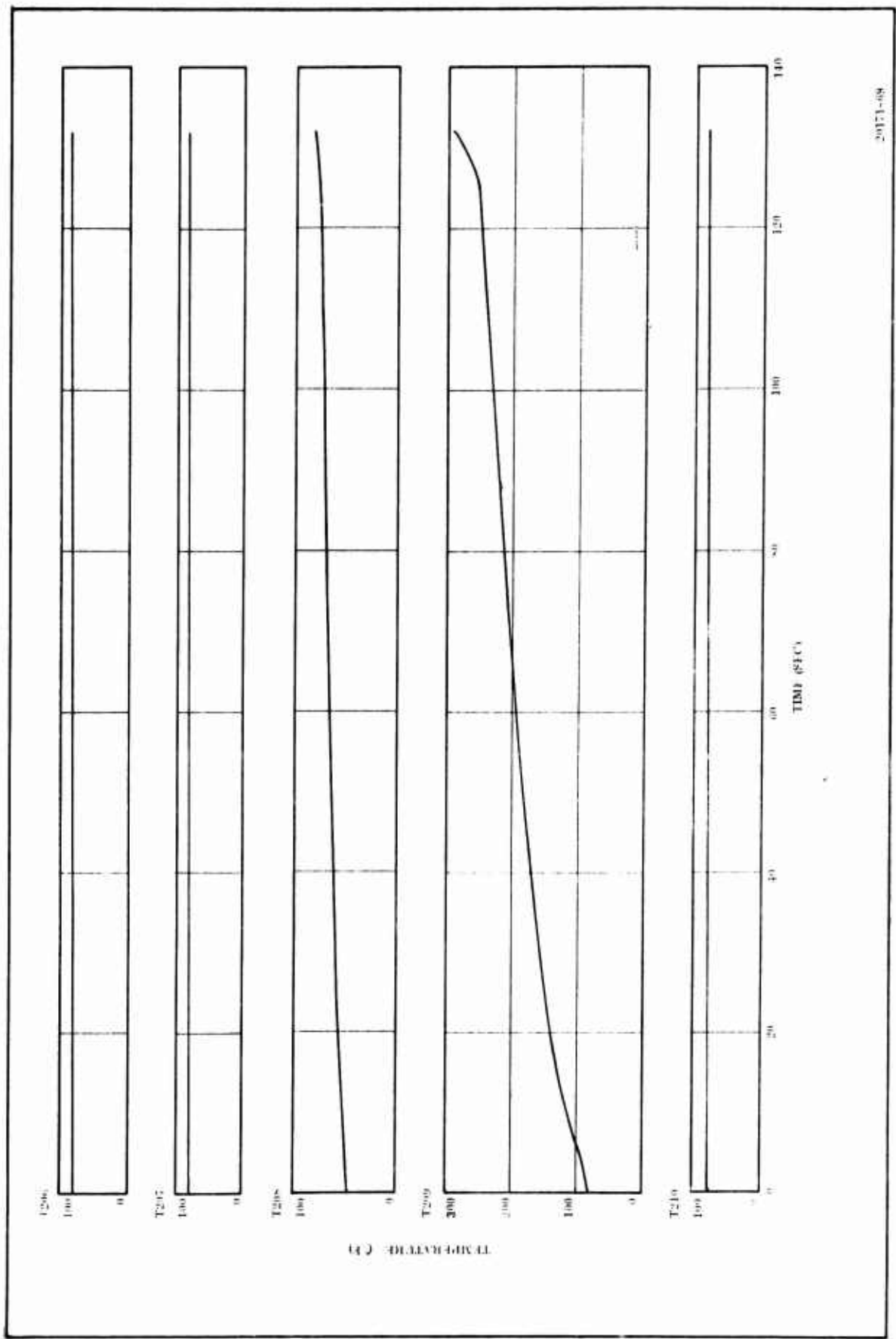
CONFIDENTIAL



(C) Figure 36. Temperature Plots (T201 thru T205)

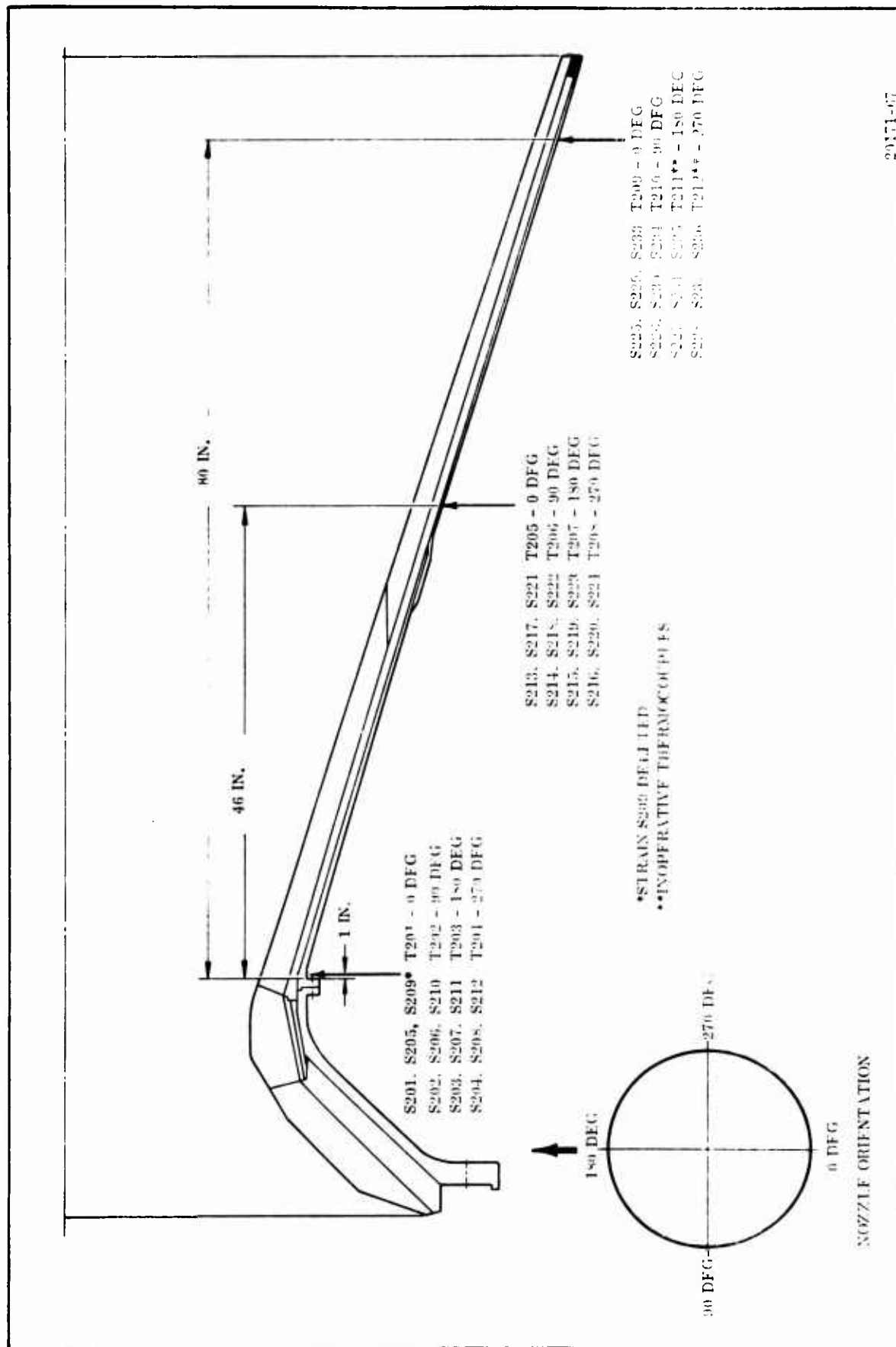
CONFIDENTIAL

CONFIDENTIAL



(C) Figure 37. Temperature Plots (T206 thru T210)

CONFIDENTIAL



(U) Figure 38. 156-8 Nozzle Instrumentation

CONFIDENTIAL

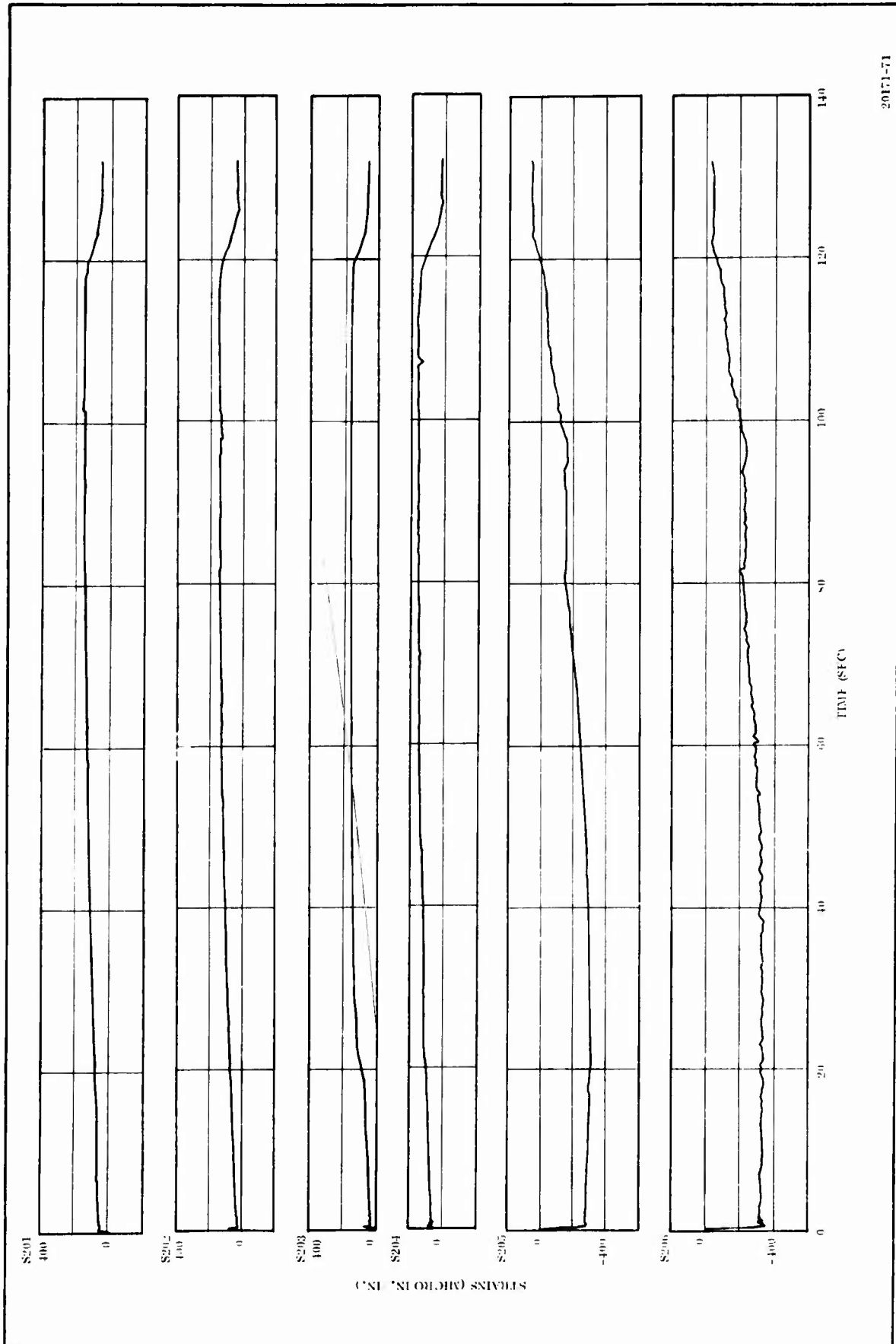
increase in temperature at time t equals 119 sec was due to gases swirling about the exit cone during heat soak. T206 and T207 remained essentially at ambient temperature throughout firing. T208 rose gradually from ambient condition (75°F) to 115°F during firing, probably due to reflection off the side of the test bay. Thermocouple T209 rose from 75 to 250°F, again due to reflection from the test bay floor. Thermocouple T210 remained at ambient condition. Thermocouples T211 and T212 were found to be inoperative during the static test dry run checkout and were not used.

- (U) (2) Strain Gages--Figure 38 shows the locations of all strain gages which were attached to the outer surface of the nozzle during the test.
- (C) Examination of the plots of strain vs time (Figures 39 thru 45) showed no anomalies. The maximum strain recorded was approximately -440×10^{-6} in./in. which is very low. This was anticipated because of the heavyweight nature of the nozzle. With the very low level strains recorded, corresponding stresses would be insignificant and therefore were not calculated.

(U) 6. ACCELEROMETER DATA

- (U) Accelerometer data were taken to document the motor vibrational characteristics during static test and to aid in analysis in case of failure.
- (U) Review of the accelerometer data revealed no abnormal conditions during firing.
- (U) The power spectral density plots (Figures 46 thru 49) show that the nozzle experienced a much higher vibrational energy than the motor harness. Also, forward locations on the nozzle experienced a lower energy level than did the aft end.
- (C) The nozzle data were further analyzed to determine g levels at the predominant frequencies. The predominant frequencies for the aft nozzle vibration in the vertical direction were 40 Hz, 200 Hz, and 700 Hz.
- (C) The predominant frequencies for the aft nozzle in the horizontal direction were 40 Hz, 370 Hz and 450 Hz.

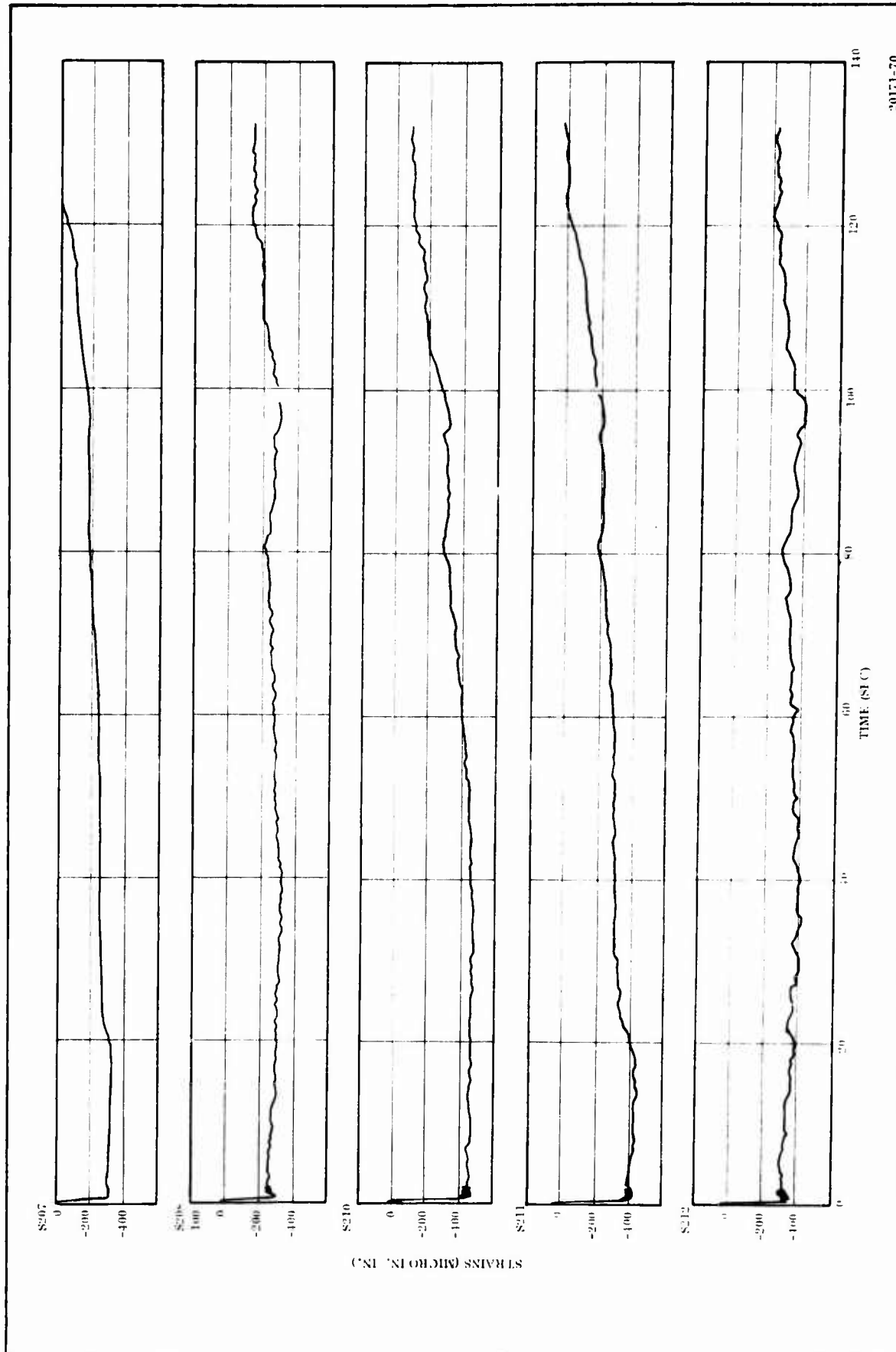
CONFIDENTIAL



(C) Figure 39. Strain Plots (S201 thru S206)

CONFIDENTIAL

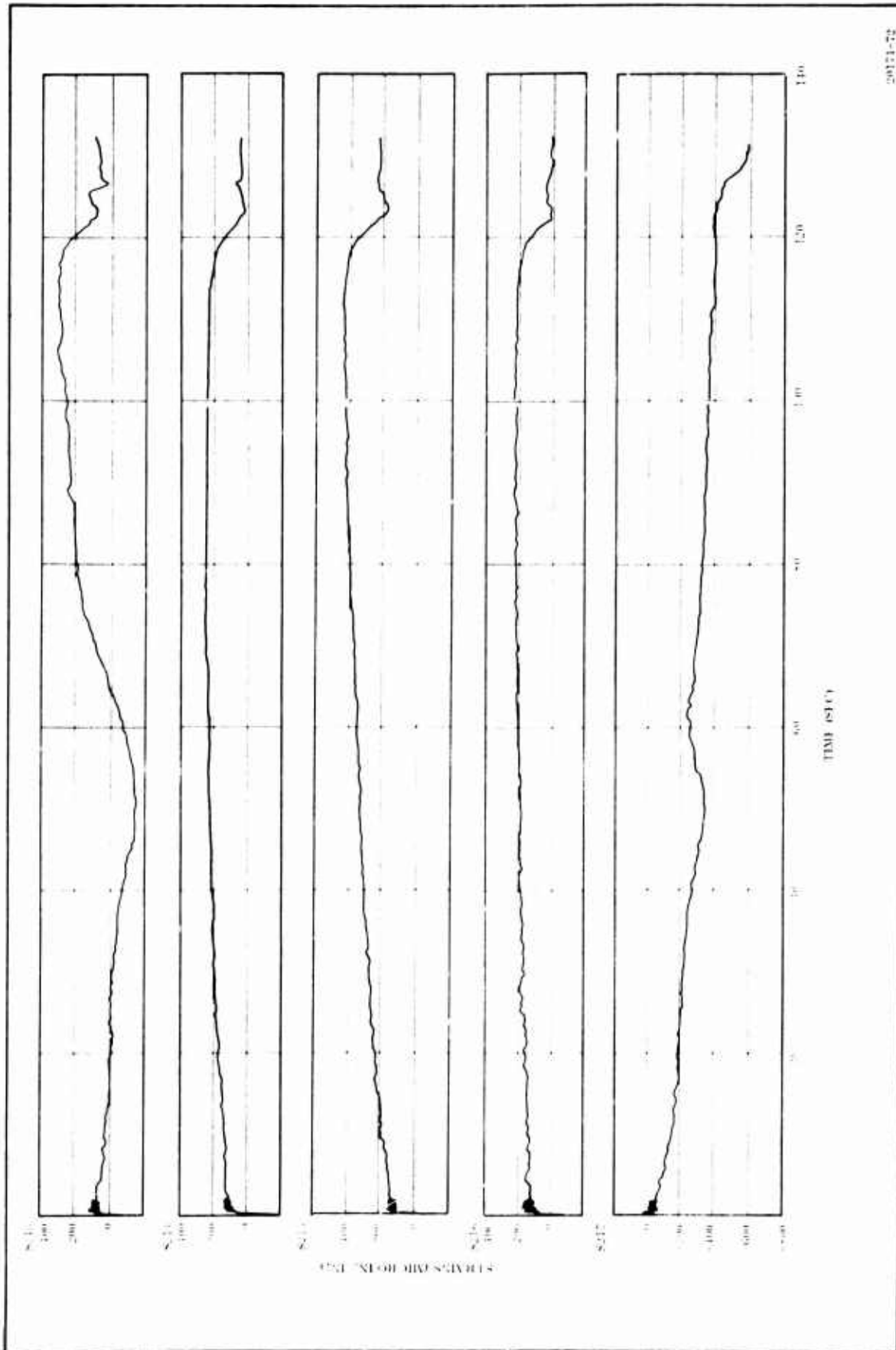
CONFIDENTIAL



(C) Figure 40. Strain Plots (S207 thru S212)

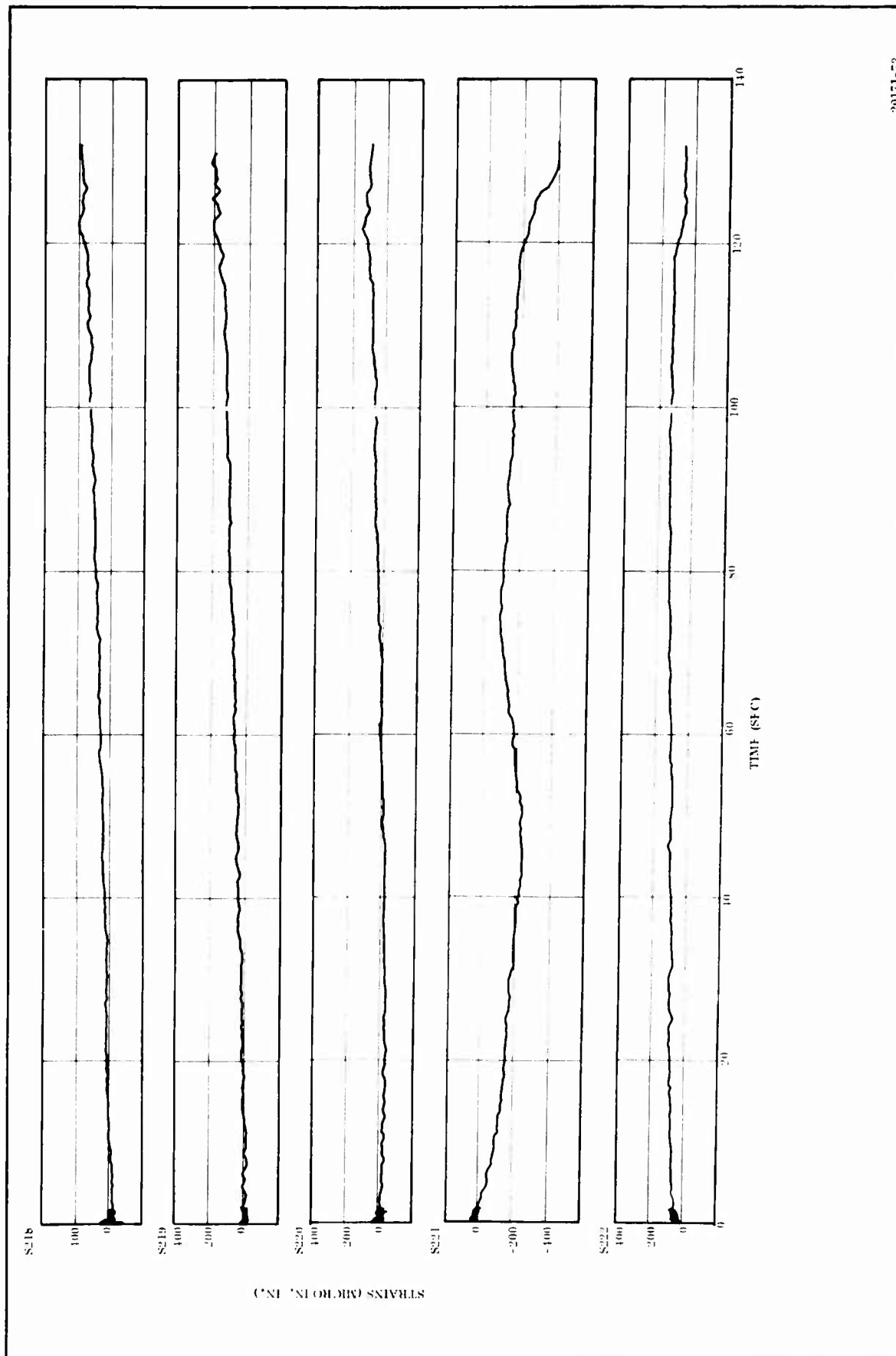
CONFIDENTIAL

CONFIDENTIAL



(C) Figure 41. Strain Plots (S213 thru S217)

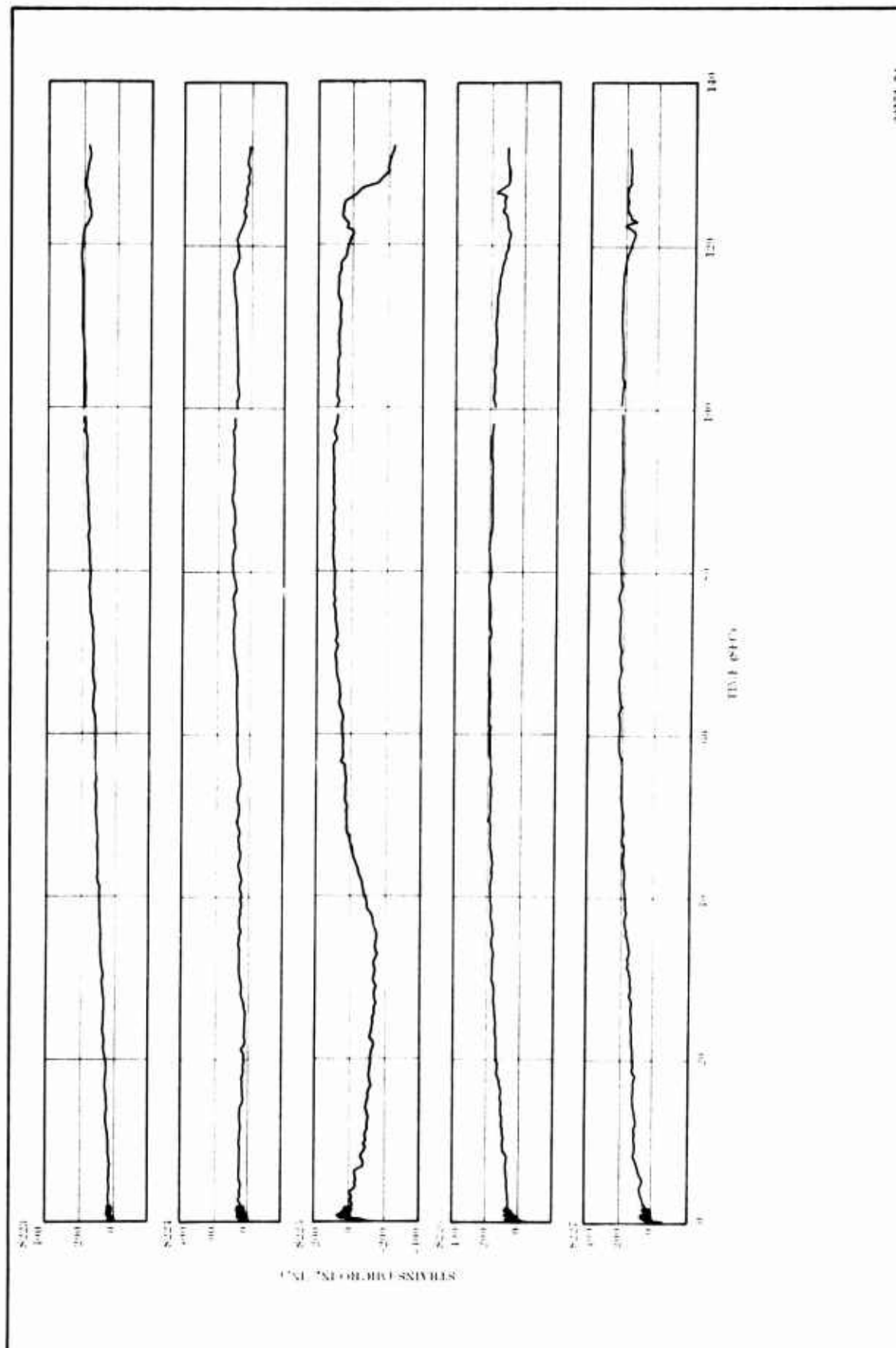
CONFIDENTIAL



20171-73

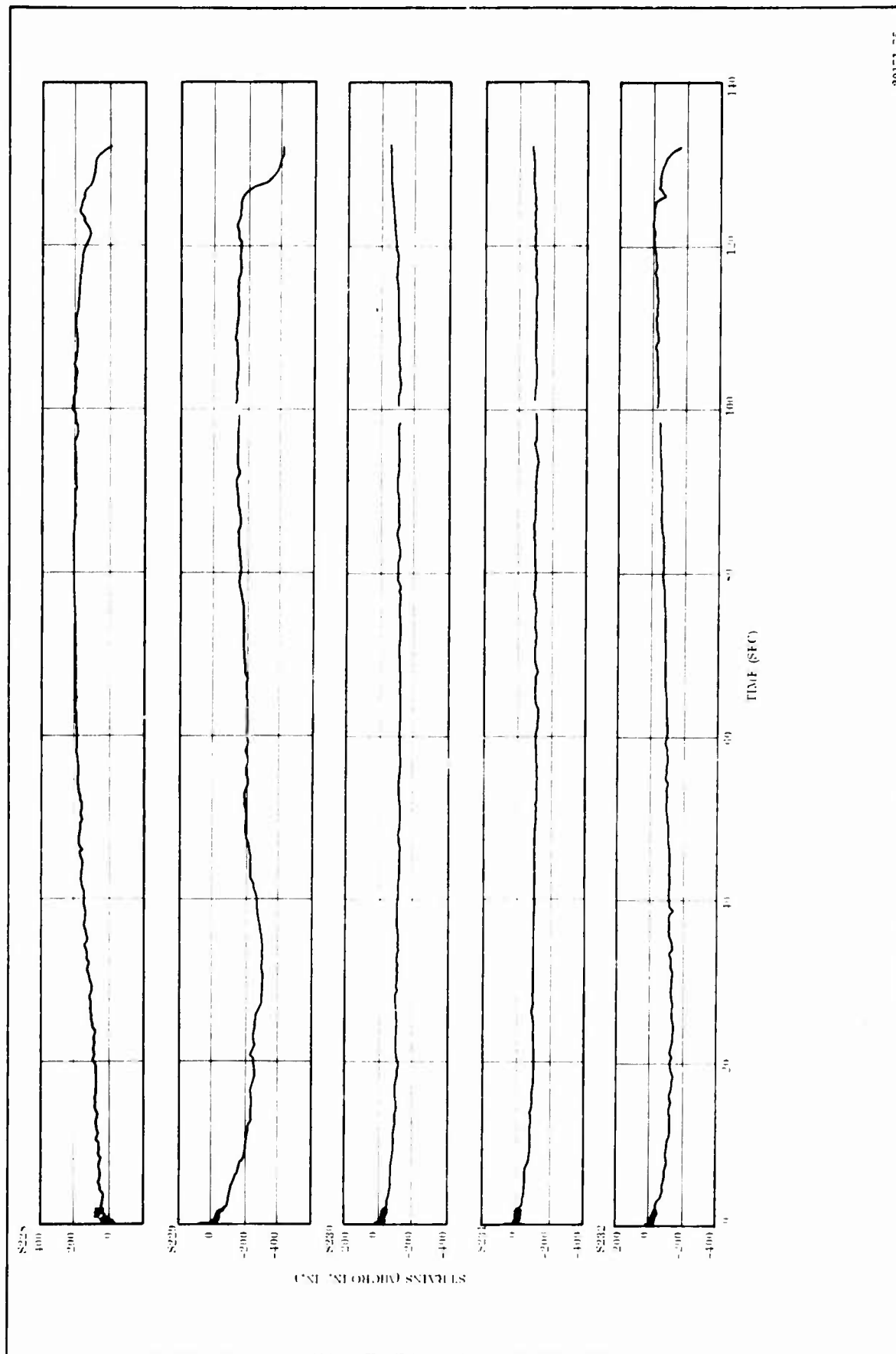
(C) Figure 42. Strain Plots (S218 thru S222)

CONFIDENTIAL



(C) Figure 43. Strain Plots (S223 thru S227)

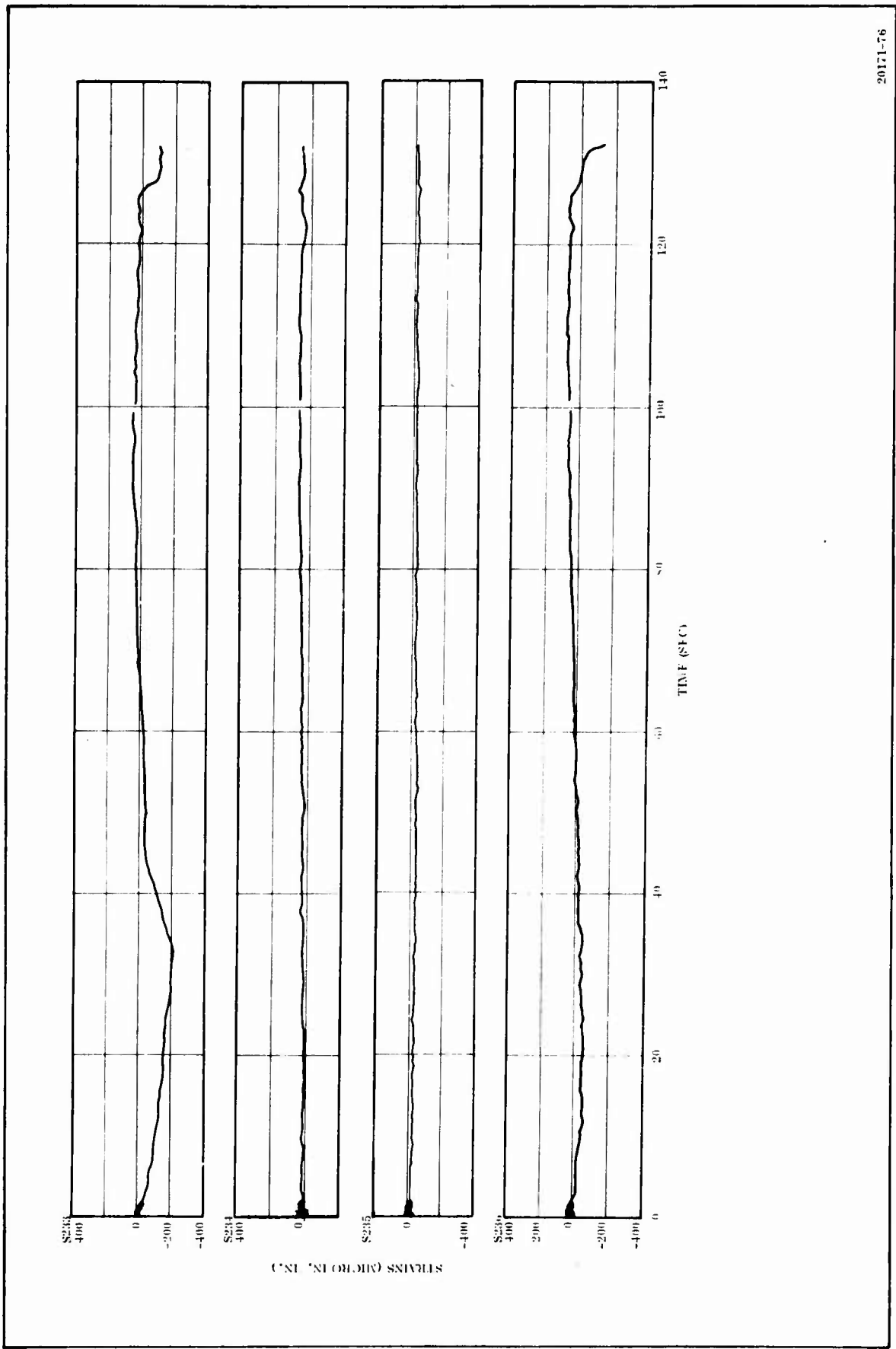
CONFIDENTIAL



20171-75

(C) Figure 44. Strain Plots (S228 thru S232)

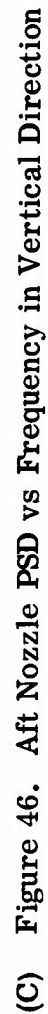
CONFIDENTIAL

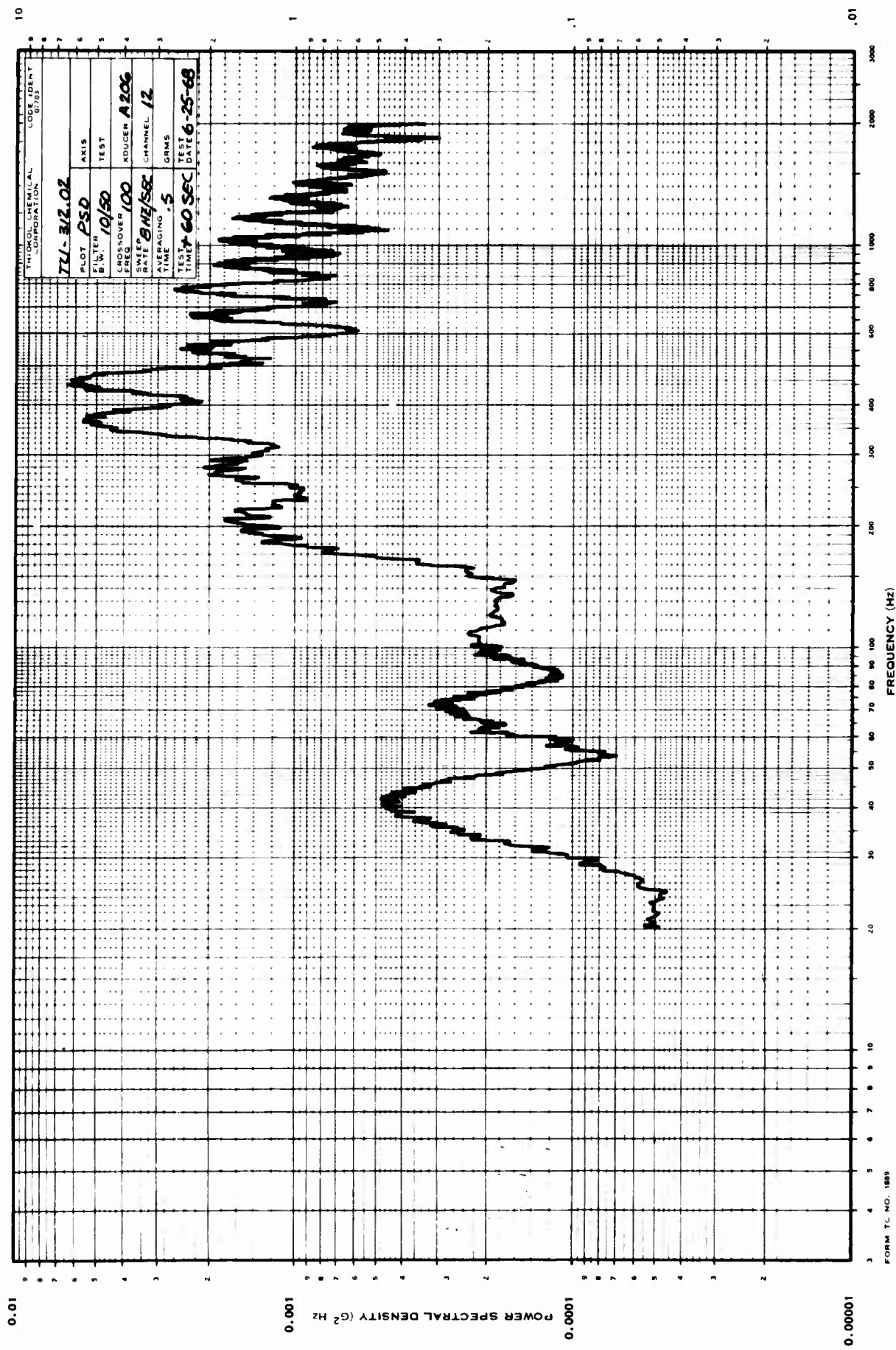


20171-76

(C) Figure 45. Strain Plots (S233 thru S236)

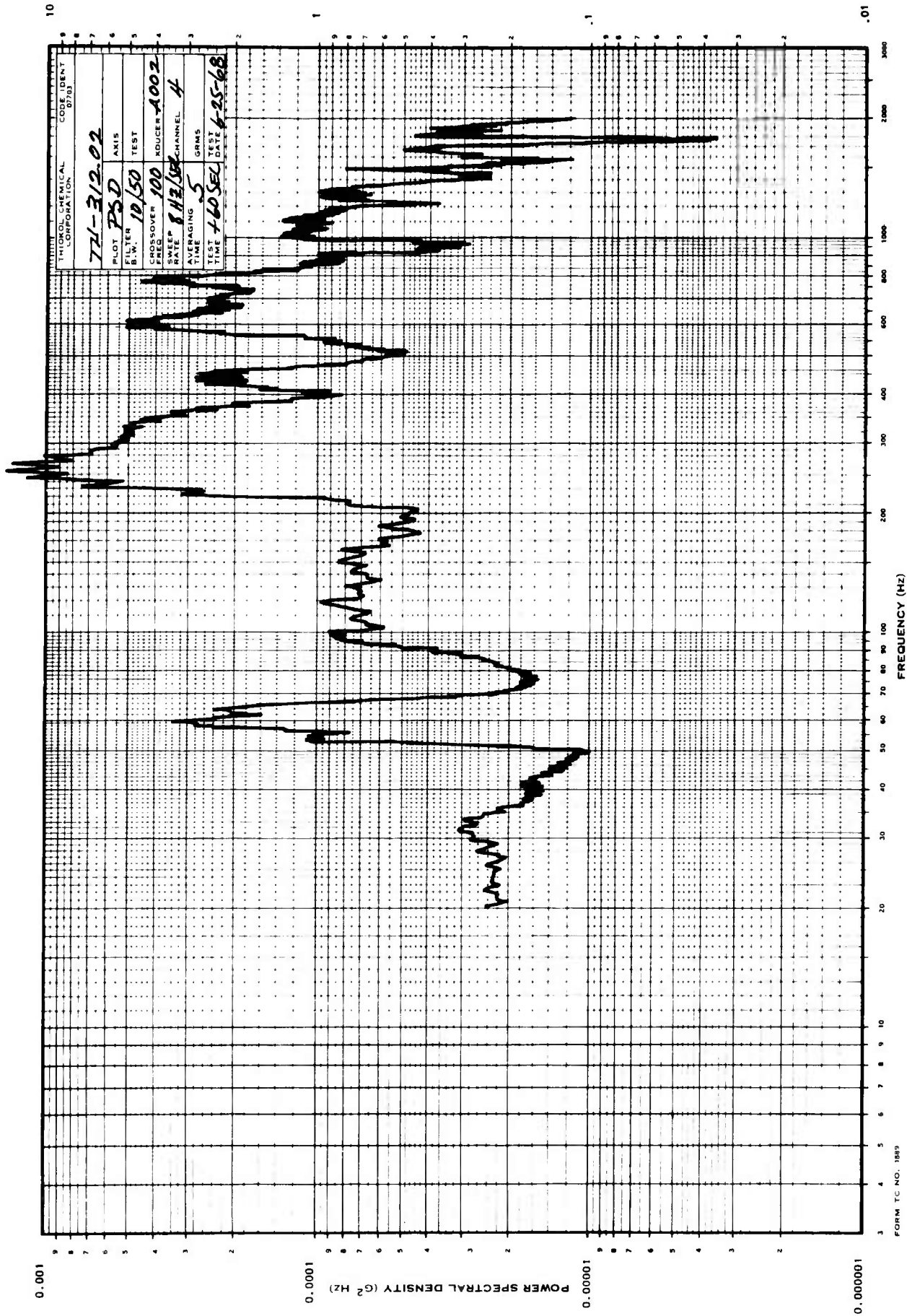
CONFIDENTIAL





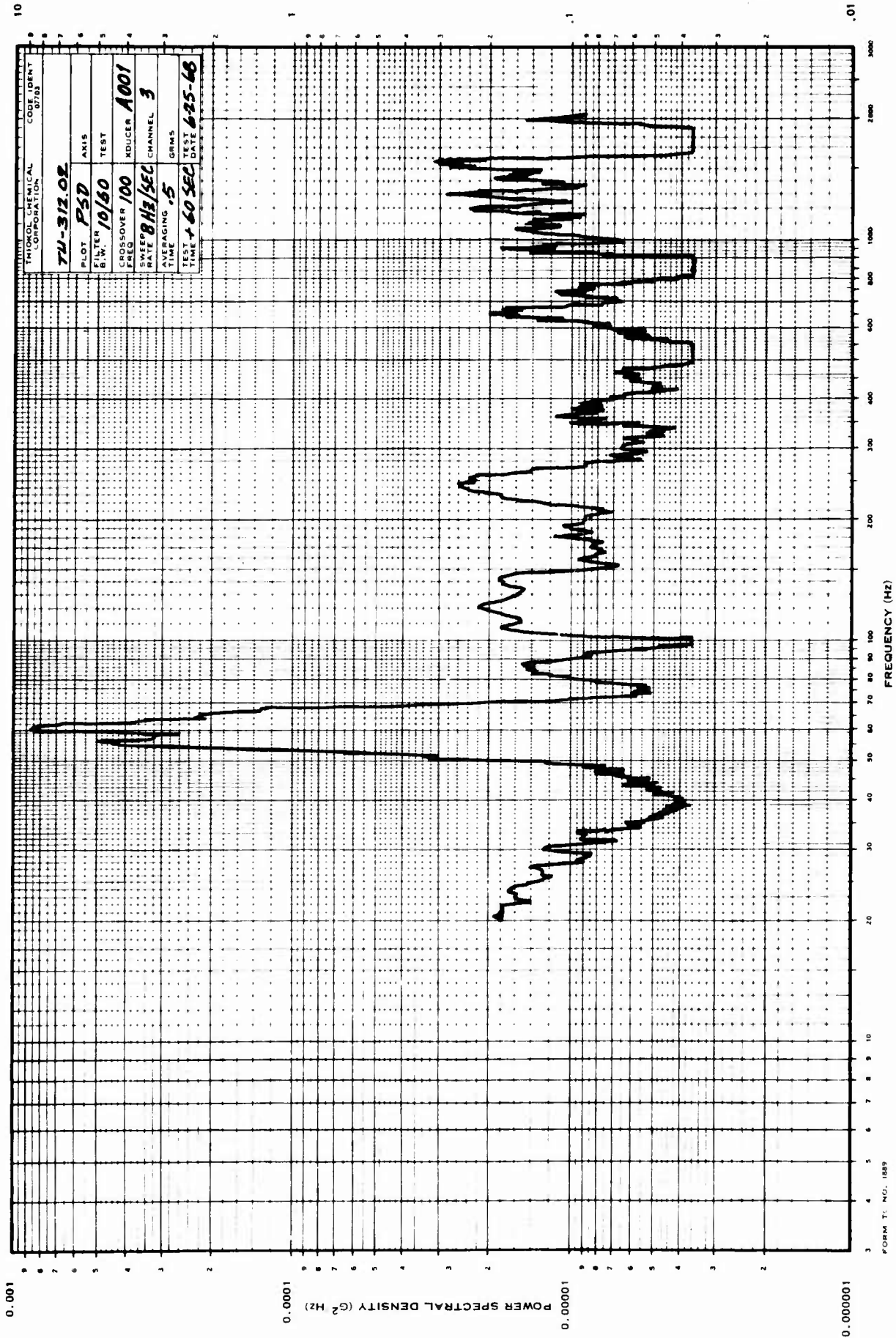
(C) Figure 47. Aft Nozzle PSD vs Frequency in Horizontal Direction

CONFIDENTIAL



(C) Figure 48. Aft Harness PSD vs Frequency in Longitudinal Direction

CONFIDENTIAL



(C) Figure 49. Forward Harness PSD vs Frequency in Vertical Direction

CONFIDENTIAL

SECTION V

(U) HYDROBURST TEST

(U) A. INTRODUCTION

(U) The hydroburst test was conducted in test stand T-17 on 8 Aug 1968. The case was pressurized at 2.5 psig/sec to 500 psig, then increased at 4.3 psig/sec up to the burst pressure of 1,095 psig.

(U) The test objectives were to:

1. Demonstrate manufacturing methods, controls, and process development for fabrication of large segmented fiberglass solid propellant motor cases.
2. Demonstrate the steel glass composite clevis joint load capability.
3. Demonstrate minimum safety factor of 1.25 (equivalent burst pressure of 1,075 psig).
4. Determine ultimate burst pressure.

(U) B. BLADDER REPAIR AND CASE INSTALLATION

(U) 1. BLADDER REPAIR

(U) The case was transported from T-24 (static test stand) to the manufacturing area for bladder repair in the assembled condition rather than disassembling the individual segments. The case was handled with brackets attached to the forward skirt and with a plate attachment on the aft boss.

(U) During static test there were areas in the case where the bladder was burned and in some locations the glass composite was damaged (see Figures 22, 23 and 24). A new bladder had to be installed before the case could be hydroburst. The forward segment required complete bladder replacement from the dome insulation to the joint insulation. The center segment also required complete bladder replacement from the forward joint insulation to the aft joint insulation. The aft segment required only local patches. The case was cleaned and the loose glass removed for bladder repair. The replacement bladder consisted of 0.030 in. V-45 sheet bonded to the case and/or insulation with Stabond T-161.

(U) The case showed no indication of leakage when tested in the horizontal position with 50 psig air. The case was pressurized to 5 psig to guard against bladder unbonding during case transportation from the manufacturing area to the test area.

(U) 2. CASE INSTALLATION

(U) The case was removed from the truck and vertically positioned with two mobile cranes. The case was then lowered into the test stand. Epocast filler was applied to the skirt to insure good contact between forward skirt and test stand. During the above procedure a leak developed in the aft joint. The aft attachment plate was removed and the leak repaired.

(U) Water was added to the case and as it reached the aft joint a leak was noted. The leak was expected to be stopped by application of internal pressure to the joint seals. The aft closure piston assembly was installed into the case and Epocast filler applied to the test stand overhead structure. The case was then pressurized to 40 psig which stopped the leak in the aft joint.

(U)

C. INSTRUMENTATION

(U)

The case was instrumented per drawing 7U37325 (see Figure 50). Eight cameras were located to provide a view of the front and rear of the case. Two cameras were high speed (200 frames per second) and six were 64 frames per second. Two pressure transducers, 24 extensometers and 45 strain gages were used to record case pressure, displacement and strain. The instrumentation was connected and checked out prior to test.

(U)

D. TEST RESULTS AND ANALYSIS

(U)

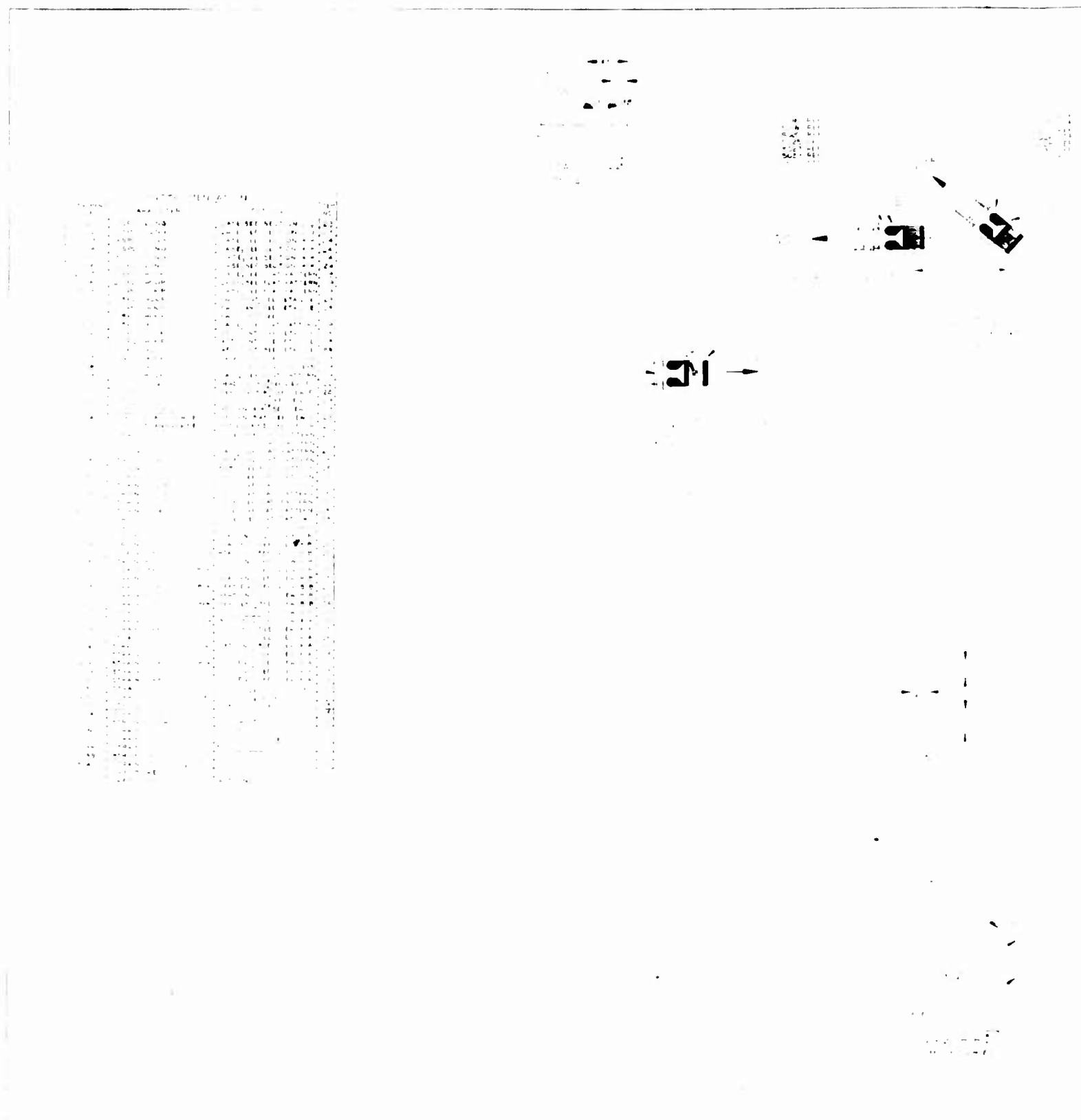
The Halliburton high pressure pumps and piping system were connected to the case pressurizing system. After reaching a manifold pressure of 75 psig, the nominal pressure rise rate was held at 2.5 psig/sec up to 500 psig and at 4.3 psig/sec from 500 psig up to burst. The case failed at 1,095 psig (Figure 51). The pressure recording device was at the aft end of the case. The pressure at the case failure location was actually 1,110 psig due to hydrostatic waterhead.

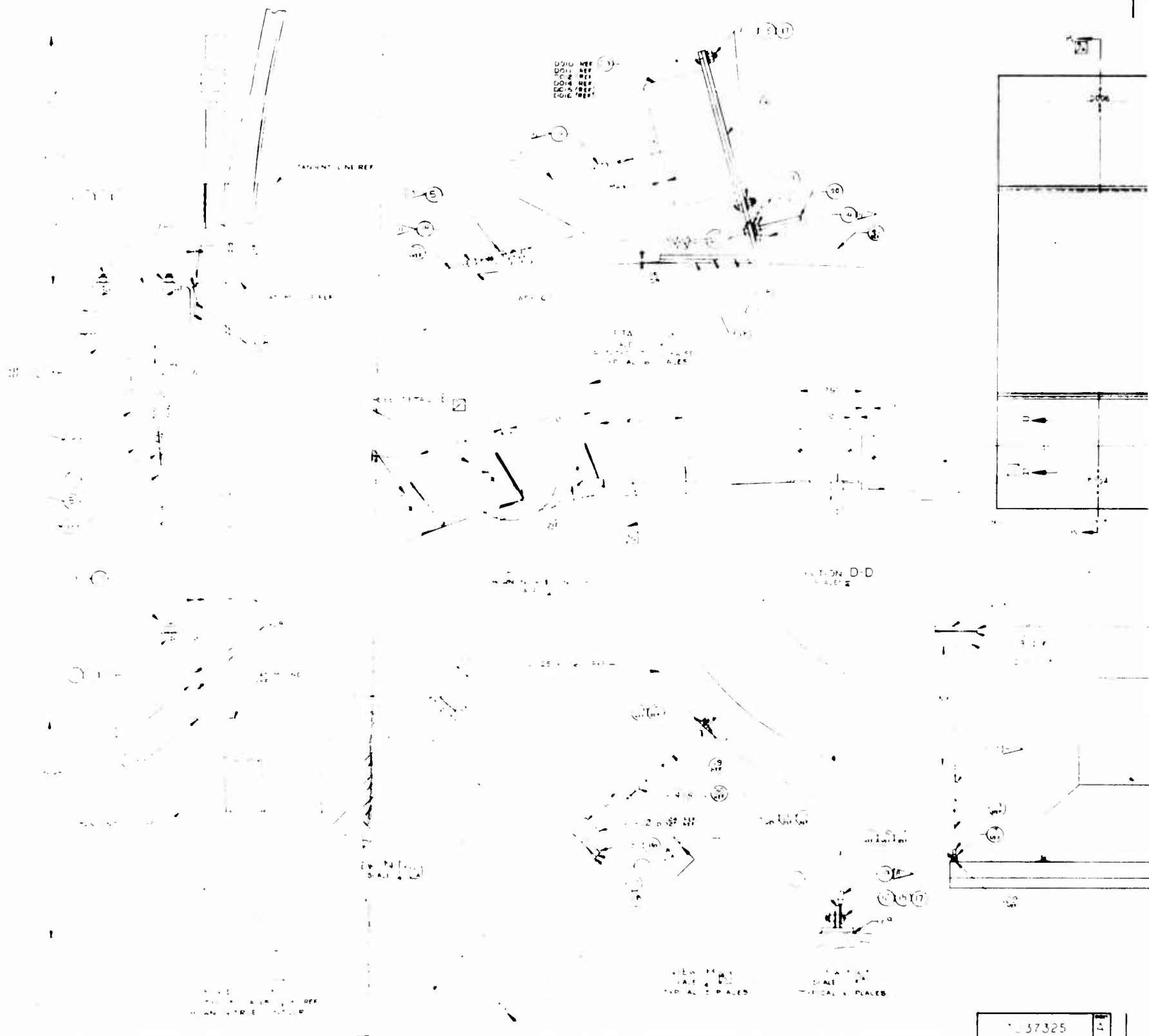
(U)

A hoop failure started about 40 in. forward of the joint in the forward segment, at the 90 to 100 deg circumferential location. The crack progressed circumferentially toward the back of the case (180 deg location) and axially through the forward joint to a point about 15 in. aft of the joint, where it again turned circumferential toward the front of the case (Figure 52). Secondary cracks followed the primary cracks above and below the joint. The joint section banana peeled outward from the case on both sides toward the 270 deg location.

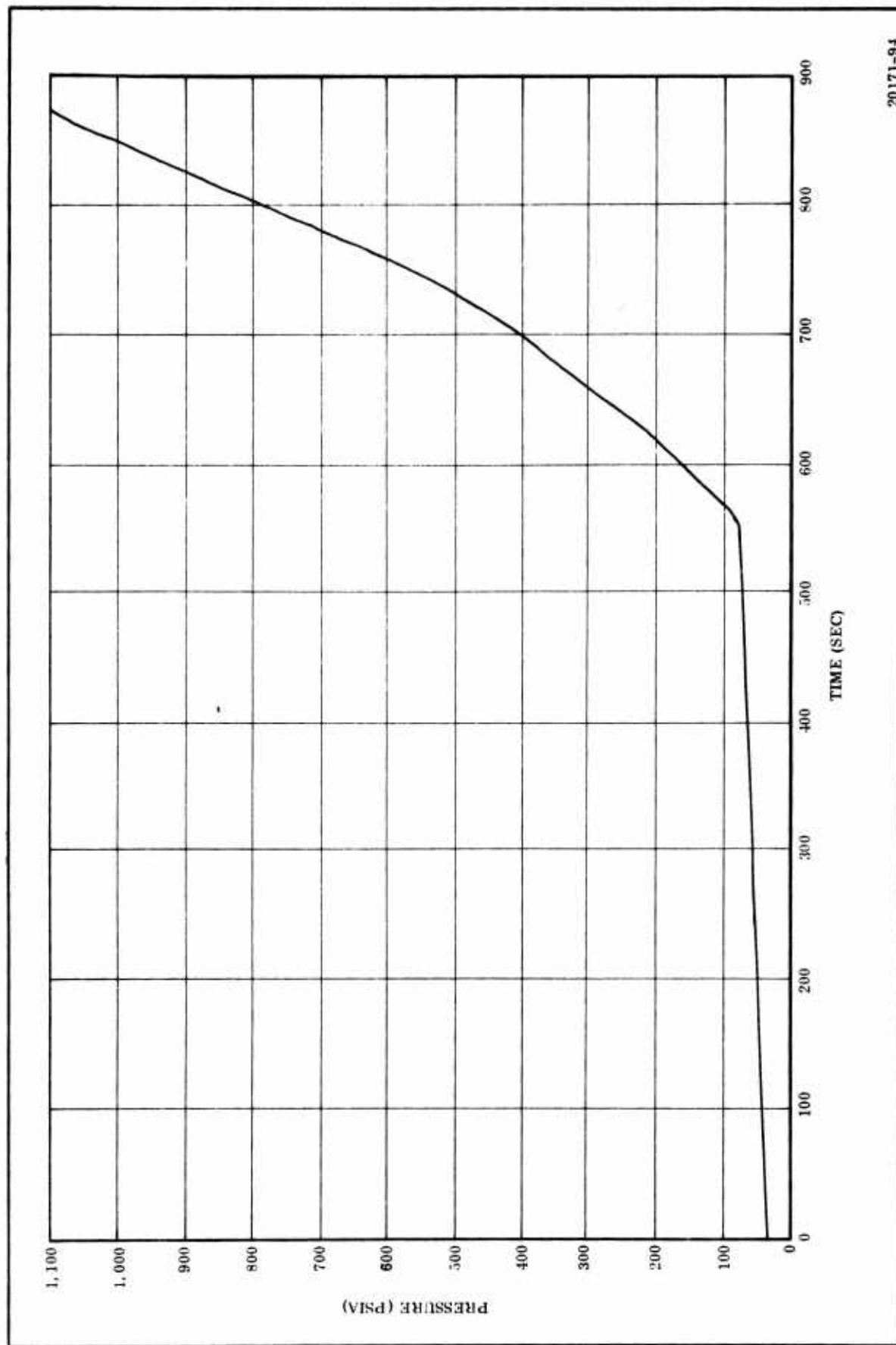
(U)

The forward skirt buckled first at the 90 deg location and rotated counter-clockwise (viewed from the front of the test stand). The forward dome was severely buckled.

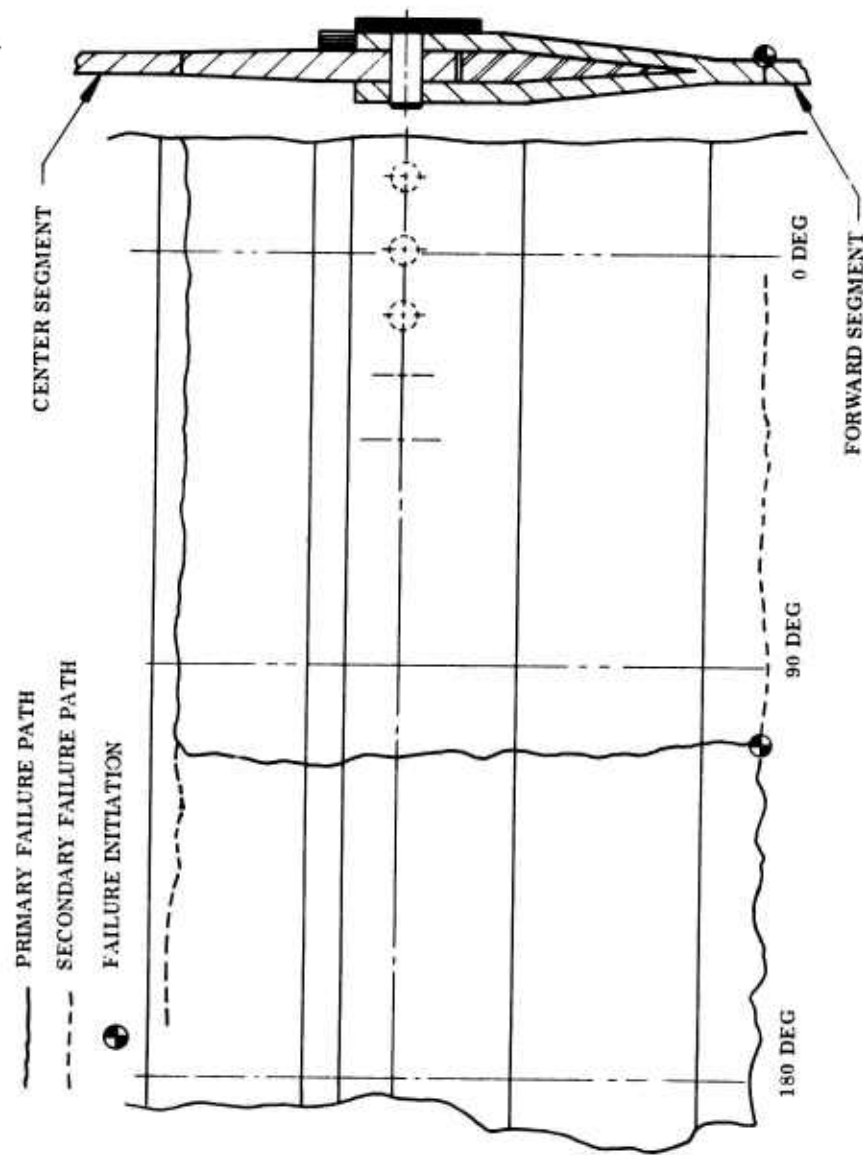




37325



(U) Figure 51. Hydroburst Pressure Chart



FLAT CASE PATTERN WITH 0 DEG AT
FRONT OF TEST STAND

20171-92

(U) Figure 52. Case Crack Propagation at Burst

(U) The center and aft segments were propelled upward inverting the aft dome and crushing the aft skirt against the top of the test stand. The cylindrical portion was severely buckled at the 90 deg location (Figure 53).

(U) Several factors caused the failure to occur in the forward segment. Inspection of sections taken from the forward segment in the failure area showed a very dry laminate. Because of the dry condition, several layers of glass were removed prior to the third hydrotest for bladder replacement. The most important factor was the insulation burning through during static test (see Figure 22). Several layers of glass were burned through and the effect of the heat soak on the remaining composite could not be determined. The calculated hoop and longitudinal stresses in the forward and center segments were as follows:

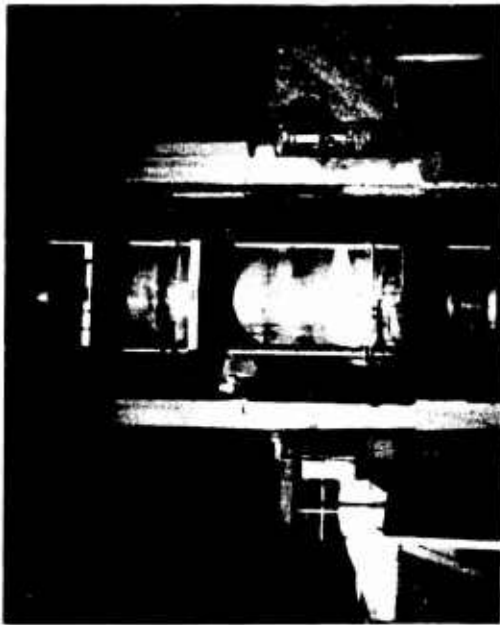
<u>Segment</u>	<u>Hoop Stress (ksi)</u>	<u>Longitudinal Stress (ksi)</u>
Forward	294	232
Center	263	238

(U) The calculations reflect the number of layers damaged, burned or removed, but they do not reflect the effect of the heat affected layers. The heat generated from the burnthrough in the static test in combination with the dry laminate caused a hoop failure at a glass stress of 294 ksi.

(U) Once the crack had propagated through the hoop ring on the inside of the joint, the added case bending caused by joint bulging created longitudinal crack propagation. The inner clevis leg failed first allowing water to flow between the clevis leg and the microballoon epoxy filler and out through the joint. The films show water bursting from the joint at the front of the case (0 deg location). The films also show that the complete longitudinal failure occurred in less than 1/200 second.

(U) During hydroburst, cracking and popping was heard at 800 to 900 psig. Strain and extensometer data show that there was some increase in hoop and longitudinal strain in the forward segment at 800 to 900 psig. Figure 54 shows an increase of

1. Failure Initiation



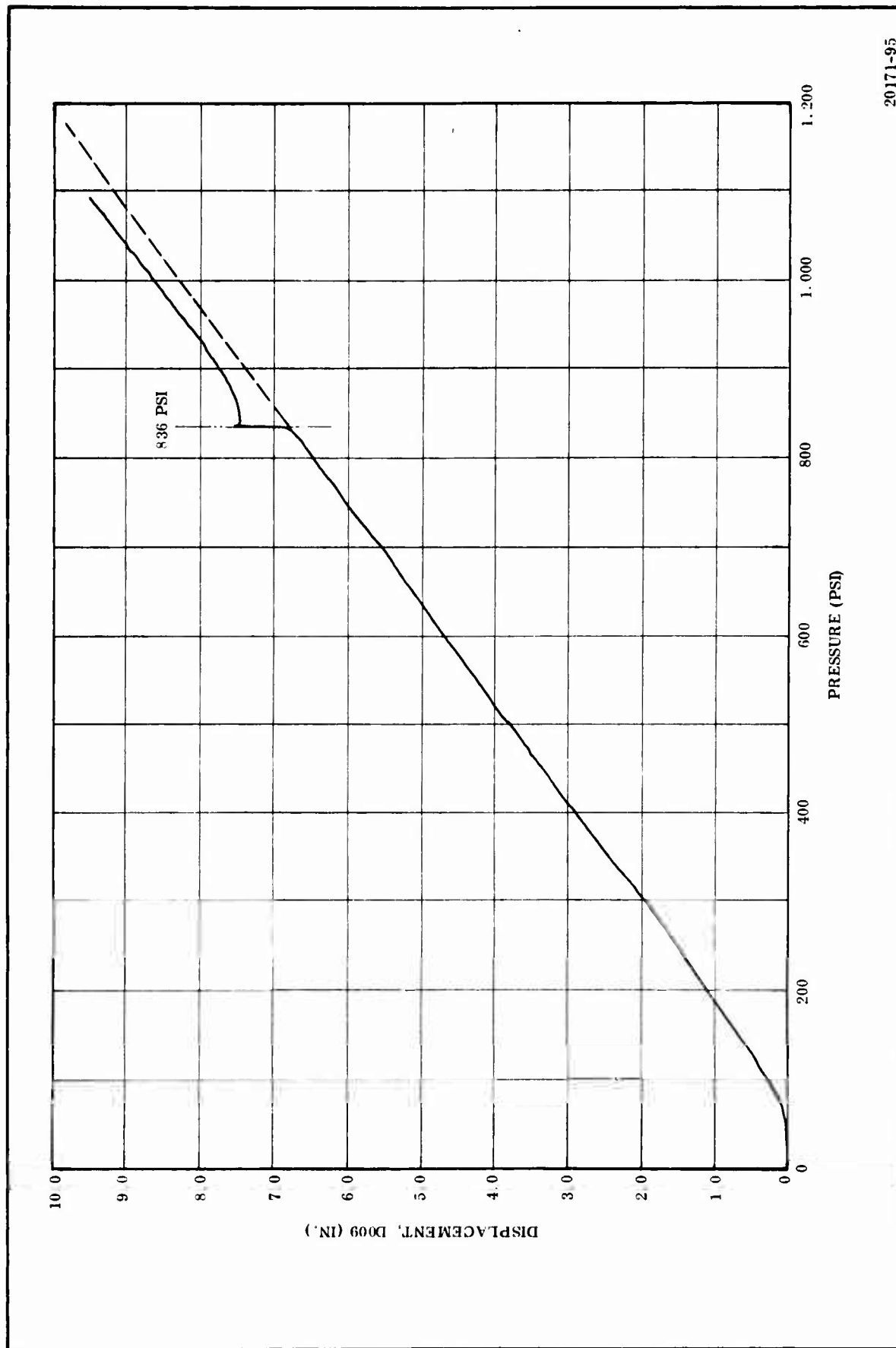
2. Skirt Buckling



3. Cylinder Buckling



(U) Figure 53. Photographic Sequence of Hydroburst (Viewed from 0 Deg Position)



20171-95

(U) Figure 54. Hoop Displacement, Forward Segment

5 percent in hoop strain. This increase in strain was attributed to partial breaking of the glass laminate.

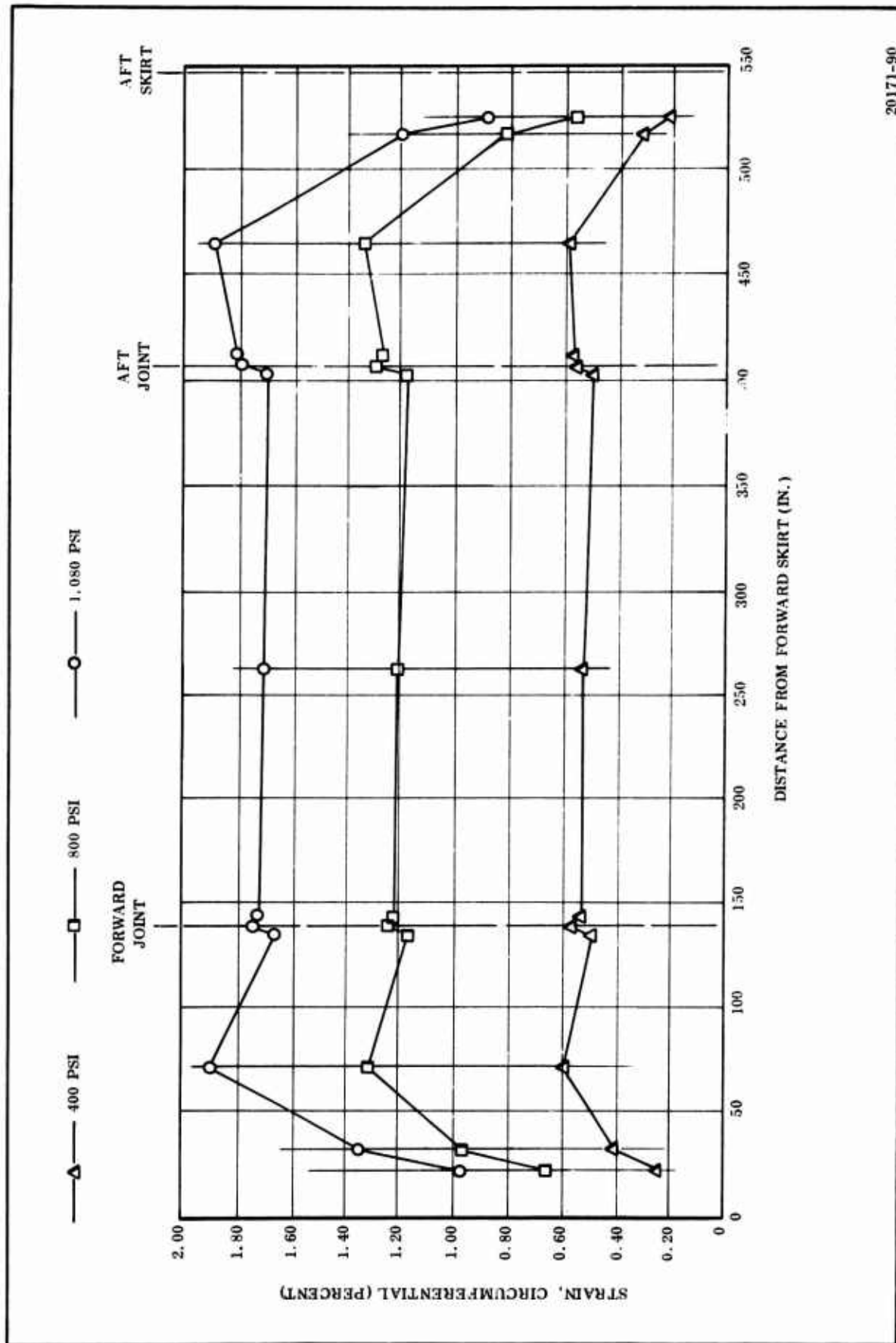
(U) Examination of the forward joint after burst showed that the failure did not start in the damaged clevis legs. The tongue and outer clevis leg remained intact with a large percent of the pins remaining in the joint. All three of the damaged clevis legs were in good condition. There was no indication of crack propagation or shim delamination. The clevis legs were completely separated from the forward segment. The tongue remained attached to the center segment over one quarter of the circumference. Strain gages used to determine load distribution in the damaged clevis legs were lost due to case crazing. The ultimate load capability of the joint was not demonstrated because of the failure in the forward segment. However, the minimum joint safety factor of 1.25 based on a MEOP of 860 psig was demonstrated.

(U) Hoop strain data at various case locations is plotted in Figure 55 for three different pressures. Strains have the same pattern as those of the third 156-8 hydrotest, but the strains from the hydroburst are about 7 percent higher. The change in strain at the joint was investigated to determine if it had an effect on the forward segment failure. The discontinuity stress at the joint induced by varying hoop stiffness would only increase the axial stress 4 percent. A 4 percent increase in axial stress did not have a significant effect on the forward segment failure.

(U) The forward skirt transmitted the thrust load as expected. No indication of buckling was exhibited. The skirt load at case failure was 3,320 lb/in. of circumference. This included the thrust load plus the weight of the water in the case.

(U) The aft joint remained intact even though the case was severely buckled during burst. The shims showed no indication of buckling or "bell mouthing." Pins remained in good condition with no indication of bearing failure.

(U) The forward and aft domes performed as expected. Several of the strain gages were lost due to dome crazing, but remaining gages provided adequate data. The polar bosses did not show indication of yielding or cracking.



(U) Figure 55. Circumferential Strain Data

20171-90




- (U) The strains and displacements at burst are shown in Tables VIII and IX. The strains in general were lower than those observed in the static test and hydrotests. The extensometer readings were about the same as those observed in other tests. A comparison of measured and calculated stresses follows.

<u>Segment</u>	<u>Hoop Stress (ksi)</u>	<u>Longitudinal Stress (ksi)</u>
Forward (calculated)	294	232
Forward (measured)	258	204
Center (calculated)	263	18
Center (measured)	264	228

- (U) The measured and calculated stresses compared within 4 percent in the center segment. In the forward segment the measured stresses were approximately 15 percent below calculated stresses. The calculated stresses in the forward segment were in the local burned area on the inside of the case. The strains were measured on the outside of the case and did not pick up the local stress concentrations.
- (U) Calculations prior to hydroburst showed that failure could occur in the damaged clevis legs at a pressure of 1,075 psig. Calculations also indicated a minimum failure pressure of 1,265 psig in the forward segment. The above calculations were based on glass ultimate strengths of 335 ksi in the hoop direction and 305 ksi in the longitudinal direction. The burned area in the forward segment, in combination with the dry laminate, reduced the ultimate strength of the material and forced the failure to occur in the forward segment.

TABLE VIII

(U) EXTENSOMETER READINGS AT BURST PRESSURE

<u>Extensometer</u>	<u>Direction</u>	<u>Displacement (in.)</u>	<u>Gage Length (in.)</u>
D001	Long.	*	--
D002		6.35	480.5
D003		**	--
D004		**	--
D005		**	--
D006		**	--
D007	Hoop	5.00	489.0
D008		7.00	490.5
D009		9.85	491.5
D010		8.75	497.5
D011		9.20	497.5
D012		8.95	492.0
D013		8.85	491.0
D014		8.75	497.5
D015		9.45	498.0
D016		9.35	492.5
D017		9.80	491.0
D018		6.30	494.0
D019	Hoop	4.60	490.5
D020	Long.	1.40	32.5
D021		1.30	30.0
D022		7.40	38.5
D023	Long.	7.35	38.5
D024	Trans	**	--
D025	Trans	**	--








NOTES: For gage locations see Figure 50.

*Gage failed at 900 psi.

**Gages showed insignificant movements.

TABLE IX

(U) STRAIN READINGS AT BURST PRESSURE

<u>Gage</u>	<u>Direction</u>	<u>Strain (%)</u>	<u>Gage</u>	<u>Direction</u>	<u>Strain (%)</u>
S001	Hoop	1.33	S024	D. Fiber***	1.14
S002	Long.	*	S025	D. Hoop	0.52
S003	Hoop	1.15	S026	D. Fiber	0.47
S004	Long.	0.75	S027	D. Hoop	0.68
S005	Hoop	1.48	S028	D. Fiber	0.83
S006	Long.	1.09	S029	D. Hoop	0.95
S007	Hoop	1.40	S030	D. Fiber	0.98
S008	Long.	1.15	S031	D. Hoop	0.83
S009	Hoop	1.59	S032	D. Fiber	1.10
S010	Long.	10.7	S033	Long.	-0.22
S011	Hoop	1.39	S034		0.17
S012	Long.	0.78	S035		-0.31
S013	D. Fiber	*	S036	Long.	0.38
S014	D. Fiber	*	S037	Radial	0.31
S015	D. Fiber	1.21	S038		-0.57
S016	D. Hoop	*	S039		0.83
S017	D. Fiber	1.18	S040	Radial	-0.31
S018	D. Hoop	0.84	S041	Long.	*
S019	D. Fiber	0.73	S042		*
S020	D. Hoop	**	S043		*
S021	D. Fiber	1.27	S044		*
S022	D. Fiber	**	S045	Long.	*
S023	D. Fiber	1.29			

NOTE: For gage locations see Figure 50.

*Gage lost to fiberglass crazing.

**Gage failure.

***D. - Designates dome gages.

SECTION VI

(U) CONCLUSIONS AND RECOMMENDATIONS

(U) A. CONCLUSIONS

- (U) 1. Large segmented fiberglass reinforced plastic (FRP) cases up to 156 in. in diameter are feasible for large solid rocket motors from a design and process standpoint.
- (U) 2. The 156-8 case was adequately designed and all areas of discrepancy or failure resulted from fabrication defects or physical damage.
- (U) 3. The 156-8 case contained a defective glass laminate low in resin content in each area where the glass laminate had been cured simultaneously and in contact with the B. F. Goodrich 39322 NBR rubber. The defective glass laminate resulted in failure of the original forward and aft skirts and necessitated their replacement and repair. This defect also necessitated removal and replacement of the bladder in all three segments as well as the removal of four to five layers of glass on the interior of each segment.
- (U) 4. A large FRP case is not particularly sensitive to damage. Damage occurred in several areas of the basic pressure vessel and joints of the 156-8 with no detrimental effect on case use.
- (U) 5. Large segmented fiberglass cases can be successfully pressure sealed by seating the seal in the internal insulation.

- (U) 6. Segmented fiberglass cases require a sophisticated joint rounding system to facilitate assembly of loaded segments in the horizontal position. The original rounding system for the 156-8 motor was inadequate.
- (U) 7. The joint insulation contour grinding tooling was inadequate and could have been improved by tool design refinements.
- (U) 8. The casting problem which ultimately led to extensive grain repair of the forward segment evolved from: (1) excessive processing time to deaerate and cast the propellant and (2) excessive distance for the propellant to flow from the bayonet to the farthest point of the grain. These deficiencies would not have existed if a vacuum casting system and/or more bayonets had been used.
- (U) 9. The X-ray of large motor grains in fiberglass cases is feasible using the type equipment used to radiographically inspect the 156-8 forward segment. The relative size and nature of the defects in the forward segment were determined quite accurately from interpretation of the X-rays.
- (U) 10. The grain repair of large solid motors can be successfully undertaken. This program has demonstrated that defects can be mechanically cut from large motor grains of PBAA-AP propellant and the grain successfully recast with the same type propellant.
- (U) 11. Techniques for accurate ballistic performance predictions for large motors are available as is demonstrated by the actual data from this test.
- (U) 12. The nozzle, which had its plastic parts cured under pressures produced by high tension shrink tape, performed essentially the same as other large nozzles in which the large plastic parts were cured in a hydroclave.

- (U) 13. The quench system design was inadequate to completely protect the motor case from post-test heating. The system did not adequately cover the forward segment due to the angle of the injection holes. This inadequacy resulted in heat damage to the case segment.
- (U) 14. Case failure during hydroburst test occurred in the heat affected area and, therefore, the full composite case strength was not determined. Strengths of 294,000 psi were demonstrated and it is, therefore, assured that obtainable strength is at least that high.
- (U) 15. When bonding of large pieces of NBR insulation into the case is required, the size and relative total void area can be greatly reduced by drilling 1/8 in. bleed holes through the parts. These holes should be drilled in areas which will experience gas flow velocities up to Mach .052. When these holes are slanted 45 deg from the direction of the gas flow, they are not detrimental to the insulative or erosion resistance of the NBR.

(U) B. RECOMMENDATIONS

- (U) 1. To avoid having defective glass laminate next to shear plies and bladder, FRP cases should be wrapped using preimpregnated roving and proven fabrication techniques. If other new processes and materials are used, appropriate prefabrication testing should be conducted to insure the glass composite is not affected by the shear ply and bladder materials.
- (U) 2. Future large motors should be vacuum cast in a vacuum bell. This method would have avoided major propellant casting problems in this program.

- (U) 3. Future large motor FRP cases, segmented or monolithic, should be wrapped over the insulation to eliminate problems of insulation fabrication and installation.
- (U) 4. On future large nozzle and large plastic insulation parts, the method of fabrication using shrink tape for compaction pressure should be considered as an acceptable state-of-the-art technique.
- (U) 5. When quench systems are required in large diameter cases, the ports into the head end dome should be oriented to direct the quench medium along the dome contour to insure complete quench of the forward section of the case.
- (U) 6. Pressure actuated seals of design similar to that of the 156-8 should be used on future segmented FRP cases.
- (U) 7. Future programs should provide for a flightweight design ignition system to allow technical advancement of this subsystem along with all other systems.
- (U) 8. It is recommended that in any large motors which do require bonding of NBR insulation into the case that 1/8 in. bleeder holes on no greater than 6 in. centers be incorporated to minimize voids behind the insulation in areas predicted to experience gas flow velocities up to Mach .052. Further investigation should be conducted to determine the effects of bleeder holes in areas which will experience velocities greater than Mach .052.

Security Classification

DOCUMENT CONTROL DATA - R & D

(Security classification of title, body of abstract and indexing annotation must be entered when the overall report is classified)

1. ORIGINATING ACTIVITY (Corporate author) Thiokol Chemical Corporation Wasatch Division Brigham City, Utah		2a. REPORT SECURITY CLASSIFICATION Confidential	
		2b. GROUP 4	
3. REPORT TITLE Final Report, Demonstration of 156 Inch Motor with Segmented Fiberglass Case and Ablative Nozzle, Volume II--Static Test and Hydroburst			
4. DESCRIPTIVE NOTES (Type of report and inclusive dates) Final Report (12 Apr 1966 thru 8 Aug 1968)			
5. AUTHOR(S) (First name, middle initial, last name) Walker, Thomas Zeigler, Robert F.			
6. REPORT DATE December 1968		7a. TOTAL NO. OF PAGES 110	7b. NO. OF REFS None
8a. CONTRACT OR GRANT NO. AF 04(611)-11603		9a. ORIGINATOR'S REPORT NUMBER(S) TC0-57-8-8	
b. PROJECT NO.		9b. OTHER REPORT NO(S) (Any other numbers that may be assigned this report) AFRPL-TR-68-159-Vol II	
c.			
d.			
10. DISTRIBUTION STATEMENT In addition to security requirements which must be met, this document is subject to special export controls and each transmittal to foreign nationals may be made only with prior approval of AFRPL (RPPR/STINFO) Edwards AFB, California.			
11. SUPPLEMENTARY NOTES		12. SPONSORING MILITARY ACTIVITY SAMSO AND AFRPL	
13. ABSTRACT The primary objectives of the program were to successfully static test fire the rocket motor followed by a hydroburst test of the fiberglass case. These objectives were attained. The motor (156-8) was static test fired 25 Jun 1968 and all systems performed satisfactorily. This test successfully demonstrated the segmented fiberglass case design and the joint seal design. All motor and nozzle components were intact and in good condition at the completion of the test. The motor operated at close to predicted ballistic values. Post-test inspection of the motor and components disclosed that the internal insulation, nozzle design, and joint seal design were satisfactory and the nozzle performed as predicted. Inadequacies in the CO ₂ quench system permitted some charring through of the insulation in the forward dome which necessitated repair prior to the hydroburst test on 8 Aug 1968. Burst occurred at 1,095 psi, starting in a heat affected area of the forward segment.			

DD FORM 1473
1 NOV 65

Security Classification